CHALMERS
UNIVERSITY OF TECHNOLOGY

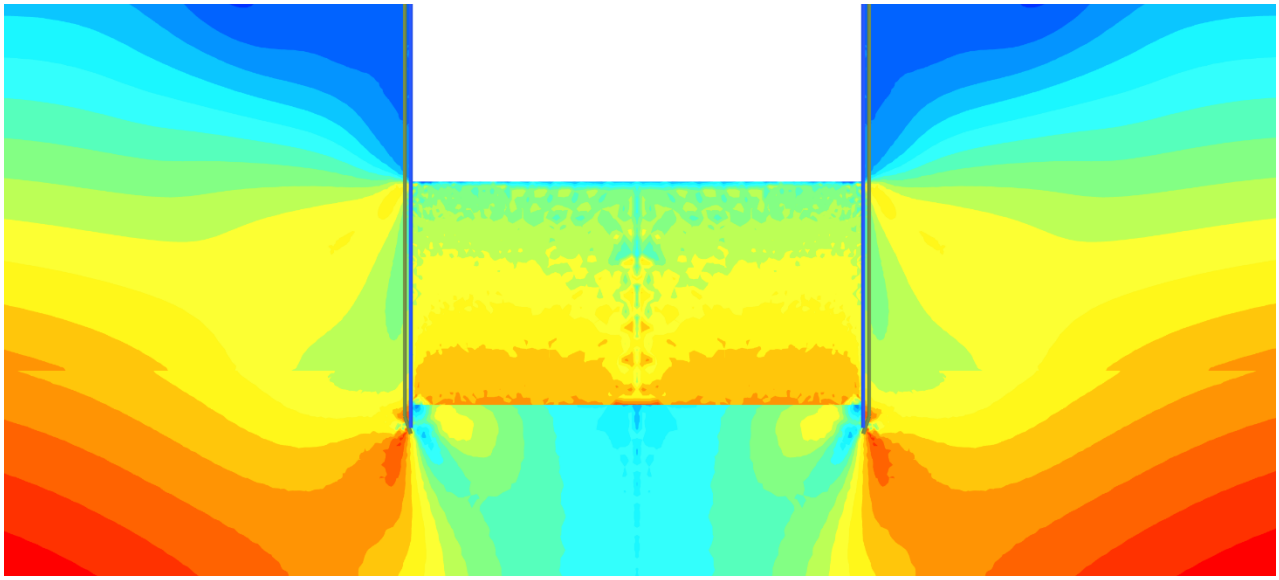

Numerical Modelling of Deep Mixing in Passive Zone of an Excavation

A Case Study based on Västlänken E02 Centralen

Master's thesis in Infrastructure and Environmental Engineering

MARCUS B. CLAESSON
OSKAR J. REHNBERG

DEPARTMENT OF ARCHITECTURE AND CIVIL ENGINEERING (ACE)
DIVISION OF GEOLOGY AND GEOTECHNICS

CHALMERS UNIVERSITY OF TECHNOLOGY
Gothenburg, Sweden 2021
www.chalmers.se

MASTER'S THESIS ACEX30

Numerical Modelling of Deep Mixing in Passive Zone of an Excavation

A Case Study based on Västlänken E02 Centralen

Master's Thesis in the Master's Programme Infrastructure and Environmental Engineering

MARCUS B. CLAESSON
OSKAR J. REHNBERG

Department of Architecture and Civil Engineering
Division of Geology & Geotechnics
CHALMERS UNIVERSITY OF TECHNOLOGY
Göteborg, Sweden 2021

Numerical Modelling of Deep Mixing in Passive Zone of an Excavation
A Case Study based on Västlänken E02 Centralen

Master's Thesis in the Master's Programme Infrastructure and Environmental Engineering

MARCUS B. CLAESSON
OSKAR J. REHNBERG

Examensarbete ACEX30
Institutionen för arkitektur och samhällsbyggnadsteknik
Chalmers tekniska högskola, 2021

Department of Architecture and Civil Engineering
Division of Geology & Geotechnics
Chalmers University of Technology
SE-412 96 Göteborg
Sweden
Telephone: + 46 (0)31-772 1000

Cover: Deviatoric stresses in the final model of the study, mirrored for symmetry.

Department of Architecture and Civil Engineering
Göteborg, Sweden, 2021

Numerical Modelling of Deep Mixing in Passive Zone of an Excavation

A Case Study based on Västlänken E02 Centralen

Master's Thesis in the Master's Programme Infrastructure and Environmental Engineering

MARCUS B. CLAESSON

OSKAR J. REHNBERG

Department of Architecture and Civil Engineering
Division of Geology & Geotechnics
Chalmers University of Technology

ABSTRACT

This report focuses on how to model the short-term system response of a deep excavation with a lime cement column grid in the passive zone. The report investigates a case site in Gothenburg where a deep excavation is made in soft Scandinavian clay for the construction of a train tunnel. The investigation is conducted using a 2D homogenization technique in a finite element software. The clay is modelled using Creep-SCLAY1S and the LC using the Hardening Soil constitutive model. Results from the numerical investigation are compared with monitoring from the case study to analyse and reiterate. The comparisons show that the best method of modelling lime cement in this study is to have a homogenous soil body to represent the inner excavation. Installation effects of the lime cement has a considerable impact on the results. The lime cement columns decrease the horizontal displacements of the sheet pile walls in the excavation and the settlements on surrounding soil, while it increases the strut forces in the excavation due to its installation effects. Overall, deep excavations are complex systems. For accurate prediction of deformations during design, an understanding of the entire system will be necessary.

Key words: Deep mixing, deep excavation, soft clay, passive zone, system response, lime cement installation effects, Creep-SCLAY1S, Hardening soil, Plaxis 2D.

Contents

1 Introduction 1
1.1 Aim and objectives 1
2 Background 2
2.1 Deep excavations in soft soil 2
2.2 Dry Deep Mixing 3
2.3 Numerical Modelling in Two Dimensions 5
2.4 Constitutive Models in Numerical Geotechnics 6
2.4.1 Hardening Soil model 7
2.4.2 Creep-SCLAY1S 10
3 E02 Centralen, Västlänken 16
3.1 Geotechnical conditions 16
3.2 Cross section 18
3.3 Field monitoring 20
4 Finite Element Analysis of E02 Centralen 24
4.1 Model geometry 25
4.1.1 Mesh and Boundaries 28
4.2 Parameter Determination 29
4.2.1 Parameter boundaries 30
4.2.2 Parameter Sensitivity Analysis 37
4.2.3 Optimization of Parameters 39
4.2.4 Structural Elements 43
4.3 Numerical investigation 44
4.3.1 Scenarios regarding LCC grid 44
4.3.2 Scenarios regarding material parameters 46
4.3.3 Scenarios regarding installation effects 47
5 Results and Discussion 48
5.1 Base Model 48
5.2 Numerical investigation results 51
5.2.1 Installation Effects 55
5.2.2 Final Model 60

5.2.3 Creep-SCLAY1S state parameters 63
5.3 Impact of LCC on Excavation 65
6 Further Discussion 68
6.1 Sources of Error 68
6.2 Further Research 69
7 Conclusion 70
References 71

Preface

This study would not have been possible without the Geotechnical experts that have supported us this semester. Especially, we would like to thank our examiner Minna Karstunen for great guidance and outstanding presence during the entire project. We would also like to thank our Chalmers supervisors Jonatan Isaksson and Sinem Bozkurt as well as our NCC supervisor Tim Björkman for the constant feedback, dedication and goodwill in every meeting and email. The study visit to E02 Centralen was of great help to us. We are proud of what this project became, and your overwhelming support has been essential the entire way.

Finally, we would like to thank our fellow geotechnical students at Chalmers for the dialogue, laughter and insight that has been exchanged this semester.

Gothenburg, June 2021

Marcus Berghamn Claesson
Oskar Rehnberg

1 Introduction

Urbanization is a global trend that is present in Sweden. In the bigger cities, new infrastructure needs to be constructed on limited space and time, and with minimum impact on its surroundings. There is also a need to construct taller structures on less stable ground, such as along riverbanks, where sensitive soft soils are found. This presents a challenge in terms of stability and settlements. Stricter environmental and emission requirements are also present, for example, Trafikverket requires contractors in their large infrastructure projects to reduce their CO^2 emissions from 2015, by 30% until 2025 (Trafikverket, 2021). Cement production contributes to 5% of manufactured CO^2 emissions (World Business Council for Sustainable Development, 2002). Since all foundation techniques involves cement, reducing its usage is key.

The use of deep mixing in the passive zone of excavations can meet many of these challenges while being cost effective. Deep mixing uses less cement than a conventional foundation with concrete cross walls, creates no spoil, eases the excavation process, and strengthens the soil with potential for reuse of the stabilized material (Wood, 2018). The method also increases the safety of the working environment by stabilizing the working foundation. It has been used in numerous projects in Norway, but so far only small-scale tests have been performed in Sweden (Wood, 2018). Therefore, more studies on how the lime cement columns behave in projects in Sweden are needed before the method can become widely used.

1.1 Aim and objectives

The purpose of this study is to increase the understanding of deep mixing in the passive zone of a deep excavation. Specifically, sheet pile wall deformations will be studied, as this is often a major factor of design. Furthermore, specific insights on the design of the case excavation will be sought after. The following research questions will be answered:

- What serviceability impact does the deep mixing technique have on the case excavation?
- How can an excavation with deep mixing be accurately modelled in Plaxis 2D?

The study focuses on a site study of E02 Centralen, which contains a deep excavation with a lime cement grid of double overlapping rows on the passive side. The study will be approaching the problem through a rigorous computational technique based on homogenisation, that can model complex 3D effects in computationally effective 2D analysis. The aim is to accurately model the construction period and short-term system response of the site. To further study the effects of complex soft clay behaviour, a complex soil model specifically designed for soft clay, Creep-SCLAY1S, will be used. Time dependency will hence be partly considered where Creep-SCLAY1S is used, that is in the soil surrounding the excavation.

The study starts with background, explaining some of the general knowledge behind the study. It is followed by a specific case description regarding the study site with its geological and geotechnical properties. Field monitoring and soil tests from the area are also shown. Tests previously carried out are described and shown, as well as recorded monitoring of the ongoing construction. The chosen methodology is then presented. Lastly, results from our study are presented and analysed, followed by some summarizing conclusions.

2 Background

In this chapter, the geotechnical problems of deep excavations in soft soils will first be introduced. The method of deep mixing will then be explained. Lastly, numerical modelling and different constitutive models for soft soils and lime cement will be presented.

2.1 Deep excavations in soft soil

Deep excavations in soft soils are one of the most challenging geotechnical constructions. The construction subjects the soil to complex stress situations in shear, compression, and extension. Moreover, soft soils can show complex behaviour because of its geological history.

Soft soils are defined as geologically young clays or silty clays that have only or mostly been consolidated solely by its own unit weight (Bjerrum, 1973). Hence little hardening of the soil has occurred. The amount of consolidation of the soil is described by a preconsolidation pressure, which is the highest pressure that the soil has endured. A soil is then overconsolidated if the current stress state is below the preconsolidation pressure, and normally consolidated if they are equal. Soft soils, such as normally or slightly overconsolidated clays, will undergo large deformations when subject to stress exceeding the preconsolidation pressure. Furthermore, soft soils are fully saturated with low undrained shear strength and are hence inclined to water flow and plastic deformations. These properties make soft soils challenging materials to work with.

A typical deep excavation design in soft soils is shown in Figure 2.1. An excavation is a site where the removal of soil has created a surface difference, hence leading to new stresses in the surrounding soil. Unsupported excavations in soft soils are limited to shallow depths of 2-3 meters to avoid failure (Heidelberg, 2006). However, these unsupported excavations must have an inclined slope as well as protection from erosion and from water movements to prevent failure. Because of these limitations, most deep excavations in soft soils are supported excavations. The support is in form of walls, often combined with struts or anchors. In soft soils, the usage of stiff walls, e.g., sheet pile walls, is preferred to reduce the displacement on surrounding soil, especially when performed in an urban area where settlements around the excavation can damage nearby constructions. The use of struts and anchors are to further reduce the deformations of the wall and hence the displacements of surrounding soils. The limited strength of soft soils also creates the possible failure mechanism of bottom heave in deep excavations. This can limit the possible depth of an excavation and must be considered in the design. A concrete slab is often installed at the bottom to stabilize against bottom heave and improve working conditions.

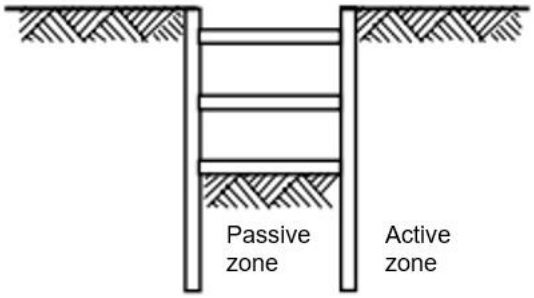

Figure 2.1 Schematic sketch of a braced excavation with double struts.

To understand the structural behaviour of a deep excavation, there are some aspects of interest that can be monitored. The first one is horizontal displacements of the excavation wall. Wall displacements can lead to ground settlements and other serviceability problems. Furthermore, it can be used as indicator of the margin to safety failure. Another important indicator is ground settlements. It can be analysed in different distances from the excavation. Close to the excavation, the ground settlements are important to determine the serviceability of the construction site. For example, cranes and other vehicles may have problems operating safely on ground with large settlement. Further away it can indicate the harm on surrounding buildings and constructions. Strut forces are also an important aspect of the excavation and should be monitored. The struts are often designed to be able to take high loads, but at normal state the monitoring can give information on the system response of the excavation. The distribution of forces in the struts can give an indication of how much earth pressure is mobilized in the passive zone.

Some soil state parameters can help in understanding the system response but are harder to monitor. Pore pressures in the excavation show areas subject to increased stress and are important indicator of weak points. Horizontal total pressures, also called earth pressures, show what force the soil is applying to the system. In the passive zone, the sheet pile walls push against the earth creating passive earth pressures, providing support together with the struts. How much earth pressure is mobilized in the passive zone is dependent on the soil stiffness and strength (Knappet & Craig, 2012).

2.2 Dry Deep Mixing

Deep mixing is a technique where a binding material is mixed into the soil, forming a stabilized soil material. A mixture of lime and cement (LC) is a frequent binder material used in clay, forming LC stabilized clay. The LC is installed using blades that rotate into the ground, forming columns in the ground called lime cement columns (LCC), see Figure 2.2. It is the leading ground improvement method in the Scandinavian countries where soft clays are highly common (Larsson S. , 2005). Deep mixing is divided into dry- and wet deep mixing where the difference is the liquid state of the cement during installation into the soil, in Scandinavia dry deep mixing is the most common method as it works well with wet clays. The mixture becomes weakly cemented resulting in higher compressive strength, but the strength and stiffness in extension is less known and may have high variability. The strength and stiffness of LCC depends on the amount of cement, which typically ranges between 40-100 kg/m^3. When installing LC into the ground, high air pressures are used to distribute the material into the soil. This causes disturbance in the pore pressures in the ground. Furthermore, the injection of new material also pushes the soil away, causing a volumetric increase in the ground. This volumetric increase tends to partially reset with time as the pressure stabilizes. Some case studies have also proven to have the opposite effects when installing the LCC, causing a volumetric decrease instead. This phenomenon is caused because of excessive amounts of clay being removed from the ground when the drill is moving back up.

LCC are most popularly used under embankments to increase the stability of soils (Hedman & Kuokkanen, 2003). The vertical load from the embankment causes the compressive behaviour of the soil under the embankment to be governing the response. However, when used in an excavation site, extension and shear behaviour of the LC is more important than the compressive. Research on the shear strength of single LCC began with (Kivelö, 1998) and has been further investigated

both in field testing (Broms, 1998) and in lab testing (Larsson, Malm, Charbit, & Ansell, 2012). A single LCC did not show significant shear strength increase compared to the initial soil. Further research focused on the combined shear strength of LCC groups in the passive zone of excavations (Kitazume, Yamamoto, & Udaka, 1999) (Kitazume & Maruyama, 2006) (Kitazume & Maruyama, 2007). The results showed that shear strength significantly increases by overlapping columns and hence creating a connected lime cement grid. Overlapping LCC has later been implemented to improve the soil in the passive side of deep excavations. Apart from increasing the safety factor, LCC may have the following positive impacts on an excavation (Wood, 2018):

- Reduce impact on surrounding soil.
- Reduce the construction loads in strut and wall.
- Stabilize excavation ground and working foundation, allowing for more efficient work, more heavy machines and facilitate transportation around the excavation.
- Reduces the ground displacements in the excavation bottom during construction, which reduces damage in the facility and enables the use of a permanent concrete bottom.
- Reduces vibrations during the construction and later potential rail/traffic vibrations if a tunnel is constructed.
- Reduces settlements in the permanent state which reduces maintenance costs.

In Norway, LCC has been successfully implemented to stabilize the passive zone in up to 18 meters deep excavations (Karlsrud, Eggen, & Nerland, 2015). However, in Sweden LCC has only been implemented in the case site of E02 Centralen in Västlänken, see chapter 3, apart from a testing site in Enköping (Ignat, 2018). Previous research has concluded that current design guidelines in Sweden (Trafikverket, 2014) are too conservative for effective design of LCC in deep excavations (Ignat, 2018), and significantly underestimates the shear strength of the LC area when overlapping columns are introduced. If the method is to be used more in Sweden as well as in the rest of the world, further understanding is required of the strength and stiffness in the passive zone. Furthermore, research on time dependent serviceability limit state (SLS) behaviour of LCC in the passive zone of a deep excavation is needed in Sweden, as it is often the design requirement for urban excavations.

Figure 2.2 Lime cement grid in Västlänken E02 Centralen. (Jonatan Isaksson, private photo)

2.3 Numerical Modelling in Two Dimensions

Numerical modelling is a method that is often used in geotechnical problems to analyse complex geometries and material behaviours. Numerical modelling often uses finite elements which divides the area of interest into a finite number of nodes and uses mathematical correlations to determine the physical relationship between the nodes (Ismail-Zadeh & Tackley, 2010). This creates a mesh that can describe deformations, stresses, pore pressures, among other characteristics depending on the input parameters and mathematical correlations. Numerical modelling demands a high number of calculations and can only be used efficiently by a computer.

The numerical model is an alternative to the analytical model which is often hand calculated and using equations where the results can be described as analytical functions (Starting Point Teaching Entry Level Geoscience, 2020). The numerical model is gradually replacing the analytical model because of its ability to take into consideration significantly more characteristics of the soil and surrounding elements. This creates a more thorough and realistic model at the expense of simplicity. Deep excavations involve several complex behaviours in the soil that affect the serviceability state. Time dependent analysis of settlements are especially complex. With the help of modern computation, numerical analysis allows for these parameters to be considered (Potts, 2003).

Numerical modelling can be performed in one, two or three dimensions, where the complexity and time investment significantly increases with more dimensions. A numerical model can be simplified to 2D if one of the directions can be assumed constant. Excavations are affected by 3D effects if the cross section of the excavation changes, however if there is a long enough stretch of

a constant cross section, 3D effects can be neglected and a 2D analysis is sufficient. A grid of LCC can be simplified to 2D using a homogenous body and material to represent the 3D grid. The effects of the simplification have been studied in the ultimate limit state by (Ignat, 2018), and can usually be justified.

2.4 Constitutive Models in Numerical Geotechnics

A constitutive model is a generalised way of expressing the stress strain relationship of a soil (Potts, 2003). Constitutive models strive to simulate any real stress path the soil takes. Numerous different constitutive models are used in geotechnical problems, all with their strengths and limitations. Following is a description of some fundamental properties of nonlinear elastoplastic models: The elastic law, yield surfaces, hardening laws, the flow rule, implementation of earth pressures and preconsolidation pressure. It is followed by a further description of the two constitutive models used in this study, Hardening soil and Creep-SCLAY1S.

Elastic law is what defines the stress-strain relationship under the elastic condition of soils. Both models in this study uses a non-linear stress dependent elastic law. The non-linearity is based on typical soil response and can be altered through changing stiffness properties.

The yield surface is the boundary between small elastic strains and large plastic strains (Phillips & Sierakowski, 1965). The surface is dependent on the principal stresses that describes the amount of volumetric and deviatoric stresses that acts on the soil. The formulations of the yield surface in Hardening Soil and Creep-SCLAY1S are different and explained more in detail in chapter 2.4.1 and 2.4.2. Some models have a failure surface integrated into the yield surface, while others have a separate failure surface. One example of a failure surface is the Mohr Coulomb theory of critical state. It assumes there is a critical state of the soil where shearing can occur with no stress or volume increase if enough stress is present (Knappet & Craig, 2012). The critical state line is defined in a relationship between normal and shear stresses.

The hardening law describe the evolution of the yield surfaces as a function of plastic increments. Most models contain a volumetric hardening law describing the change in size of the yield curve because of plastic deformations (Wheeler, Näätänen, Karstunen, & Lojander, 2003). A shear hardening law is present in both models with the plastic shear strain as the relevant parameter (Schanz, 1999). The representation of the law differs between the two models, see chapter 2.4.1 and 2.4.2. In Hardening soil, the cone yield surface relates hardening to plastic deviatoric strain, while the Creep-SCLAY1S model has an additional hardening law to describe rotational hardening.

The flow rule determines which stress path the soil will take in the plastic zone. Associated flow rule assumes that plastic strains follow the inclination of the elastic strains in the stress space, see Figure 2.3. In models with separate Mohr-Coulomb failure condition such as Hardening Soil, non-associated Flow is assumed. Then, the direction of plastic strains is determined through additional surfaces which is more mathematically complex. Assuming an associated flow rule for soft soil has however been proven sufficient (Wheeler, Näätänen, Karstunen, & Lojander, 2003).

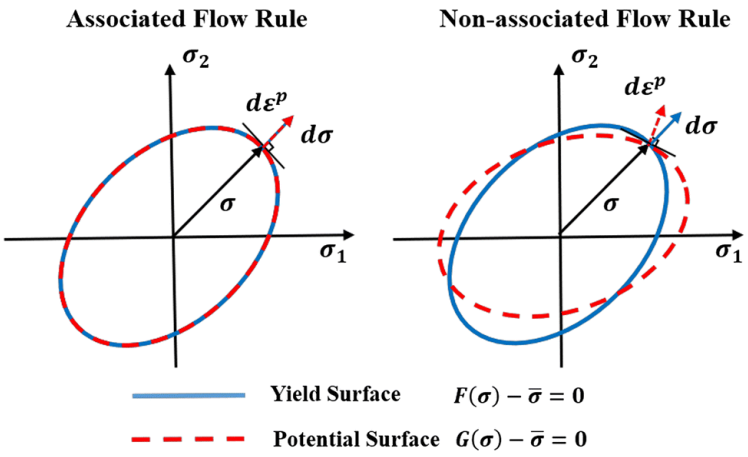

Figure 2.3 Associated Flow Rule. (Wu, o.a., 2020)

Although each constitutive model has its own set of parameters, there are some parameters that can be seen in most advanced models. The lateral earth pressure coefficient, *K0*, describes the lateral earth pressure from the soil (Graham, Nooman, & Lew, 1983). The normally consolidated value, $K0_{NC}$, is often calculated by Jaky's formula, see Equation (2.1). It can be implemented if the soil is not heavily overconsolidated. The formula bases the value solely on friction angle, with the logic of two extreme cases. If friction angle is equal to 0, no frictional forces hold the earth and lateral loading is equal to vertical loading ($K0_{NC}$=1). If the friction angle is equal to 90, the earth holds itself up entirely and no lateral earth pressure is present ($K0_{NC}$=0).

$$K0_{NC} = 1 - Sin(\phi) \tag{2.1}$$

The overconsolidated ratio (OCR) is the ratio between the preconsolidation pressure and the in-situ vertical stress, see equation (2.2), while pre-overburden pressure (POP) is the difference between the two values see equation (2.3). Most models contain an OCR or POP as required model input, including the models in this study.

$$OCR = \frac{\sigma'_p}{\sigma'_v} \tag{2.2}$$

$$POP = \sigma'_p - \sigma'_v \tag{2.3}$$

2.4.1 Hardening Soil model

Hardening soil is a complex soil model well suited for a variety of soils, especially those with complex stiffness behaviour. Its input parameters are displayed in Table 2.1. It contains several surfaces in the triaxial stress space, see Figure 2.4: a volumetric cap, a shear hardening cone, and a Mohr-Coulomb failure condition (Karstunen & Amavasai, 2017). The Mohr-Coulomb theory of critical state assumes that there is a critical state of the soil where shearing can occur with no stress or volume increase if enough stress is present. The critical state is defined in the σ-τ space by the critical state line and its inclination, friction angle ϕ.

Table 2.1 Input parameters for Hardening Soil model. (Schanz, 1999)

Index	Parameter Description
ϕ	Friction angle
c	Cohesion
Ψ_p	Dilatancy angle
OCR/POP	Overconsolidation ratio or Pre-overburden pressure
E_{50}^{ref}	Secant stiffness in standard drained triaxial test
E_{oed}^{ref}	Tangent stiffness for primary oedometer loading
m	Power for stress level dependency of stiffness
E_{ur}^{ref}	Unloading/reloading stiffness
ν_{ur}	Poisons' ratio for unloading-reloading
P_{ref}	Reference pressure for stiffnesses
K_0^{NC}	K_0-value for normal consolidation
R_f	Failure ratio

The model contains two hardening laws. Initial volumetric hardening is defined by an OCR or POP value, together with the initial stress condition. A separate shear hardening yield surface is defined by K_0^{NC}, the lateral earth pressure coefficient at normally consolidated state, see equations (2.4), (2.5) and (2.6). (Schanz, 1999)

$$f_{12} = \frac{q_a}{E_{50}} \frac{(\sigma_1 - \sigma_2)}{q_a - (\sigma_1 - \sigma_2)} - \frac{2(\sigma_1 - \sigma_2)}{E_{ur}} - \gamma^p \tag{2.4}$$

$$f_{13} = \frac{q_a}{E_{50}} \frac{(\sigma_1 - \sigma_3)}{q_a - (\sigma_1 - \sigma_3)} - \frac{2(\sigma_1 - \sigma_3)}{E_{ur}} - \gamma^p \tag{2.5}$$

With the definition

$$\gamma^p \coloneqq \varepsilon_1^p - \varepsilon_2^p - \varepsilon_3^p = 2\varepsilon_1^p - \varepsilon_v^p \approx 2\varepsilon_1^p \tag{2.6}$$

The stress-strain relationship is hyperbolic and based on drained stiffness parameters. The stiffness moduli are not model constants but reference stiffnesses, see Figure 2.5. The stiffnesses and the reference pressure P_{ref} must be specified as inputs. In a triaxial test, P_{ref} is the confining pressure σ_3, while in an oedometer test it is a pressure slightly higher than the preconsolidation pressure. The shear cone and volumetric cap allow a rotational hardening which can alter the stress path.

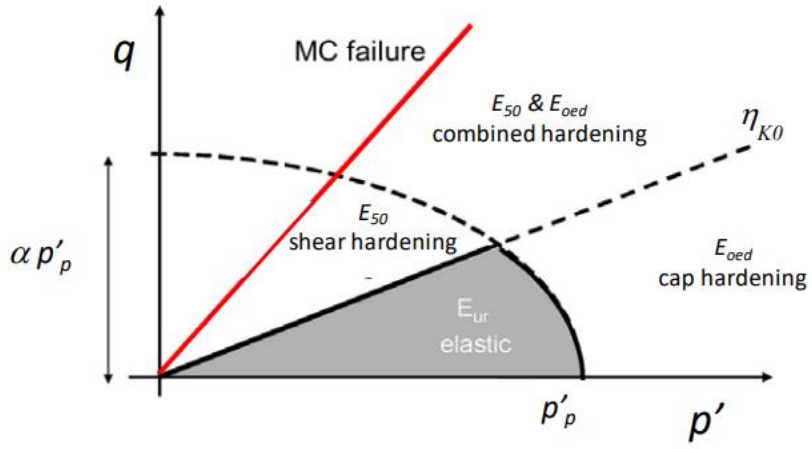

Figure 2.4 Yield surfaces of Hardening Soil model. (Karstunen & Amavasai, 2017)

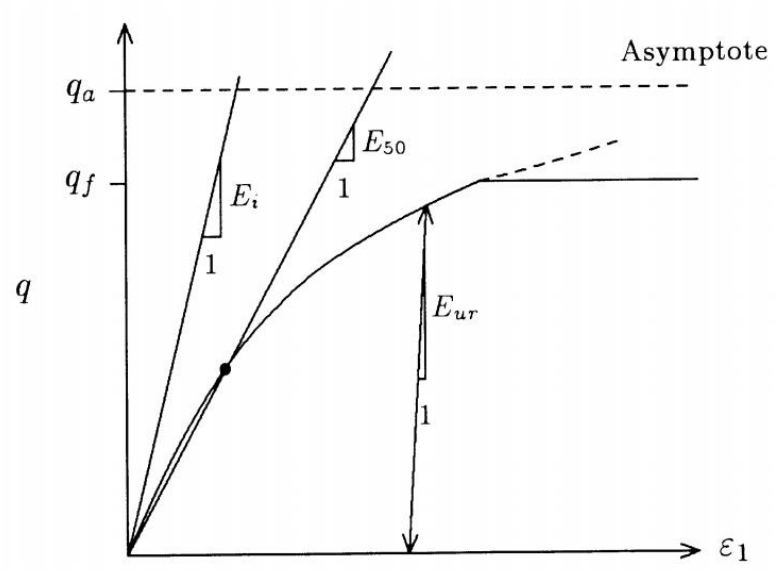

Figure 2.5 Illustration of the moduli used in Hardening Soil, also showing the hyperbolic stress-strain relation. (Schanz, 1999)

An associated flow rule is used on the cap surface, but non-associated flow is used on the shear hardening and Mohr-Coulomb envelope. The potential surface is determined through the dilatancy angle ψ', but for soft clays it is set to 0, thus in practice assuming associated flow on all envelopes (Karstunen & Amavasai, 2017). The stiffness is calculated based on Ohde-Janbu type of non-linear relationship from the drained stiffness E_i^{ref}, see equation (2.7).

$$E'_i = E_i^{ref} \left(\frac{\sigma'_i + a}{p_{ref} + a} \right)^m \tag{2.7}$$

where a=c' cot (ϕ'). For soft clays, m is usually equal to 1 and c' is equal to 0, which results in a semi logarithmic stress-strain relationship. The stiffnesses E_{50} and E_{ur} for the case with c'=0 kPa and m=1 is equal to equation (2.8) and (2.9), respectively.

$$E'_{50} = E_{50}^{ref}\left(\frac{\sigma'_3}{p_{ref}}\right) \tag{2.8}$$

$$E'_{ur} = E_{ur}^{ref}\left(\frac{\sigma'_3}{p_{ref}}\right) \tag{2.9}$$

where E_{50}^{ref} and E_{ur}^{ref} are the reference values of E'_{50} and E'_{ur}. More theory regarding the Hardening Soil model can be found in (Schanz, 1999).

2.4.2 Creep-SCLAY1S

The Creep-SCLAY1S model is an advanced model designed to accurately simulate normally- or slightly overconsolidated soft clays. The model is a combination of the Creep-SCLAY1 and SCLAY1S models, both originating from the SCLAY1 model. Creep-SCLAY1S can therefore simulate both anisotropy, creep, bonding, and destructuration.

The model demands a total of 14 input parameters shown in Table 2.2, most of which can be retrieved from laboratory tests, while a few need to be derived through a sensitivity analysis. The theory behind the model has been proved to accurately reflect the behaviour soft soils in numerous papers. (Karstunen, Krenn, Wheeler, Koskinen, & Zentar, 2005) (Yu Yin & Karstunen, 2011) (Sivasithamparam, Karstunen, Brinkgreve, & Bonnier, 2013)

Table 2.2 Input parameters for Creep-SCLAY1S.

Notation	Input Parameter
κ^*	Modified swelling index
λ_i^*	Modified intrinsic compression index
μ_i^*	Modified intrinsic creep index
OCR/POP	Overconsolidation ratio or Pre-overburden pressure
ν_i^*	Poisson's ratio
M_C	Inclination of critical state line in compression
M_E	Inclination of critical state line in extension
τ	Reference time
ω	Absolute rate of surface rotation
ω_d	Relative rate of surface rotation
α_0	Initial anisotropy of yield surfaces
χ_0	Initial amount of bonding
a	Absolute rate of destructuration
b	Relative rate of destructuration

The Creep-SCLAY1S model uses the correlations between mean effective stress, p', and deviatoric stress, q, to define the behaviour of the soil in a triaxial load state. The volumetric strain rates, $\dot{\varepsilon}_v$, and the deviatoric strain rates, $\dot{\varepsilon}_q$, are defined as the sum of elastic and creep strain rates as described in equation (2.10) and (2.11). Plastic strains are always assumed to be present.

$$\dot{\varepsilon}_v = \dot{\varepsilon}_v^e + \dot{\varepsilon}_v^c \tag{2.10}$$

$$\dot{\varepsilon}_q = \dot{\varepsilon}_q^e + \dot{\varepsilon}_q^c \tag{2.11}$$

The theory assumes that plastic strains are dominant. Therefore, for simplicity, elastic strains are assumed to be isotropic. This leads to the definition of elastic strains as defined by equation (2.12) and (2.13). The notation K represents the elastic bulk modulus and G the elastic shear modulus, see equation (2.14) and (2.15).

$$\dot{\varepsilon}_v^e = \frac{p'}{K} \tag{2.12}$$

$$\dot{\varepsilon}_d^e = \frac{q}{G} \tag{2.13}$$

$$K = \frac{p'}{\kappa^*} \tag{2.14}$$

$$G = \frac{3K(1-2v')}{2(1+v')} \tag{2.15}$$

The shear modulus is defined using poisons ratio, *v'*, while the elastic bulk modulus uses the modified swelling index κ^*. The stiffness theory in the Creep-SCLAY1S model describes soft clays by using the correlation between void ratio and stress (Sivasithamparam, Karstunen, & Bonnier, 2015). The assumption is that soft soils follow a compression- or a swelling line, see Figure 2.6, when a drained, isotropic load is implemented, depending on whether the soil is normally- or overconsolidated. The modified compression- and swelling indices, $\lambda^*$and κ^*, can be derived in a $\dot{\varepsilon}_v - \ln(p')$ space. The relationship between the stress state and the preconsolidation pressure, p'_m, defines if the soil is normally or overconsolidated. When deriving the values from a semi logarithmic plot rather than a linear plot, non-linear elasticity stress paths related to a constant *q/p'* ratio is achieved, which is realistic in a soft soil.

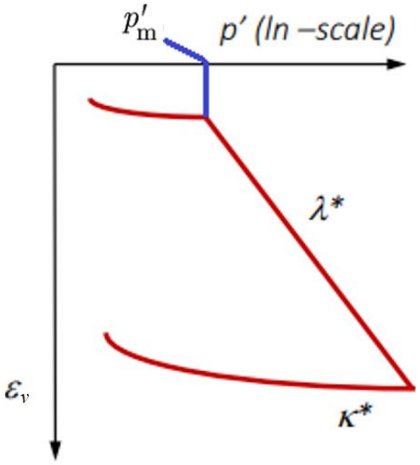

Figure 2.6 *The behaviour of clay in relation to the preconsolidation pressure according to the Creep-SCLAY1S model.*

A normally consolidated surface (NCS) is used to describe the yield surface in a *p'⁄q* plane at normally consolidated state. The preconsolidation pressure, p'_m, defines the size of the surface. The Creep-SCLAY1S model uses a theory of anisotropy as defined in the SCLAY1 model (Wheeler, Näätänen, Karstunen, & Lojander, 2003). The yield surface is described by equation (2.16), in the form of a sheared ellipse. The parameter α describes the amount of shearing of the ellipse by determining the position of the right-most vertical tangent, see Figure 2.7. If α is equal to 0, no shearing is present.

$$p'_m = p' + \frac{(q-\alpha p')^2}{(M^2-\alpha^2)p'} \tag{2.16}$$

The critical state stress envelope, M, is taking into consideration the different behaviour of the soil in extension, M_e and compression, M_c. The theory behind the parameter can be found in (Sivasithamparam, Karstunen, & Bonnier, 2015). To determine the initial shearing of the yield curve, α_{K0}, an associated flow rule is assumed (Wheeler, Näätänen, Karstunen, & Lojander, 2003). When using an inclined yield surface on natural soils, the simplification of assuming an associated flow rule is determined to be justified and neglectable. The assumption is supported by studies from e.g., (Korhonen & Lojander, 1987) and (Graham, Nooman, & Lew, 1983). The theory of anisotropy has been proved to accurately represent soft clays in numerous studies (Karstunen, Krenn, Wheeler, Koskinen, & Zentar, 2005) (Wheeler, Näätänen, Karstunen, & Lojander, 2003). (Koskinen, Karstunen, & Wheeler, 2002) (Karstunen & Koskinen, 2004).

Creep-SCLAY1S accounts for forces of natural bonding between clay particles and the effect of destructuration of these bonds during prolonged strain, using the same theory as in the SCLAY1S model. The bonding is introduced in the form of an intrinsic compression surface (ICS) with a smaller size, p'_{mi}, depending on the amount of bonding, see equation (2.17) (Koskinen, Karstunen, & Wheeler, 2002). The size of the yield curve then approaches the regular state without bonding, the NCS, as the bonds are destroyed. A current state surface (CSS) describes the current state of the yield surface with its size p'_{eq} derived from in situ effective stresses. The ICS and CSS yield curves are described by equation (2.16) but exchanging p'_m to p'_{mi} or p'_{eq} , hence, they have the same form as the normal consolidated surface (NCS). Here, χ describes the bonding of the soil and the initial bonding, χ_0, is related to sensitivity of the soil (Gras J.-P. , Sivasithamparam, Karstunen, & Dijkstra, 2018).

$$p'_m = p'_{mi}(1 + \chi) \tag{2.17}$$

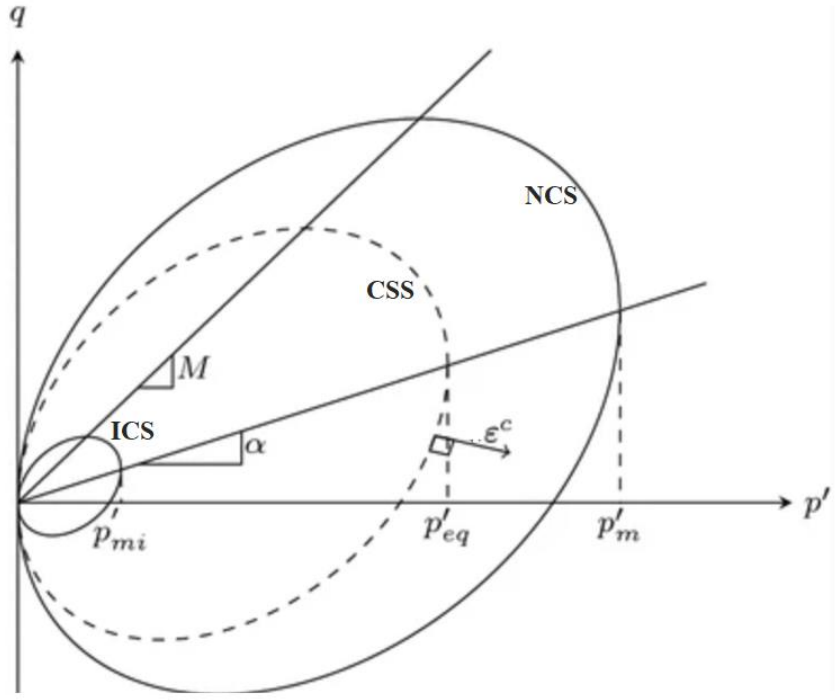

Figure 2.7 Current State Surface (CSS) and Normal Consolidation Surface (NCS) of the Creep-SCLAY1 model and the direction of viscoplastic strains (triaxial stress space). (Sivasithamparam, Karstunen, & Bonnier, 2015).

In addition, a modified intrinsic value for the compression index, λ_i^*, is used to account for bonding and the ICS over the modified compression index λ^*. This parameter must be determined from tests where all bonds have been destructurated which can be represented after large strains. This method of modelling bonding and destructuration is proved to accurately display these behaviours of the soil and increase the accuracy of the constitutive model. (Karstunen, Krenn, Wheeler, Koskinen, & Zentar, 2005) (Yu Yin & Karstunen, 2011).

To consider creep behaviour of the clay because of prolonged stress in the Creep-SCLAY1S model, the theory from the Creep-SCLAY1 model is implemented. (Sivasithamparam, Karstunen, & Bonnier, 2015). The creep strain rates are described by equation (2.18) and (2.19), using the theory of constant rate of a viscoplastic multiplier, $\dot{\Lambda}$. (Grimstad, Degado, Nordal, & Karstunen, 2010)

$$\dot{\varepsilon}_v^c = \dot{\Lambda} \frac{dp'_{eq}}{dp'} \tag{2.18}$$

$$\dot{\varepsilon}_q^c = \dot{\Lambda} \frac{dp'_{eq}}{dq'} \tag{2.19}$$

The modified intrinsic creep index, μ_i^*, is added as an input parameter together with the reference time, τ, where 1 is equal to 24 hours. These parameters are used to determine the viscoplastic multiplier in equation (2.20). This creep theory has been proven to accurately display creep behaviour in soft clays with high sensitivity (Sivasithamparam, Karstunen, Brinkgreve, & Bonnier, 2013).

$$\dot{\Lambda} = \frac{\mu_i^*}{\tau} \cdot \left(\frac{p'_{eq}}{p'_m}\right)^{\frac{\lambda_i^* - \kappa^*}{\mu^*}} \cdot \left(\frac{M_c^2 - \alpha_{K0}^2}{M_c^2 - \eta_{K0}^2}\right) \tag{2.20}$$

The Creep-SCLAY1S model uses three hardening laws. The first hardening law is used to describe the isotropic hardening of the ICS. The hardening law for Creep-SCLAY1S is described in equation (2.21) where p'_{mi} is the size of the ICS and the hardening is dependent on the creep rate of volumetric strains, $\dot{\varepsilon}_v^c$.

$$\dot{p}'_{mi} = \frac{v p'_{mi}}{\lambda_i^* - \kappa^*} \dot{\varepsilon}_v^c \tag{2.21}$$

The second hardening law accounts for rotation of the yield surfaces, see equation (2.22) (Wheeler, Näätänen, Karstunen, & Lojander, 2003). The hardening law describes the change in the anisotropy of the yield curve $\dot{\alpha}$ as the rate of volumetric creep strain $\dot{\varepsilon}_v^c$ and deviatoric creep strain $\dot{\varepsilon}_q^c$ increases. The "<.>" brackets around $\dot{\varepsilon}_v^p$ indicate that if the value is below 0, it is instead equal to 0. Here η describes the stress ratio q/p' and two new parameters are introduced. The first one, ω, describes the absolute effectiveness of the rotational hardening. The second, ω_d, describes the relative effectiveness of hardening considering the relative impact of volumetric- and deviatoric strain. If $\omega_d = 0$, volumetric creep strains determine the effectiveness. If $\omega_d = 1$, deviatoric creep strains are instead dimensioning. In all other cases were $0 < \omega_d < 1$, both strains have an impact.

$$\dot{\alpha} = \omega\left[\left(\frac{3\eta}{4} - \alpha\right) < \dot{\varepsilon}_v^p > + \omega_d\left(\frac{\eta}{3} - \alpha\right)|\dot{\varepsilon}_q^p|\right] \tag{2.22}$$

The third hardening law takes into consideration the destructuration of bonds in the soft soil with increased creep strain rates, see equation (2.23), and introduces a debonding rate, $\dot{\chi}$. With this

equation, two new input parameters are introduced. The first one, *a*, describes the rate of destructuration. The second, *b*, describes the relative efficiency that volumetric- and deviatoric creep strain rates has on destroying the bonds. These parameters must be determined by a sensitivity and optimization method.

$$\dot{\chi} = -a\chi(|\dot{\varepsilon}_v^c| + \mathrm{b}|\dot{\varepsilon}_d^c|) \tag{2.23}$$

Even if the Creep-SCLAY1S model demands a lot of different input parameters to use to its full potential, it can also be altered and simplified if data is missing or unnecessary. The effects of bonding and destructuration can be neglected by setting $\chi_0 = 0$ and using the regular modified compression- and creep indexes, λ^* and μ^* . The model then becomes identical to the Creep-SCLAY1 model. Furthermore, if creep behaviour in the model can be neglected or if necessary data is missing, values for μ_i^*, *a* and *b* can be set to zero and the Creep-SCLAY1S model becomes equal to the SCLAY1S model.

3 E02 Centralen, Västlänken

Västlänken is an urban train tunnel in the city of Gothenburg, Sweden. The train tunnel is a double tracked high speed railway to transport people under the city of Gothenburg. It is 8 kilometres long of which 2 kilometres are built in Gothenburg soft clay (Trafikverket, 2020). It is a part of a big investment project, the west Swedish agreement, where one of the goals is to strengthen the railway infrastructure around Gothenburg as the city expands (Västsvenska paketet, u.d.). Västlänken is divided into four subprojects for easier management. Subproject "E02 Centralen" contains the biggest area wise excavation of the four subprojects (Trafikverket, 2020). The subproject is in writing moment under construction, the urban environment set demanding conditions during the construction because of the effect that deep excavations have on its surroundings. The project must follow guidelines not only for its own stability and safety, but for all surrounding activity and infrastructure. This includes acceptable deformations, vibrations, and noise in the surrounding area. Therefore, a serviceability limit state (SLS) approach is necessary in the design of the project. LCC have been used in the passive side on some sections of the excavation to meet the demands and guidelines.

3.1 Geotechnical conditions

The ground on the site consists of a highly homogenous, slightly overconsolidated soft clay down to large depths over 40 meters. The clay is typical around the riverbanks of Gothenburg. It was deposited during the last glacial period around 10 000 years ago when the water table was higher and there was a lower current in the Göta river, causing the fine clay to settle. The undrained shear strength increases slightly with depth. The groundwater table is 2 meters below the initial ground surface.

Diverse types of soil tests have been carried out in the area throughout the course of planning and production. In addition to tests on the clay, some tests have also been carried out on the LCC used. Field mixed tests on 80kg/m3 LC and lab mixed tests on 100kg/m3 LC have been made. The types of tests carried out can be seen in Table 3.1.

Table 3.1 Tests carried out in E02 Centralen, Västlänken.

Test	Clay	LCC
Consolidated Anisotropic Undrained Compression (CAUC)	Yes	Yes
Consolidated Anisotropic Undrained Extension (CAUE)	Yes	Yes
Consolidated Anisotropic Drained Compression (CADC)	Yes	No
Consolidated Anisotropic Drained Extension (CADE)	Yes	No
Constant Rate of Strain Cell (CRS)	Yes	No
Incremental Loading Oedometer Test (IL)	Yes	Yes
Uniaxial Test	Yes	Yes

One of the IL tests of the clay is shown in Figure 3.1, displaying stress/strain. This shows a typical stress path for soft soil behaviour. The clay is stiff until reaching a preconsolidation pressure, where high plastic deformations then occur with small stress increases. A triaxial CADC test of the clay is shown in Figure 3.2, displaying a p'/q curve, this also shows a typical soft soil path.

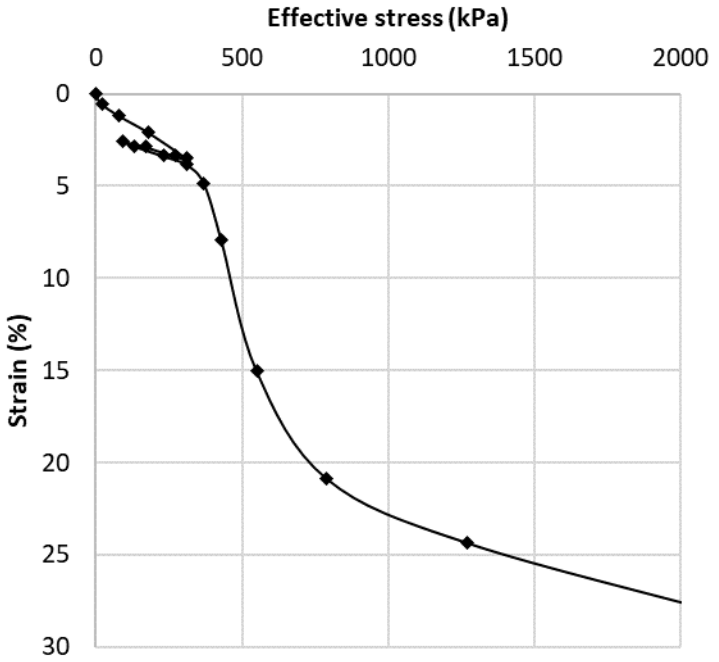

Figure 3.1 IL stress/strain curve from field testing of the E02 Centralen Västlänken site (Björkman, Isaksson, & Yannie, 2020).

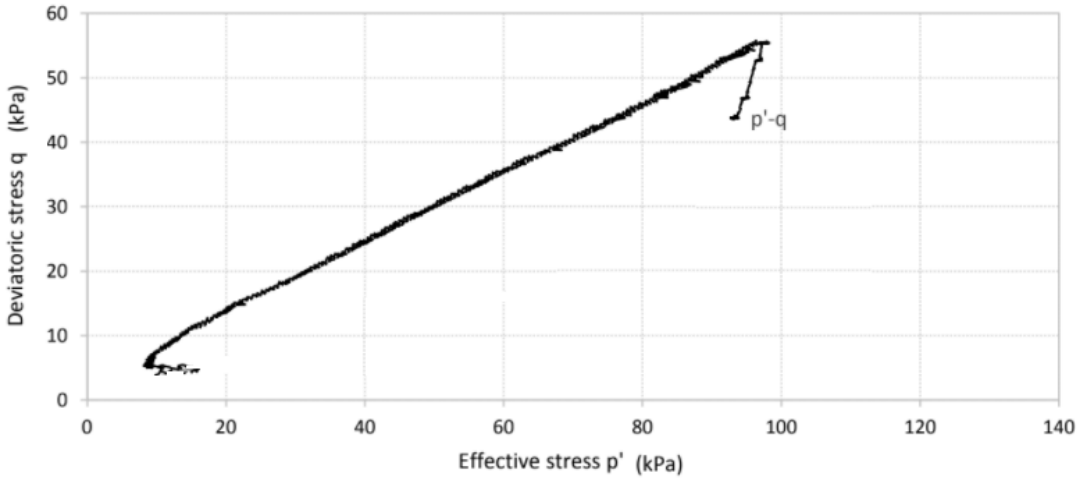

Figure 3.2 Triaxial p-q curve from field testing of the E02 Centralen Västlänken site (Björkman, Isaksson, & Yannie, 2020).

3.2 Cross section

This report will focus on the cross section where LCC are installed in the passive zone of a deep excavation retained by a sheet pile wall (SPW) with two support levels, it is a part of E02 Centralen and is shown in Figure 3.3. The excavation of this cross section has been finished and the tunnel has been installed, see Figure 3.4. It is a part of the main train tunnel, 10 meters from an emergency exit excavation to the east (area 2430) and 30 meters from the central station excavation to the west.

The cross section uses SPW AZ-38-700N combined with two rows of circular struts at -1 and -6 meters (Björkman, Isaksson, & Yannie, 2020). The struts are connected to the wall with HEB500 walers in the upper row and with HEB800 walers in the lower row. All structural elements are made from S355.

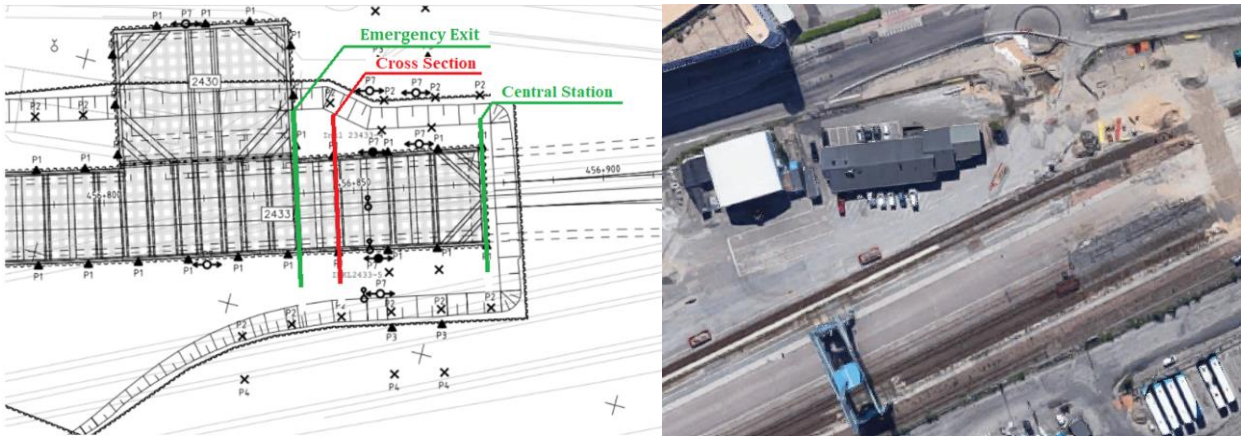

Figure 3.3 Site description (left) (Björkman, Isaksson, & Yannie, 2020) and satellite image of site before construction (right). North is down. (Google, 2021).

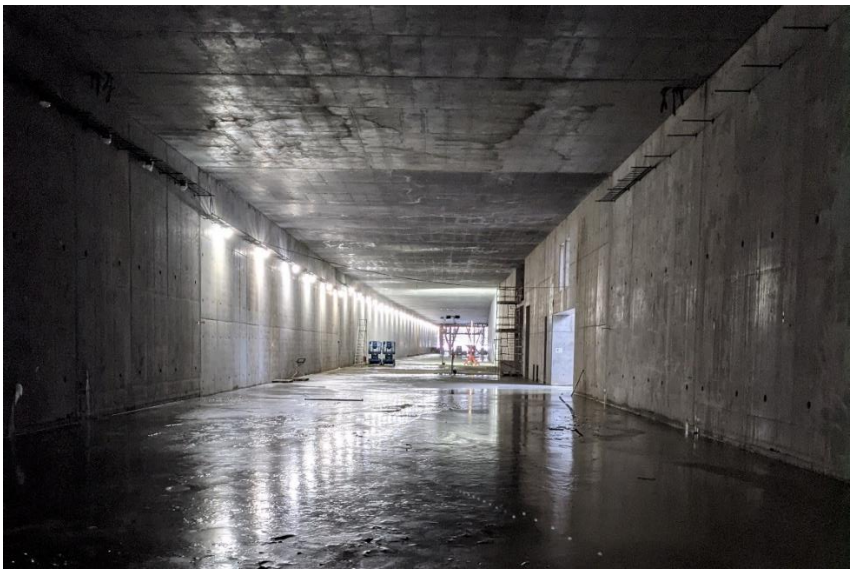

Figure 3.4 Inside the finished tunnel of the case study's cross section.

The cross section is shown in Figure 3.5. At the start of construction, a 2.5 meter deep and 50-meter-wide pit was excavated followed by the installation of a working platform (Wood, 2018). From the bottom of the pit, SPW for the deep excavation were installed followed by the installation of LCC between the walls down to -22 meters below the pit surface. The LCC were installed in a grid formation as can be seen in Figure 3.5, where double overlapping rows are used both parallel and perpendicular to the wall. Above the excavation bottom at -11,2m, 40 kg/m^3 LC was used, below it 80 kg/m^3 was used.

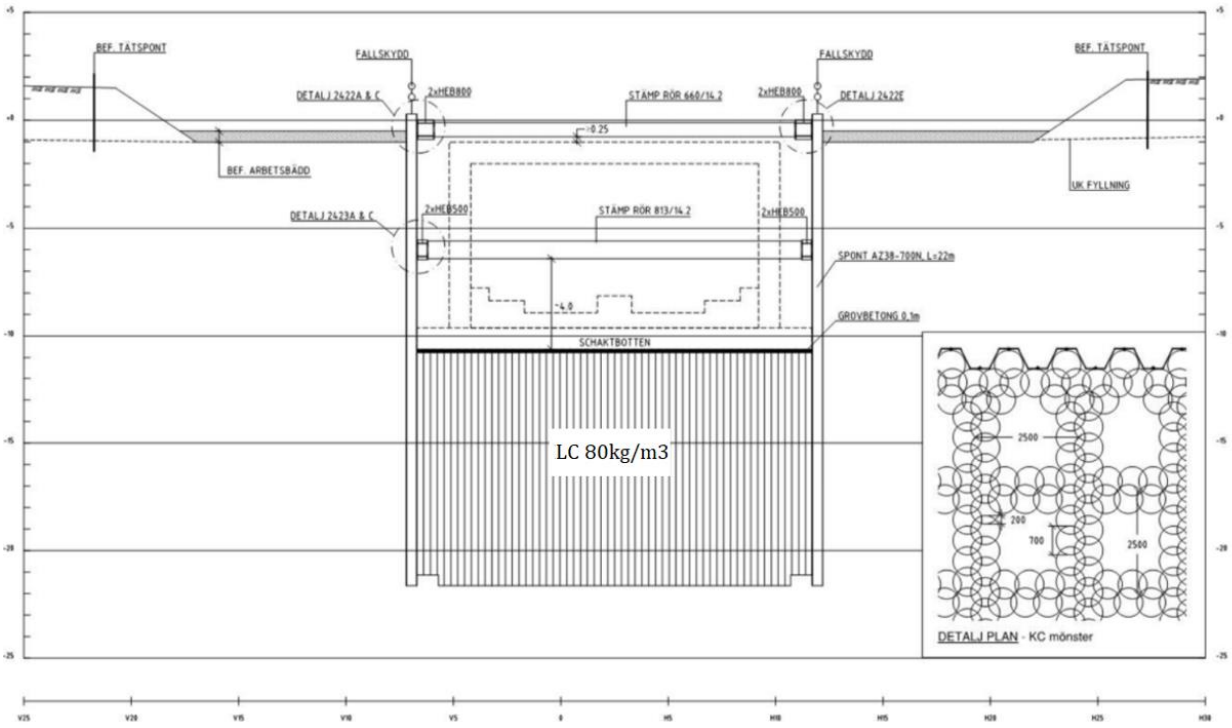

Figure 3.5 Cross section of the excavation, LCC grid formation in the down right corner (Wood, 2018).

After installation of LCC, the deep excavation was initiated with the following phases shown in Table 3.2. The timespan of the entire excavation was 5 months, and the cross section was finished 2020-01-15.

Table 3.2 Excavation procedure with time.

Stage	Time
Installation of LCC	2019-08-09
Excavation down to -2m, installation of upper strut	2019-09-25
Excavation down to -7,2m, installation of lower strut	2019-10-17
Excavation down to -11,2m	2019-11-24
Casting of bottom concrete	2019-11-24
Casting of Permanent bottom plate	2019-12-12
Dismantling of lower strut	2020-01-15

3.3 Field monitoring

During the excavation and following consolidation period, monitoring has been executed in the ground and in structural elements using inclinometers, prisms, and strain gauges. The displacements were measured from 2019-06-17 to 2020-02-17, one month after the excavation was finished.

To measure the displacements and forces in the structural elements, inclinometers and strain gauges were used. The placements of different inclinometers and strain gauges are shown in Figure 3.6. Horizontal displacements from inclinometer 5 is of interest because it is placed at the SPW and hence can display its horizontal displacements. Too large displacements can create serviceability issues such as problems in the working foundation, fractures resulting in water leakage, problems for construction on site and further installations. Wall displacements can also be measured in inclinometer 4, however this inclinometer is close to the emergency exit (area 2430) which creates disturbance in the monitoring. The horizontal displacements of inclinometer 5 is shown in Figure 3.7, both including and excluding displacements that have occurred during the installation of the LCC. The exclusion of installation effects is done by setting the displacements to zero on 2019-08-09, the end date of the LCC installation process. The strut forces from the strain gauges are shown in Figure 3.8.

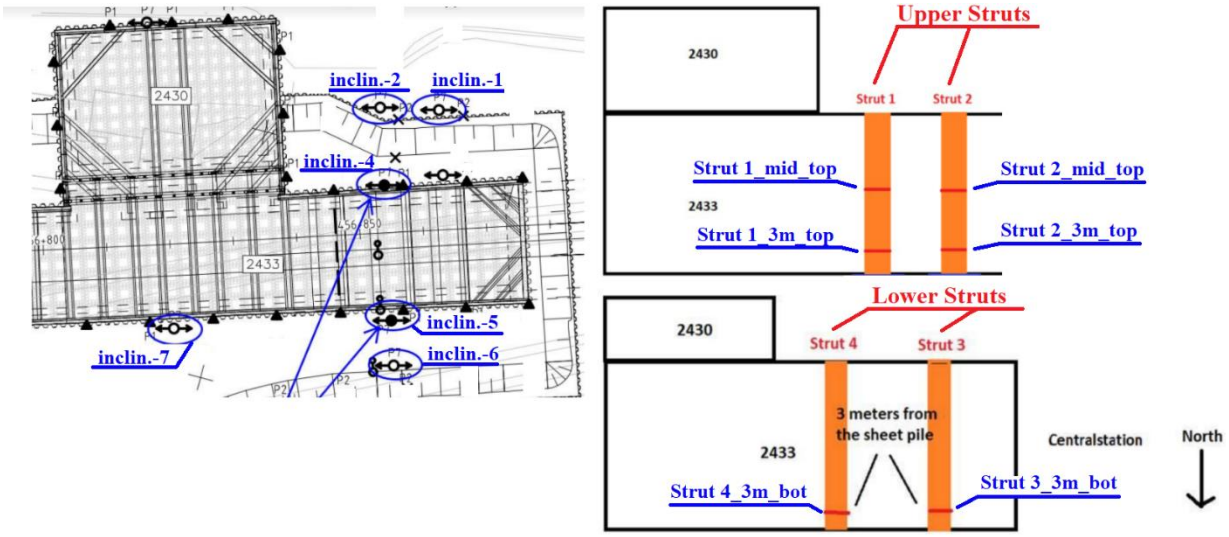

Figure 3.6 Inclinometer and strain gauge placements.

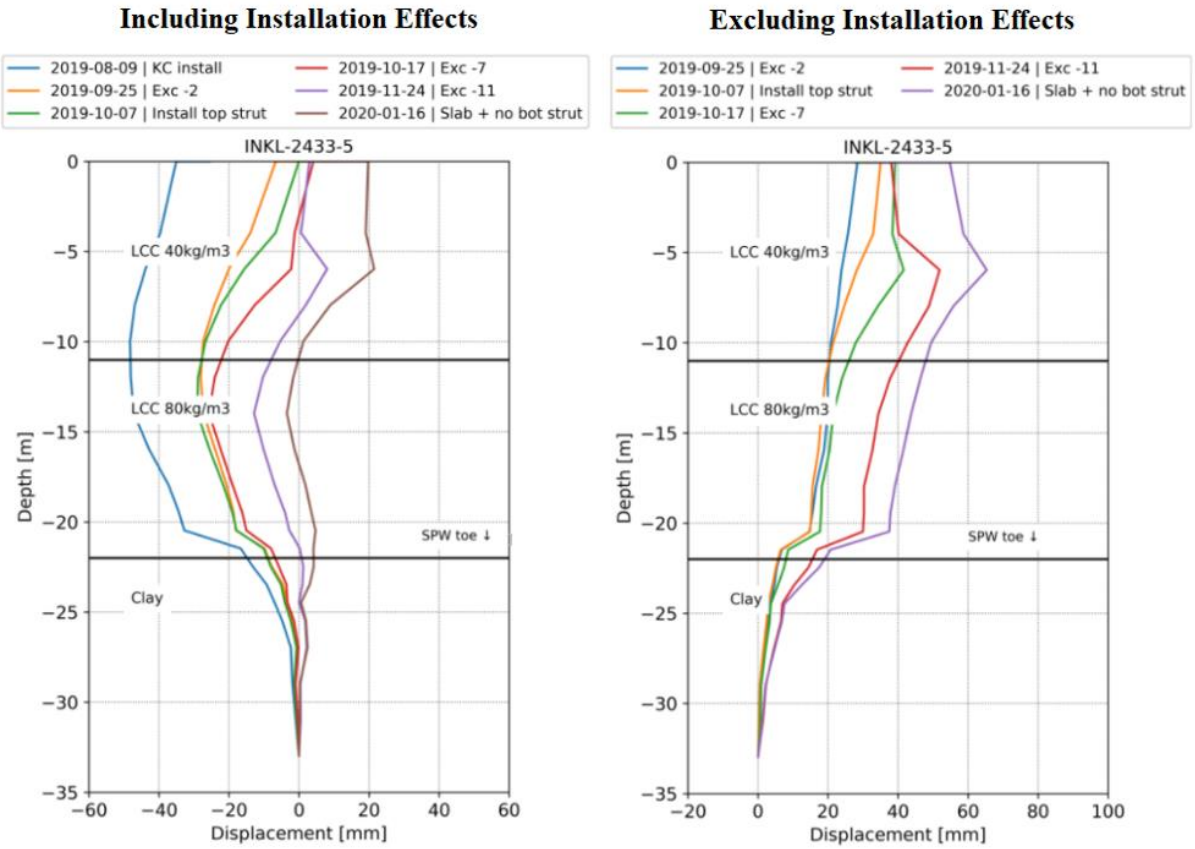

Figure 3.7 Horizontal Displacements of inclinometer 5.

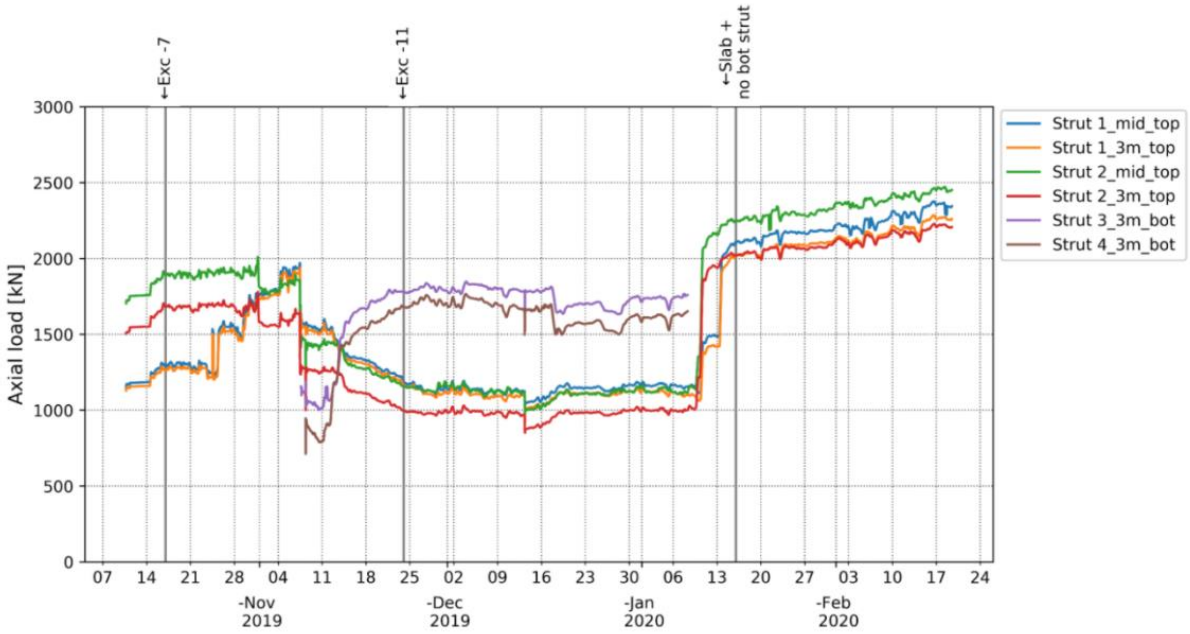

Figure 3.8 Strut forces from strain gauges.

The placements of the prisms are shown in Figure 3.9, and their vertical displacements represent the settlements on the surrounding soil. The vertical displacements of these prisms are shown in Figure 3.10. The SP3005 Prism is an outlier because of the sudden displacement at the first excavation phase, which is due to local displacements not connected to the system response.

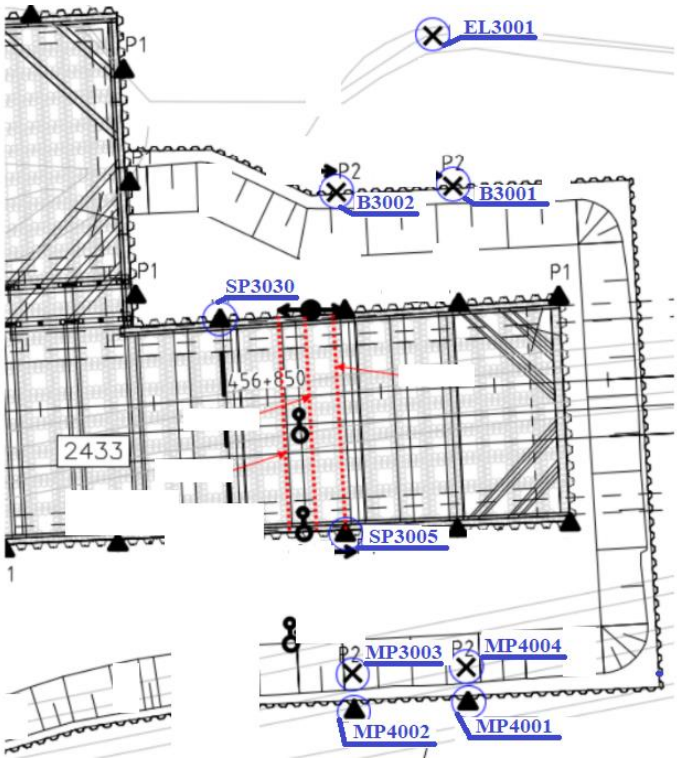

Figure 3.9 Prism placements in blue.

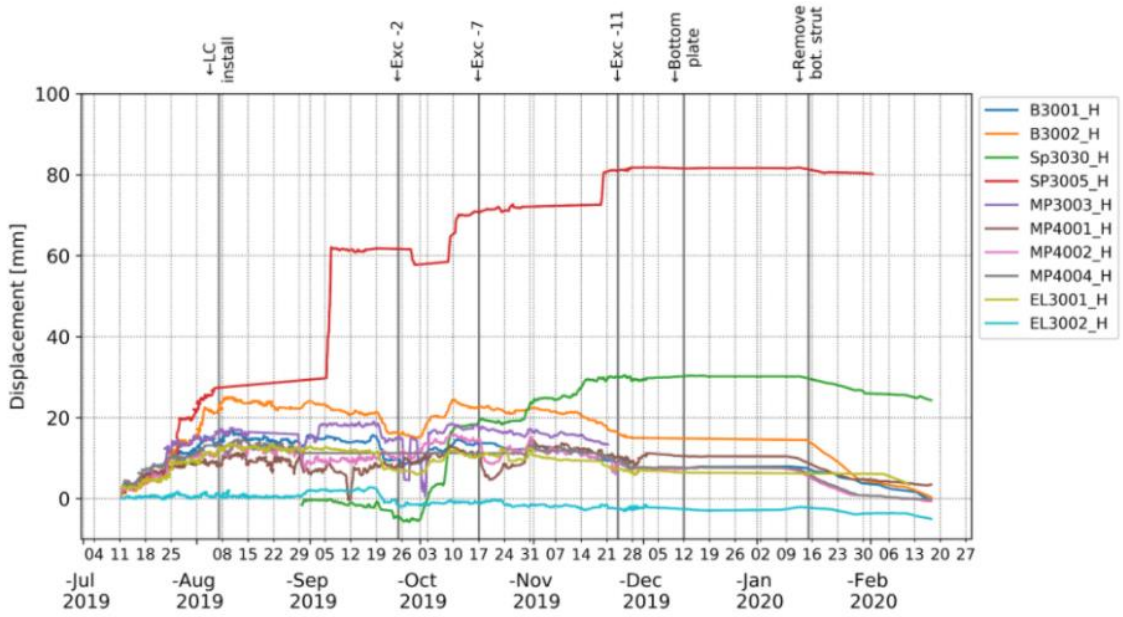

Figure 3.10 Vertical displacements of prisms.

4 Finite Element Analysis of E02 Centralen

A numerical 2D analysis in the software Plaxis 2D will be used to simulate the cross section. The LC on the passive side of the excavation will be simulated using the Hardening Soil model while the surrounding clay will be modelled with the Creep-SCLAY1S model. Hardening soil parameters for clay will also be calibrated to simulate simplified areas in the 2D space where both LCC and clay are present in the 3D space, this is further explained in Chapter 4.3.1.

The Creep-SCLAY1S model is chosen to get a broad understanding of the system response. It is an advanced model for modelling soft sensitive clay and can consider both creep, anisotropy, bonding, and destructuration. However, some of these properties may prove insignificant for this specific case study, so it will be studied what parameters have an effect. Hardening Soil is a tested constitutive model for LC and has been proven to successfully represent the material (Ignat , Baker, Karstunen, Liedberg, & Larsson, 2020). The concrete similar properties of LC can be simulated by a high OCR value, resulting in a constantly overconsolidated material (Alén, Sällfors, Bengtsson, & Baker, 2006).

Horizontal and homogenous soil layers are assumed for computational simplicity. This assumption should lead to minimal error sources since the ground conditions are horizontal and highly homogenous, see Chapter 3.1. The cross section has some disturbances in the monitoring due to 3D effects from e.g., the emergency exit area (see Figure 3.3), but since monitoring have been executed on many parts of the excavation, they can be managed.

Schematic cross section drawings of the site were used to model the geometry. To determine different soil layers, plots of OCR values and water content with depth are used. The water contents have been measured using undisturbed boreholes, OCR values are derived using oedometer tests which is described in Chapter 3.1. These graphs, see Figure 4.1, show trends that indicate two layers for the clay, 0-20 and 20-45 meters. The LCC have different amount of cement above and below the excavation bottom, which leads to two layers, 0-11,2 meters and 11,2-22 meters. However, the parameters above the excavation bottom are not as relevant because the soil there is excavated away, so this will only be considered in a numerical investigation.

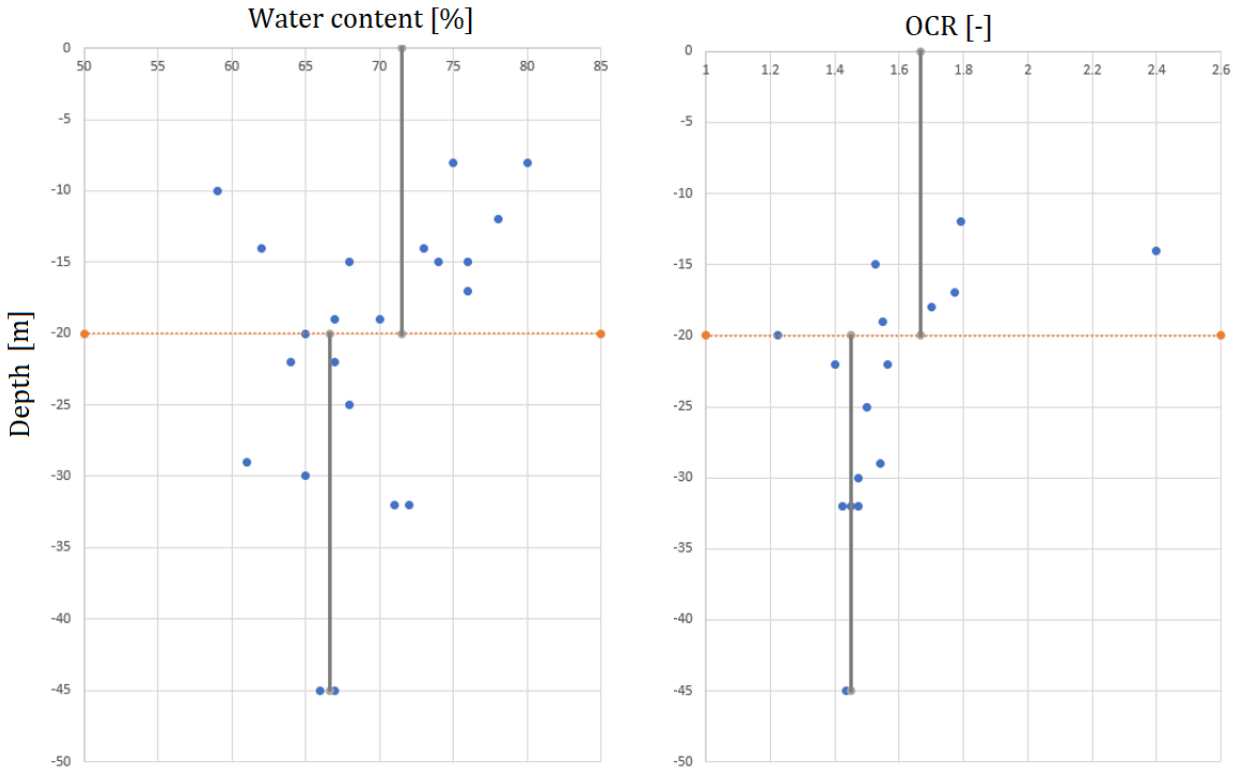

Figure 4.1 Water content and OCR with depth, indicating two layers.

4.1 Model geometry

The cross section will be simulated using a symmetry line in the middle of the excavation, this is done to reduce the simulation time. The calculation phases of the excavation are shown in Table 4.1 and are based on the construction stages in Table 3.2. All phases are consolidation phases except the initial which is *K0* procedure. The phases are illustrated in the model in Appendix B.

Table 4.1 Description of construction phases used in the model.

Phase	Simulation	Duration [days]
Initial Steady State	Initial state of the soil	-
1	Excavation of pit	30
2	Installation of sheet pile wall	1
3	Installation of LCC	1
4	Excavation down to -2m	49
5	Excavation down to -7,2m, installation of upper strut	23
6	Excavation down to -11,2m, installation of lower strut	38
7	Casting of Concrete Slab	18
8	Dismounting of lower strut	34
9	Consolidation	33

A base version of the cross section is shown in Figure 4.2. The excavation is set to a dry excavation, hence assuming that water will be removed from the excavation. An interface is implemented in the wall active in flow, leading to an impermeable wall. An example of flow conditions chosen for the model is shown in Figure 4.3. Numerical issues occurred when flow was activated in the entire interface, so it is only active in the positive side when clay exists on both sides. This should give the desired effect of the SPW being impermeable.

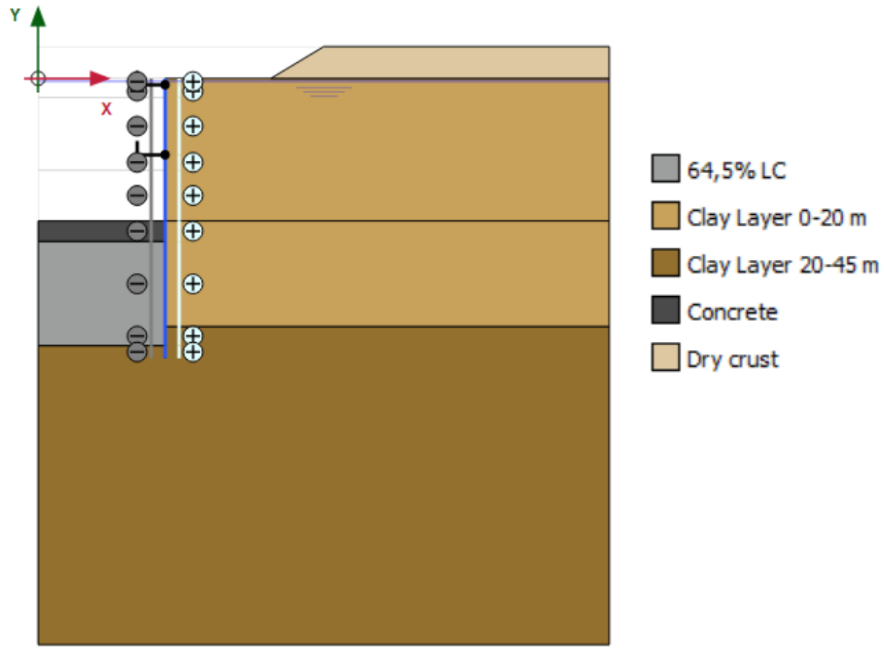

Figure 4.2 Base version of the Plaxis model, final consolidation stage.

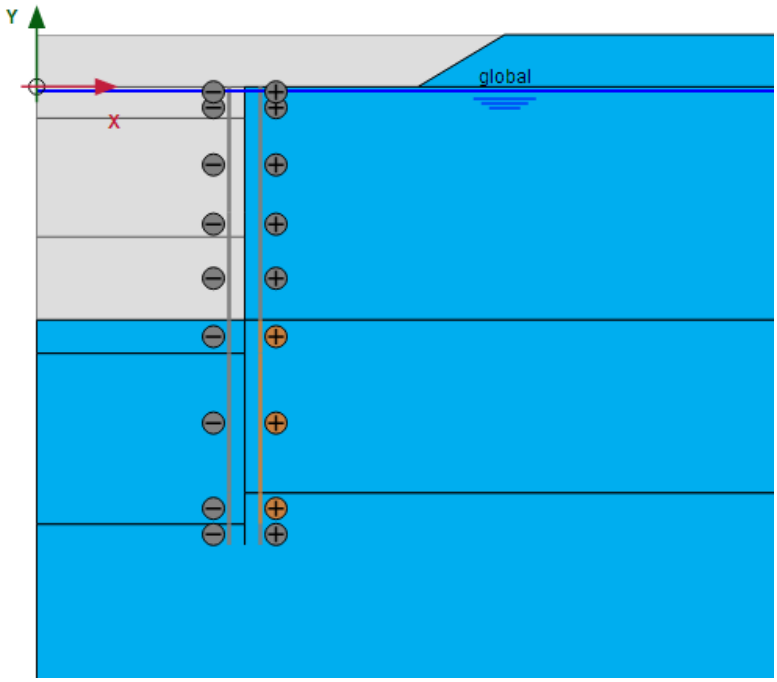

Figure 4.3 Flow conditions in Phase "Excavation to level -11,2".

4.1.1 Mesh and Boundaries

A mesh that is too fine or too coarse can have a negative effect of the model's response. It can cause local discrepancies that are not realistic, or globally influence the settlements of the soil. To ensure that an appropriate mesh is used, different mesh coarseness will be applied and compared. Furthermore, the response with different model geometries is compared in this study. Since the different model geometries result in different mesh discretization, their meshes will be compared as well. Relevant measurement points have been selected and will be showed. The models overall response in terms of deformations and pore pressures have also been studied to ensure there are no significant local discrepancies.

The results from the mesh sensitivity analysis are shown in Table 4.2 and Table 4.3. The points used for deformation monitoring are shown in Figure 4.4 and chosen based on deformation hotspots from an initial deformation result with a medium coarse mesh. The mesh has local refinement at the wall and on the passive side of the excavation, which is used in all tests, as well as local coarseness in the excavated pit. The results show that a medium mesh is sufficient. The final mesh used with the different geometries are shown in Appendix B.

The mesh fineness is most sensitive at point A at the surface beside the excavation because it is a weak point in terms of the geometry of the mesh. It is located at the ground surface, near the SPW and the upper strut. Point A was also the first point to become numerically unstable in some other analyses conducted in this study. It is also overly sensitive around point C because of the boundaries between the columns. These boundaries force the mesh to form around them and hence can create coarse areas in between. This can lead to unnatural stress paths if local refinement is not implemented.

Table 4.2. Mesh sensitivity analysis for mesh with columns. Maximum values of total displacements.

Mesh Fineness [nodes]	A: 0,5m from wall [m]	B: Lower strut level [m]	C: Excavation bottom [m]
Very Coarse [4461]	0,033	0,060	0,054
Coarse [5887]	0,016	0,059	0,053
Medium [7817]	0,016	0,058	0,053
Fine [12055]	0,016	0,058	0,053
Very Fine [18235]	Collapse of soil body	Collapse of soil body	Collapse of soil body

Table 4.3. Mesh sensitivity analysis for mesh without columns. Maximum values of total displacements.

Mesh Fineness [nodes]	A: 0,5m from wall [m]	B: Lower strut level [m]	C: Excavation bottom [m]
Very Coarse [3071]	0,015	0,06	0,054
Coarse [4961]	0,014	0,059	0,053
Medium [7353]	0,015	0,058	0,053
Fine [12215]	0,015	0,058	0,053
Very Fine [19109]	Collapse of soil body	Collapse of soil body	Collapse of soil body

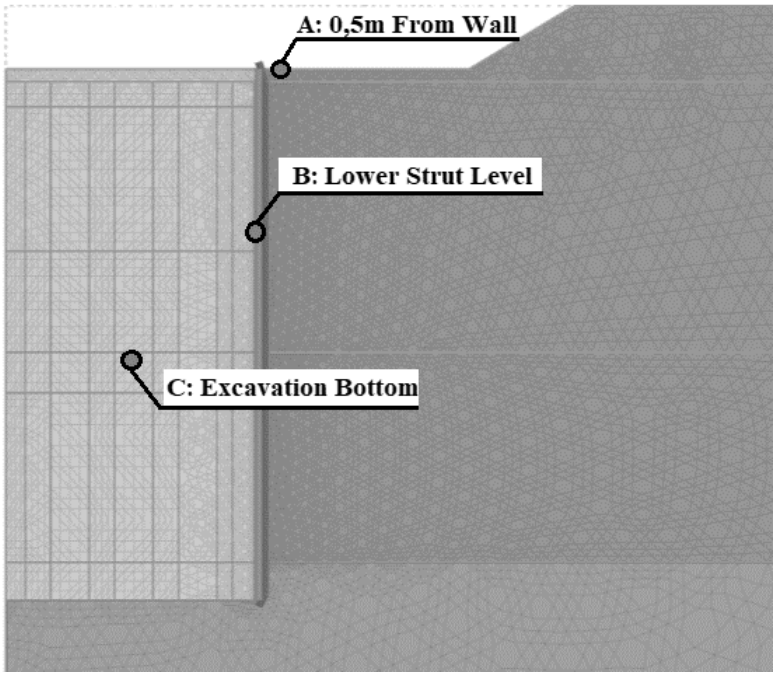

Figure 4.4 Measurement points used in the mesh sensitivity analysis.

4.2 Parameter Determination

Extracting soil parameters from available lab tests is a crucial part to get a reliable numerical model. A parameter determination method is needed to consistently gain reliable results and to avoid human errors and misinterpretations. This study's method is illustrated in Figure 4.5. Parameter optimization is a method to optimize values retrieved from different soil tests. The optimization is done by matching the curves of different output responses (e.g., p'/q or ε - σ_1

graphs) from simulated soil tests with the derived values to the lab tests. The tests are simulated using the Plaxis soil test tool, which is a tool that uses the constitutive models to simulate soil tests such as CAUC, CADE and IL tests. Before the optimization process can begin, an acceptable range of the parameters with upper and lower boundaries are needed. Furthermore, a sensitivity analysis is needed to understand how the different parameters affect the output graphs and what soil tests and outputs are most suited for the different parameters.

In a study by (Gras J. , Sivasithamparam, Karstunen, & Dijkstra, 2017), a quantitative sensitivity analysis for outputs of the most common soil tests has been made for the Creep-SCLAY1S model. The method in this study is a simplified version of that, it is described in Figure 4.5. The method begins with determination of range of parameters based on lab tests or theoretical boundaries, where the quality and relevance of each lab test are evaluated. Tests have been neglected if they lack proper documentation, or if they are done with significantly different conditions than the case study in situ conditions. The boundary determination is followed by a simplified sensitivity and optimization analysis. A simple sensitivity analysis is carried out in this study by using a graphical method, where parameters are incrementally changed to study the effect on the output graph. Furthermore, the quantitative sensitivity analysis by (Gras J. , Sivasithamparam, Karstunen, & Dijkstra, 2017) is used to compare and adjust the sensitivity results. The method for parameter optimization takes use of the variety of soil tests carried out on the site. Each parameter is optimized toward the most appropriate test and outputs. is used to compare and adjust the sensitivity results. The method for parameter optimization takes use of the variety of soil tests carried out on the site. Each parameter is optimized toward the most appropriate test and outputs.

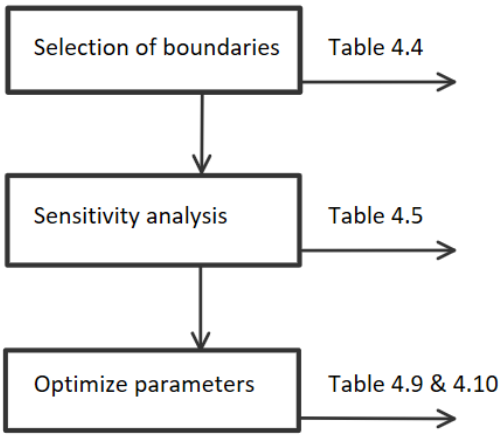

Figure 4.5. Schematic overview of the optimization method.

4.2.1 Parameter boundaries

Boundaries of the parameters are determined by theoretical and empirical relations as described in the following subheadings. The upper and lower boundaries will be taken from the highest and lowest values calculated from the tests. Some boundaries are increased as according to the study of (Gras J. , Sivasithamparam, Karstunen, & Dijkstra, 2017). The Hardening Soil clay parameters are later derived from the Creep-SCLAY1S model through curve matching with the Plaxis soil test tool. This is done to get a close resemblance between the two models, as they represent the same soil.

The critical state envelopes in compression and extension, M_c and M_e are derived from the inclination of triaxial *p-q* plots (CAUE & CAUC), as seen in Figure 4.6. The Creep-SCLAY1S model uses both triaxial extension and compression parameters to determine the value of M. Hardening soil is only used in the passive zone, hence the extension parameter M_e is derived. The hardening soil's friction angle ϕ is determined through the relationship with M_e seen in equation (4.1). The initial value for K_0^{NC} is calculated using Jaky's formula, equation (2.1).

$$\phi = sin^{-1}\left(\frac{3M_c}{6+M_c}\right) \tag{4.1}$$

$$K0_{NC} = 1 - Sin\phi \tag{2.1 bis}$$

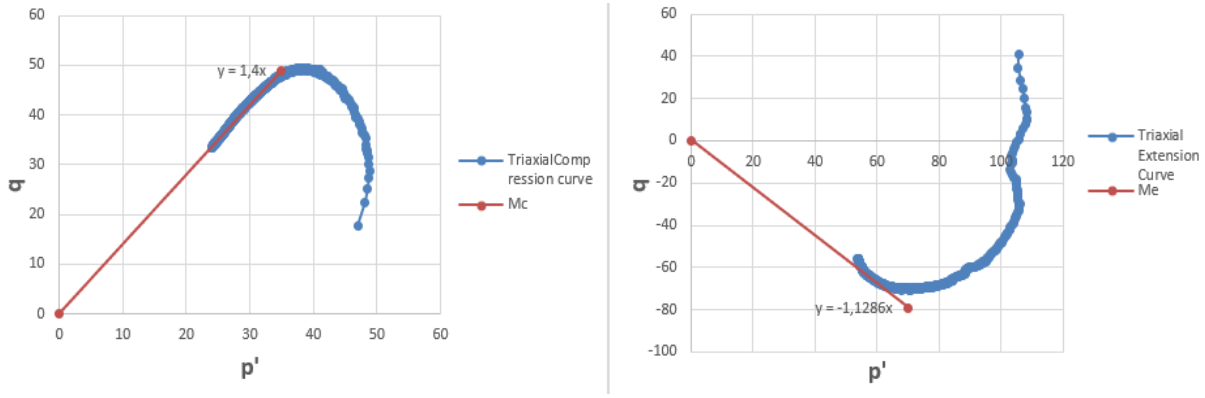

Figure 4.6. Critical state envelope derivation from triaxial tests.

To determine whether to use OCR or POP for the clay, the preconsolidation pressure, σ_p, must be estimated for a variety of IL tests at different depths and their relationship studied. The OCR and POP values are defined in equation (2.2) and (2.3). The parameter that best describes the depth-σ_p relationship is selected. To estimate the preconsolidation pressure from the IL tests, a graphical method is used where values for the modified swelling and compression index, κ^* and λ^*, were estimated and their trend lines drawn, see Figure 4.7. The κ^* value was taken as the mean inclination of the unloading/reloading curve before preconsolidation pressure was reached. This inclination is used over the initial part of the curve to avoid bedding errors and water suction. The λ^* value was taken as the steepest inclination of the oedometer curve. Where the trendlines of $\kappa^*$and λ^* meet, the preconsolidation pressure is measured. Results from all oedometer tests are drawn in a graph to get a relationship between the preconsolidation pressure and the vertical stress, see Figure 4.8. Since the lines are not fully perpendicular and instead moves apart with increased depth, and since the OCR values have a smaller variance, OCR is best suited for this clay.

The modified intrinsic compression index, λ_i^* is usually retrieved from reconstituted clays under IL tests. However, no reconstituted clay has been tested. Instead, the last loadings are used since regular compression index approaches the modified intrinsic compression index in the end of the test. Therefore, the parameter is taken as the inclination of the last part of the same IL curves as the modified compression index, λ^*, see Figure 4.7. This way, the effect of bonding is not affecting the value since all bonds have been destroyed.

$$OCR = \sigma'p\sigma'v \quad (2.2)$$

$$POP = \sigma'_p - \sigma'v \quad (2.3)$$

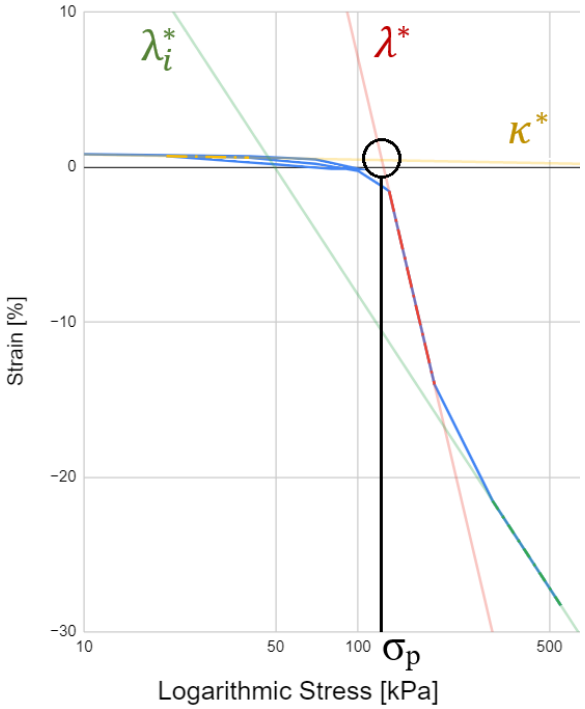

Figure 4.7 *Graphical method used to retrieve preconsolidation pressure, modified swelling index, modified compression index, and modified intrinsic compression index in an IL graph.*

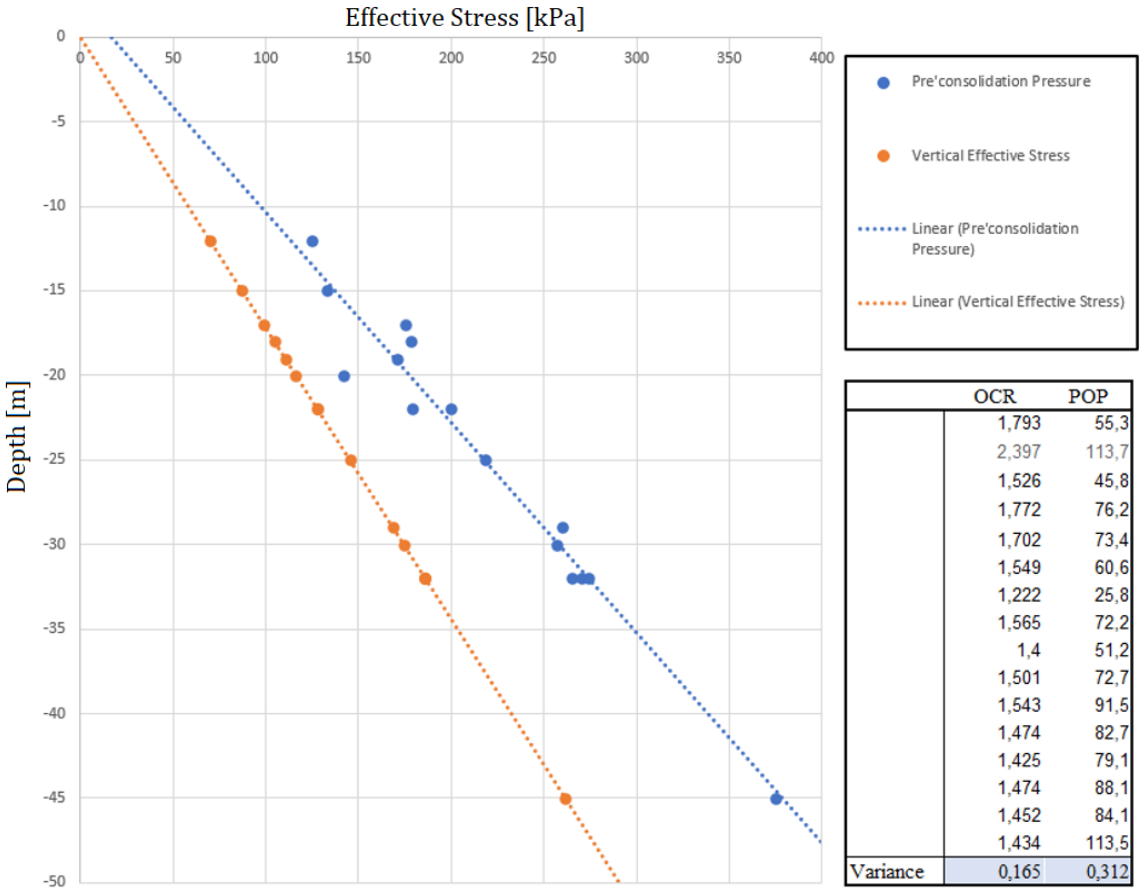

	OCR	POP
	1,793	55,3
	2,397	113,7
	1,526	45,8
	1,772	76,2
	1,702	73,4
	1,549	60,6
	1,222	25,8
	1,565	72,2
	1,4	51,2
	1,501	72,7
	1,543	91,5
	1,474	82,7
	1,425	79,1
	1,474	88,1
	1,452	84,1
	1,434	113,5
Variance	0,165	0,312

Figure 4.8 Preconsolidation pressure and vertical stress with depth.

The creep index is retrieved from Ln(time)-strain oedometer curves. To retrieve a good approximation of the modified intrinsic creep index, μ_i^*, the final loading curves must be used and preferably loaded for a lengthy period, this way all bonds are destroyed and not affecting the creep index. Only the oedometer curves that fill this requirement have been used, one of those is seen with the graphical method in Figure 4.9.

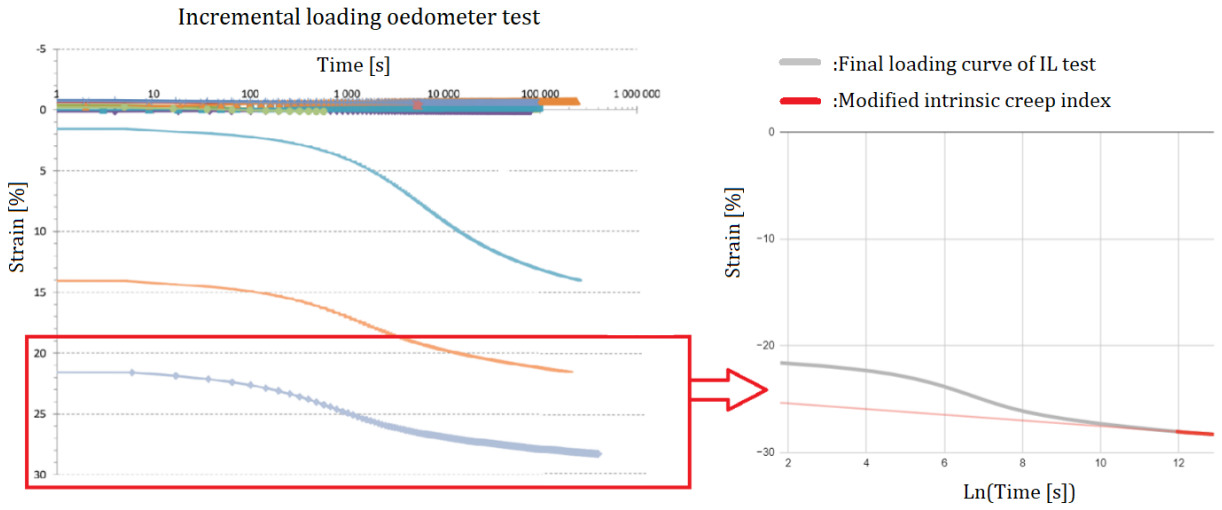

Figure 4.9 Graphical determination for retrieving modified intrinsic creep index μ_i^*, using data from the last loading step of an IL test.

For the LC, E_{50} is retrieved through triaxial CAUE data. E_{oed} is retrieved through the IL test data. Usually, E_{ur} is calculated using unloading/reloading triaxial curves. However, no unloading/reloading curve was retrieved from the triaxial tests on the LC, hence E_{ur} is instead calculated based on the relationship of $E_{ur} = 2 \cdot E_{50}$. The stiffness parameters in Hardening Soil describe the drained behaviour, but the lab tests at hand for this study are undrained. Therefore, a theoretical relationship to convert the undrained test stiffnesses into drained parameters is required. The formula is based on elastic law and described in equation (4.2) and (4.3).

$$f = \frac{1+v}{1+v_u} \tag{4.2}$$

$$E'_u = f * E_u \tag{4.3}$$

The advanced Creep-SCLAY1S parameters for anisotropy, bonding and destructuration are based on theoretical boundaries from (Gras J. , Sivasithamparam, Karstunen, & Dijkstra, 2017). Firstly, the initial bounding, χ_0, is based on the sensitivity, S_t, of the soil and calculated using equation (4.4). The sensitivity of the clay is retrieved from undisturbed boreholes in E02 Centralen. Secondly, with the associated flow rule assumed, an initial inclination of the yield surfaces, α_{K0}, is derived from equation (4.5). The value for the initial stress ratio for $K0_{NC}$, η_{K0} , is determined by Jaky's formula as $\eta_{K0} = 3 \cdot M_c/(6 - M_c)$. The value of the relative rate of surface rotation, ω_d, can be directly derived from M_c by equation (4.6). Thirdly, for the value of absolute rate of surface rotation, ω, the study from (Leoni, Karstunen, & Vermeer, 2008) suggests equation (4.7), using the difference between modified swelling index and modified intrinsic compression index (Gras J. , Sivasithamparam, Karstunen, & Dijkstra, 2017). Lastly are bonding and destructuration parameters *a* and *b*. According to (Gras J. , Sivasithamparam, Karstunen, & Dijkstra, 2017), the relative efficiency, *b*, typically range between 0,2 and 0,4 since the deviatoric strains can be assumed to have lesser impact then volumetric strains in soft clays. The absolute rate of destructuration, *a*, has suggestions for upper and lower bounds from (Gras J.-P. , Sivasithamparam, Karstunen, & Dijkstra, 2018), assuming an anisotropic material that is normally- or lightly overconsolidated, see equation (4.8).

$$\chi_0 = S_t - 1 \tag{4.4}$$

$$\alpha_{K0} = \frac{\eta_{K0}^2 + 3\eta_{K0} - M^2}{3} \tag{4.5}$$

$$\omega_d = \frac{3(4M_c^2 - 4\eta_{K0}^2 - 3\eta_{K0})}{8(\eta_{K0}^2 - M_c^2 + 2\eta_{K0})} \tag{4.6}$$

$$\omega = \frac{1}{\lambda_i^* - \kappa^*} \cdot \ln\left(\frac{10M_c^2 + \alpha_{K0} \cdot \omega_d}{M_c^2 + \alpha_{K0} \cdot \omega_d}\right) \tag{4.7}$$

$$\frac{ln2}{[\ln(2+2\chi_0) - \ln\left(1+\frac{\chi_0}{2}\right)] \cdot (1+b) \cdot (\lambda_i^* - \kappa^*)} < a < \frac{1+\chi_0}{\chi_0 \cdot (\lambda_i^* - \kappa^*) \cdot (1+2b\frac{\alpha_{K0}}{M_e^2})} \tag{4.8}$$

With the usage of OCR, the parameter boundaries for the two clay layers are shown in Table 4.4. The parameter boundary for the LC is shown in the same table. Here an OCR of 1 where the LC is always normally consolidated is used, as well as an OCR of 15 to represent a state of always being overconsolidated. These OCR values are used to avoid getting a LC material that changes behaviour because of an exceeded preconsolidation pressure, as this is not how the LC behaves.

Table 4.4 Selected parameter boundaries.

Model/Material	Parameter	Minimum Value 0-20m	Maximum Value 0-20m	Minimum Value 20-45m	Maximum Value 20-45m
Clay/CreepSCLAY1S	κ^*	0,00436	0,00863	0,00542	0,0132
	λ_i^*	0,103	0,118	0,103	0,121
	μ_i^*	0,00250	0,00640	0,00250	0,00430
	OCR	1,40	1,79	1,22	1,60
	χ_0	7	30	7	30
	a	3,53	10,0	3,39	10,0
	b	0,200	0,400	0,200	0,400
	M_C	1,36	1,43	1,40	1,77
	K_0	0,350	0,450	0,318	0,450
	ω_d	0,900	0,970	0,900	0,970
	α_0	0,521	0,734	0,521	0,734
	M_E	1,00	1,250	1,000	1,250
	ω	16	50	16	50
LCC/Hardening soil	OCR [-]	1,00	15,0		
	E_{oed} [kPa]	40.000	100.000		
	E_{50} [kPa]	70.000	150.000		
	E_{ur} [kPa]	140.000	300.000		
	K_0 [-]	0,300	0,500		
	Φ [°]	31	37		
	m [-]	0,700	1,00		

4.2.2 Parameter Sensitivity Analysis

The results of the sensitivity analysis for the two constitutive models are shown in Table 4.5, the curves used in the analysis can be seen in Appendix A. The results are ranked from "None" to "Very High" to explain the impact of changing the parameter for the specific lab test. "Very Low" is barely visible change, "Low and "Medium" indicate change in the curve values, while "High" and "Very High" indicate impactful changes that can alter the shape and form of the curve.

Table 4.5 Results of sensitivity analysis.

Model/Material	Parameter	IL	CAUC	CAUE
Creep-SCLAY1S	κ^*	High	Low	Low
	λ_i^*	Very High	Low	Low
	μ_i^*	Medium	Medium	Medium
	OCR/POP	High	High	High
	χ_0	High	Very Low	Very Low
	a	Very High	High	High
	b	Medium	Medium	Medium
	M_C	None	High	None
	K_0	Small	Medium	Medium
	ω_d	None	Low	None
	α_0	Small	High	High
	M_E	None	None	High
	ω	None	None	High
Hardening soil	OCR/POP	Very High	-	High
	E_{oed}	High	-	High
	E_{50}	Medium	-	Very High
	E_{ur}	Medium	-	Very High
	K_0	Medium	-	Medium
	ϕ	Low	-	High
	m	Medium	-	High

The results from the sensitivity analysis are combined with the theory and results from (Gras J. , Sivasithamparam, Karstunen, & Dijkstra, 2017) to determine which parameters should be optimized with which test. These decisions can be seen in Table 4.6, Table 4.7 and Table 4.8, together with the graph used. A CADE test is used for the Hardening soil clay parameters over CAUE as it can be simulated in the Plaxis soil test and hence no conversion to drained parameters are needed. The OCR value in the LCC will not be optimized but instead tested in a numerical investigation discussed in chapter 4.2.5.

Table 4.6 Lab tests and output graphs used for optimizing the different parameters for Creep-SCLAY1s clay.

Test	Output graph	Parameters optimized
Oedometer Test	ε - σ_1	$\kappa^*, \lambda_i^*, \mu_i^*, \chi_0$, a, b, OCR/POP
Oedometer Test	ε - time	μ_i^*
Triaxial CAUC	p'- q	$M_C, K_0, \omega_d, \alpha_0$
Triaxial CAUE	p'- q	M_E
Triaxial CAUE	ε - q	ω

Table 4.7 Lab tests and output graphs used for optimizing the different parameters for Hardening Soil clay.

Test	Output graph	Parameters optimized
Oedometer test	ε - σ_1	E_{oed}
Triaxial CADE	ε - q	$E_{50}, E_{ur} K_0$, ϕ

Table 4.8 Lab tests and output graphs used for optimizing the different parameters for Hardening Soil LCC.

Test	Output graph	Parameters optimized
Triaxial CAUE	ε - q	$E_{oed}, E_{50}, E_{ur}, K_0$, ϕ, m

4.2.3 Optimization of Parameters

The optimization process is initiated by optimizing the oedometer tests, followed by triaxial compression tests and lastly the triaxial extension tests. The method is aided by the Plaxis soil test tool. It is possible to change single parameters and see the effect directly. With this tool, soil parameters are changed individually, and the effect is studied. If a positive effect is seen (the test simulation looks more like the lab data), the parameter is changed again until no positive effect. The oedometer/triaxial lab tests that the simulated tests are optimized into is chosen based on a summarized plot of all tests for the specific layer. The chosen test should represent all the tests for that layer as a mean, should have a good estimate of the initial effective stress, and should not have defects and outlying trends. A summary of lab tests as well as the chosen test for the optimization process is showed in Appendix A.

Optimized graphs for Creep-SCLAY1S layer 0-20m is shown for IL in Figure 4.10, for triaxial CAUC in Figure 4.11, and for triaxial CAUE in Figure 4.12. Same procedure is made for clay layer 20-45m. The hardening soil clay parameters were optimized with IL and triaxial CADE curves using the optimized Creep-SCLAY1S parameters as initial values. The optimized curves for clay layer 20-45m and for hardening soil clay are shown in Appendix A.

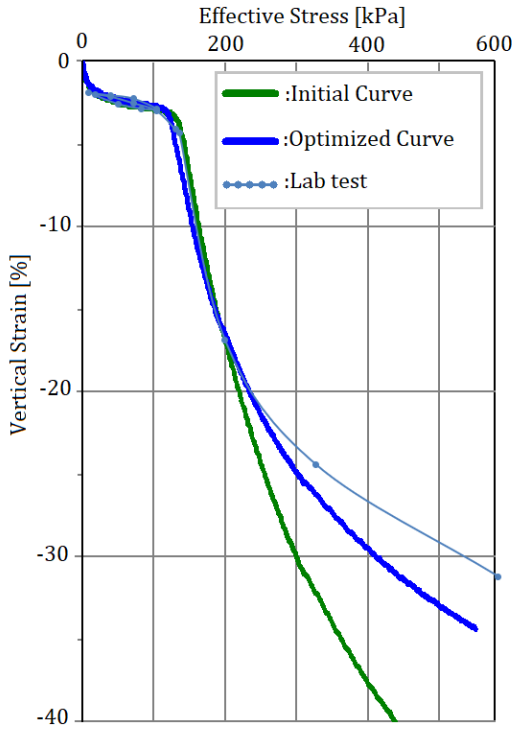

Figure 4.10 Optimized IL stress/strain curve for Creep-SCLAY1S layer 0-20m.

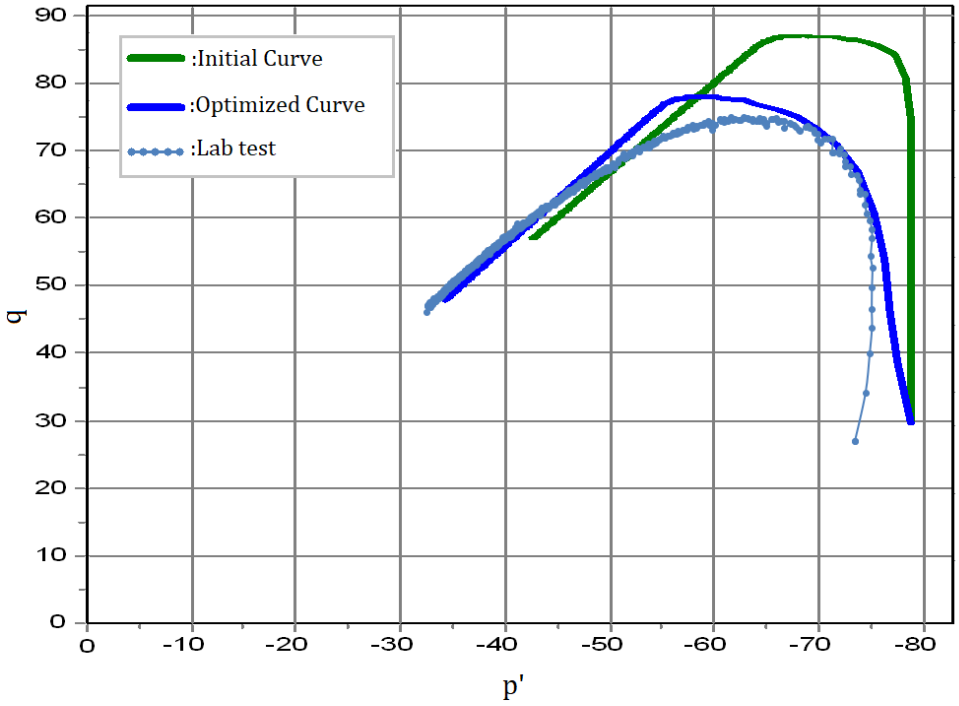

Figure 4.11 Optimized Triaxial CAUC p-q curve for Creep-SCLAY1S layer 0-20m.

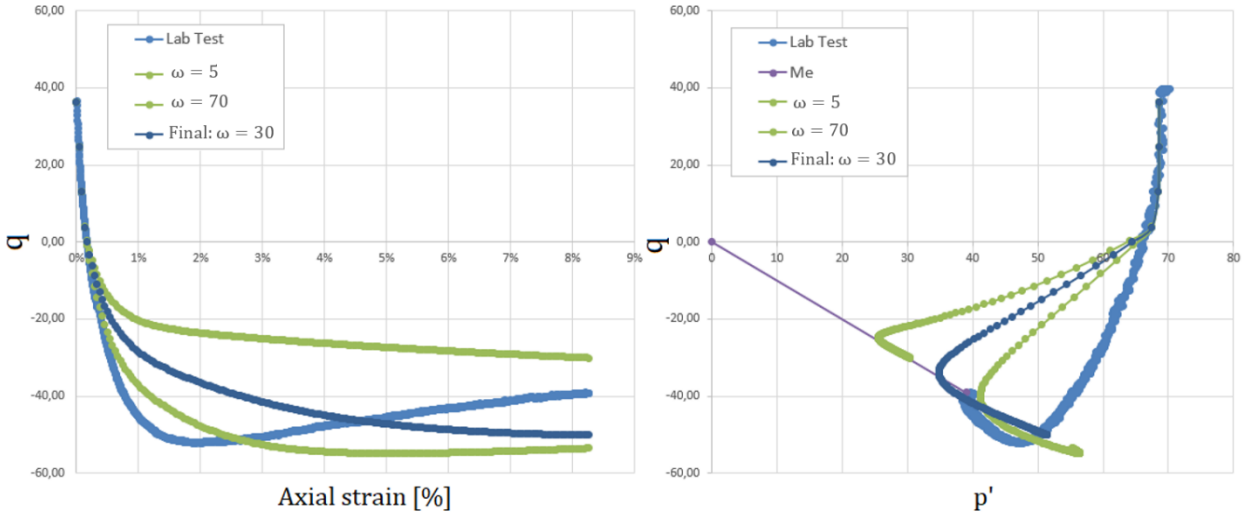

Figure 4.12 Optimized Triaxial CAUE Axial Strain/q and p'/q curves for Creep-SCLAY1S layer 0-20m, where ω =30 is the final optimized curve.

The LC was optimized with a triaxial CAUE field test, using ε - q output. The optimization is shown in Figure 4.12-Figure 4.13 for OCR 1 and 15.

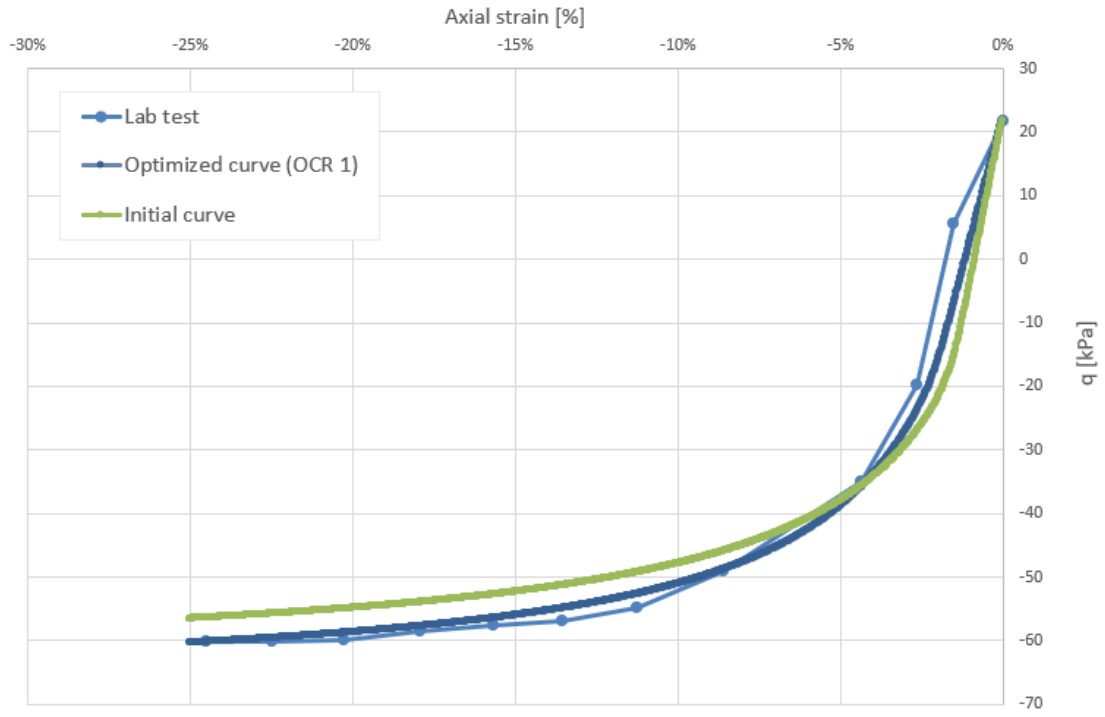

Figure 4.13 Optimized Triaxial CADE ε - q curve for the LC, OCR=1.

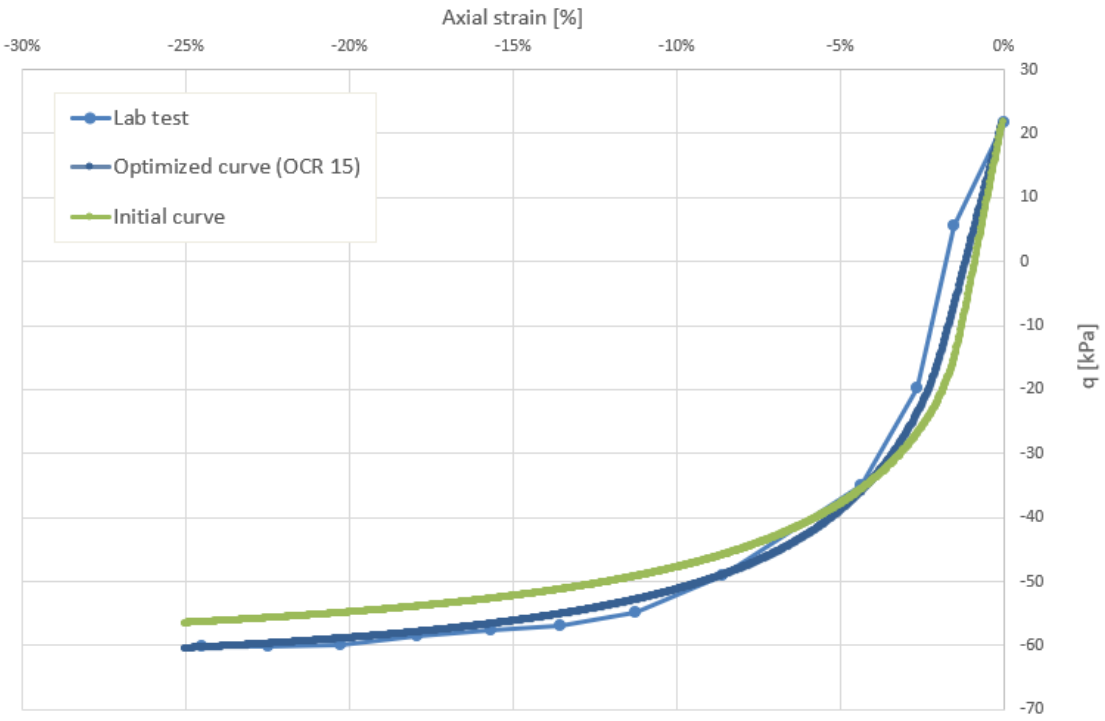

Figure 4.14 Optimized Triaxial CADE strain/q curve for LCC, OCR 15.

The results from the optimization process, and hence the final values used in the numerical analysis, is shown for Creep-SCLAY1S in

Table 4.9 and Hardening Soil model in Table 4.10. Two set of parameters are set for the LC to use in the numerical investigation. A P_{ref} value of 135 kPa is used for all Hardening soil materials as this is in the normally consolidated zone. An effective cohesion, c', of 1 is used to avoid unrealistic failure at the top of the excavation.

Table 4.9 Creep-SCLAY1S optimized parameters used in the numerical model.

Parameter	Clay Layer 0-20m	Clay Layer 20-45m
κ^*	0,0055	0,0061
λ_i^*	0,103	0,103
μ_i^*	0,0025	0,0025
OCR	1,67	1,42
χ_0	7,00	8,00
a	7,00	7,00
b	0,32	0,25
M_C	1,43	1,47
K_0	0,43	0,41
ω_d	0,97	0,99
α_0	0,55	0,57
M_E	1,00	1,12
ω	30	20

Table 4.10 Hardening Soil optimized parameters used in the numerical model.

Parameter	LC Parameter set 1	LC Parameter set 2	Clay Parameters
OCR	15	1,00	1,67
E_{oed} [kPa]	78.000	95.000	420
E_{50} [kPa]	115.000	128.000	1.400
E_{ur} [kPa]	230.000	257.000	21.000
K_0	0,47	0,40	0,49
ϕ [°]	32	37	30
m	0,85	0,80	1

4.2.4 Structural Elements

The input parameters for the SPW and struts are shown in Table 4.11, and are based on the members found in the specific cross section in the case study. The walers are not simulated in the numerical analysis. Their function is to spread the load to the entire wall, which is automatically simulated in Plaxis 2D. It is therefore assumed that the walers do not fail. The SPW is assumed linear elastic. The interface will have an initial interface reduction coefficient (R_{inter}) value of 0,5 to represent a connection between clay and steel. This value will be further tested in the numerical investigation.

Table 4.11 Model parameters for the structural members in the numerical model.

Parameter	Sheet pile wall	Strut	
		Upper strut	Lower strut
Cross Section [-]	AZ-38-700N	Circle	Circle
E [kPa]	210.000.000	210.000.000	210.000.000
I [m^4/m]	0,0948	-	-
A [m^2/m]	2,3	0,0288	0,0356
EA [kN/m]	483.000.000	6.050.000	7.480.000
EI [kNm^2/m]	1.990.000	-	-
Spacing [m]	-	9,52	4,82

4.3 Numerical investigation

After the first results are retrieved from the numerical analysis, a numerical investigation will be made to determine how to best simulate the case study. This is done by comparing the results to inclinometer, prism, and strain gauge monitoring. Table 4.12 shows all numerical investigations that will be carried out and will be further explained in Chapter 4.3.1-4.3.3.

Table 4.12 Description of numerical investigation scenarios.

Numerical investigation		Implementation
LCC grid	LC weaker layer 0-11m	Implement a -25% Strength/Stiffness in the LC material 0-11m to consider 40 kg/m^3 is used there instead of 80 kg/m^3.
	Vertical LCC grid	Vertical grid with 40%, 64,5% & 100%.
	Horizontal LCC grid	Horizontal grid with 40%, 64,5% & 100%.
Material parameters	Weaker Strength/Stiffness in LCC	Implement a -20% Strength/Stiffness in the LC material to compensate for the use of a field test
	Change the Interface reduction coefficient	R_{inter}=0,8 in the wall interface to represent a connection between clay and steel
	OCR of LCC	Using values for OCR=1 (always NC) or for OCR=15 (always OC).
LC Installation Effects		Including or excluding installation effects from the LCC.

4.3.1 Scenarios regarding LCC grid

To simulate the grid of LCC in Plaxis 2D, simplifications must be made. The impact of different approaches of modelling the grid will be tested in the numerical investigation. The models will contain materials to represent a combination of clay and LCC. In the base model, a material with 64,5% LCC will be installed to simulate the entire LCC grid. Different model approaches of horizontal and vertical LCC are then tested in the numerical investigation to better represent the

real LCC grid. The percentages are based on drawings from the case study, see Figure 4.15. For simplicity, 64,5% LCC are used instead of 70% in the horizontal and vertical column approaches. The 18cm small clay column closest to the walls will not be simulated in the geometry as it creates an unstable mesh. It will instead be taken into consideration in the interface reduction factor, R_{inter}, discussed in chapter 4.3.2. The material parameters for the mixed materials are calculated using Equation (4.9), the same equation can be used for different percent LCC and with different parameters.

$$E_{64,5\%} = \left(E_{LCC} - E_{clay}\right) * 64{,}5\% + E_{clay} \tag{4.9}$$

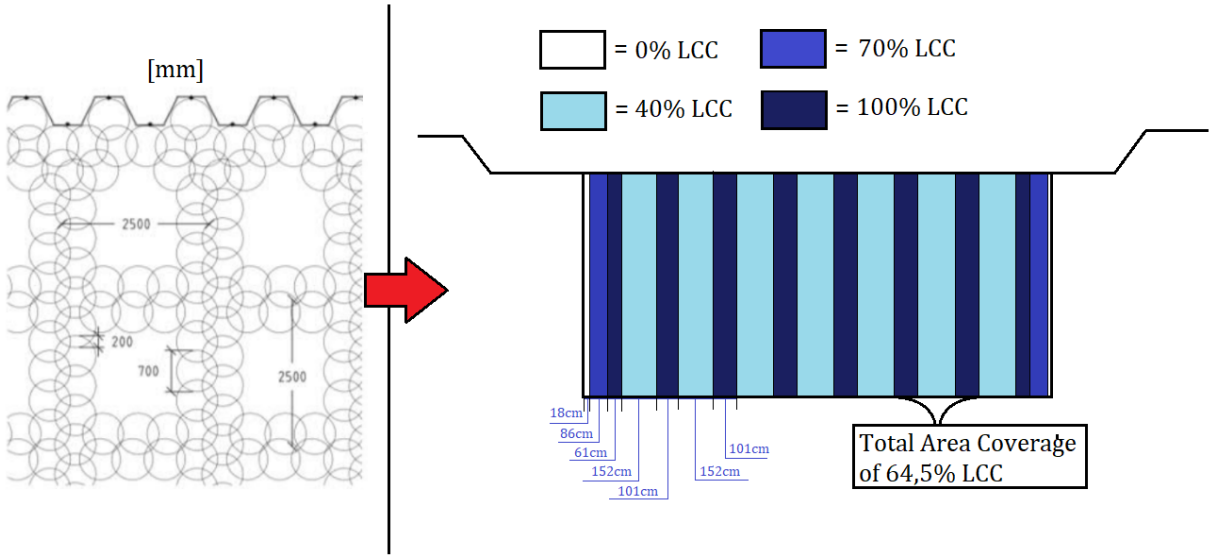

Figure 4.15 Drawing and measurement of LC grid from the case study (Björkman, Isaksson, & Yannie, 2020) (left), and the adopted percentages of LCC in the excavation (right).

To take into consideration the difference of having 40 kg/m^3 LC above the excavation bottom and 80 kg/m^3 LC below the excavation bottom, a LC material with 25% decreased strength and stiffness will be installed above the excavation bottom in the numerical investigation. The parameters affected are E_{oed}, E_{50}, E_{ur}, ϕ and K_0. The percent decreased is not necessarily accurate, but it will show if the weaker columns have an impact. Figure 4.16 shows the different scenarios in the numerical model.

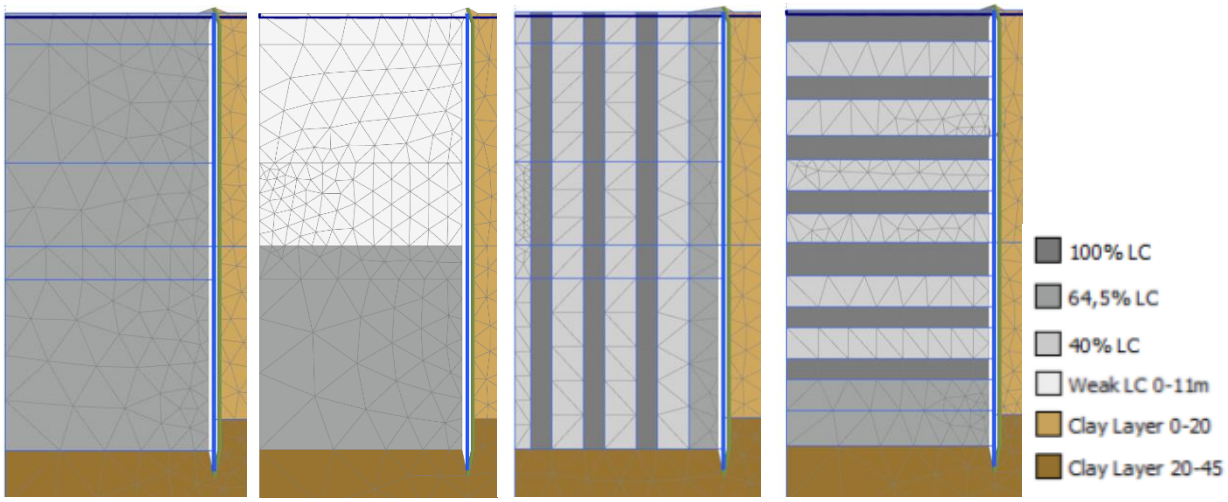

Figure 4.16 Modelling versions of the LCC grid. From left to right: base model, Weak LC 0-10 m, vertical columns, horizontal columns.

4.3.2 Scenarios regarding material parameters

Several sensitivity analyses will be carried out with different material parameters. As presented in the chapter 4.2.3, there are two set of parameters for the LC with different OCR. One set is to represent a material that is always normally consolidated and one that is always overconsolidated, both will be tested.

The interface between the wall and the LCC will be modelled differently in the numerical investigation. The concrete similar tendencies of the LCC suggests an interface reduction factor R_{inter}=0,8, however most of the wall is interfacing untouched clay as can be seen in Figure 4.17, which suggests a value of R_{inter}=0,5. Both these values will be tested.

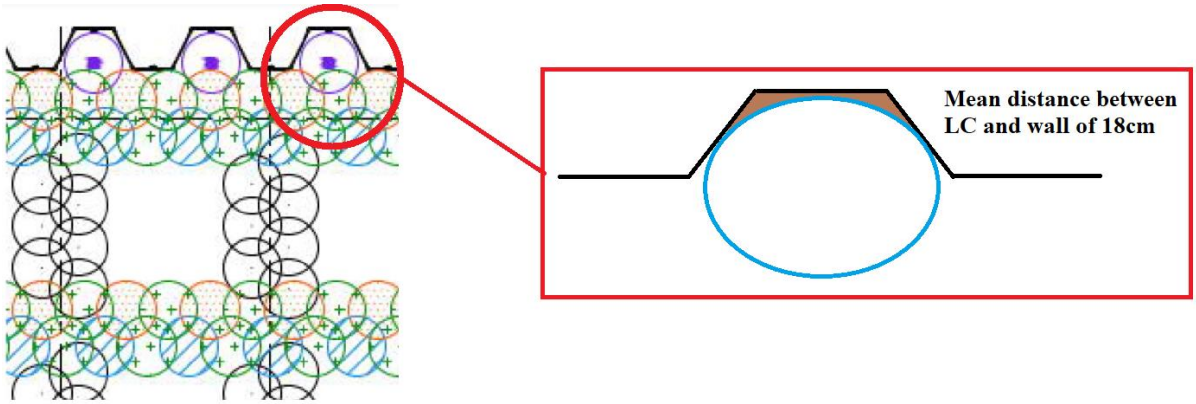

Figure 4.17 Illustration of area between wall and LCC.

The laboratory tests that the LC material parameters have been retrieved from have been mixed in the lab and taken from the field. The test used in the optimization process was a field test. When tests are taken from the field it is important to note that a lot of samples must be taken and only a few survive the process and keep intact when transported into the lab. The intact tests are always

the strongest parts of the LC and hence the parameters can be over predicted. To compensate for this, a numerical investigation will be made where the LC strength and stiffness are decreased by 20% in the entire area. This is because the field test has similar results as lab mixed tests with 100% kg/m3 LC. Reducing this with 20% can result in a material representative for 80kg/m3 LC. The affected parameters are E_{oed}, E_{50}, E_{ur}, ϕ and K_0.

4.3.3 Scenarios regarding installation effects

The monitoring from inclinometer 5, see Figure 3.7, show that installation effects have a significant effect on the wall deformations. The LC installation causes a volume expansion which alters the measured displacements both in the wall and on surrounding soil. If this is not considered in the numerical model, it will not accurately predict the system response. If not modelled, these effects must be implemented in the displacements by hand, using assumptions and predictions, or be ignored in the modelling and their effect only discussed. The investigation will focus on the potential of accurately predicting the deformations caused by installation of LCC in the Plaxis model, and if this is a viable method.

The installation effects are simulated using the volume strain function in Plaxis. The volumetric increase is anchored on the amount of LC installed (40-80 kg/m^3). The mixed soil is 64,5% of the entire area, leading to a theoretical total volumetric increase of just above 1%. However, the volumetric increase is altered to perfectly fit the inclinometer 5 displacements in the installation phase to see if the method can predict the displacements of the wall in later stages.

5 Results and Discussion

Results from the numerical model and numerical investigation is shown and discussed in this chapter. A base model with initial setup is described in Table 5.1. In the following subchapter it is presented and discussed. It is followed by the numerical investigation in Chapter 5.2. Lastly, the final model is compared with a model excluding LCC in Chapter 5.3.

Table 5.1 Description of model approach for the base model.

Model aspect	Choice for base model
Geometry of LCC	Homogenous soil to represent the entire LCC grid.
OCR of LC	OCR = 15
Value for R_{inter}	R_{inter}=0,5
LC material in excavation	No consideration of the weaker LC material above excavation bottom.
Strength reduction of LCC	No strength reduction in the LCC.
LC Installation Effects	No installation effects.

5.1 Base Model

Results from the numerical model is shown in the following figures. Horizontal wall displacements are compared with inclinometer 5 displacements in Figure 5.1. Positive values represent displacements towards the excavation while negative values represent displacements away from the excavation. The result show similar trends in displacements as the field monitoring but underestimates the maximum displacements with approximately 20 mm and improvements on the model is possible. The top of the wall is held in place in the base model results which is due to the top strut being rigid compared to the soil which is to be expected. The underestimation can partly be because of the soil creeping back after the installation effects.

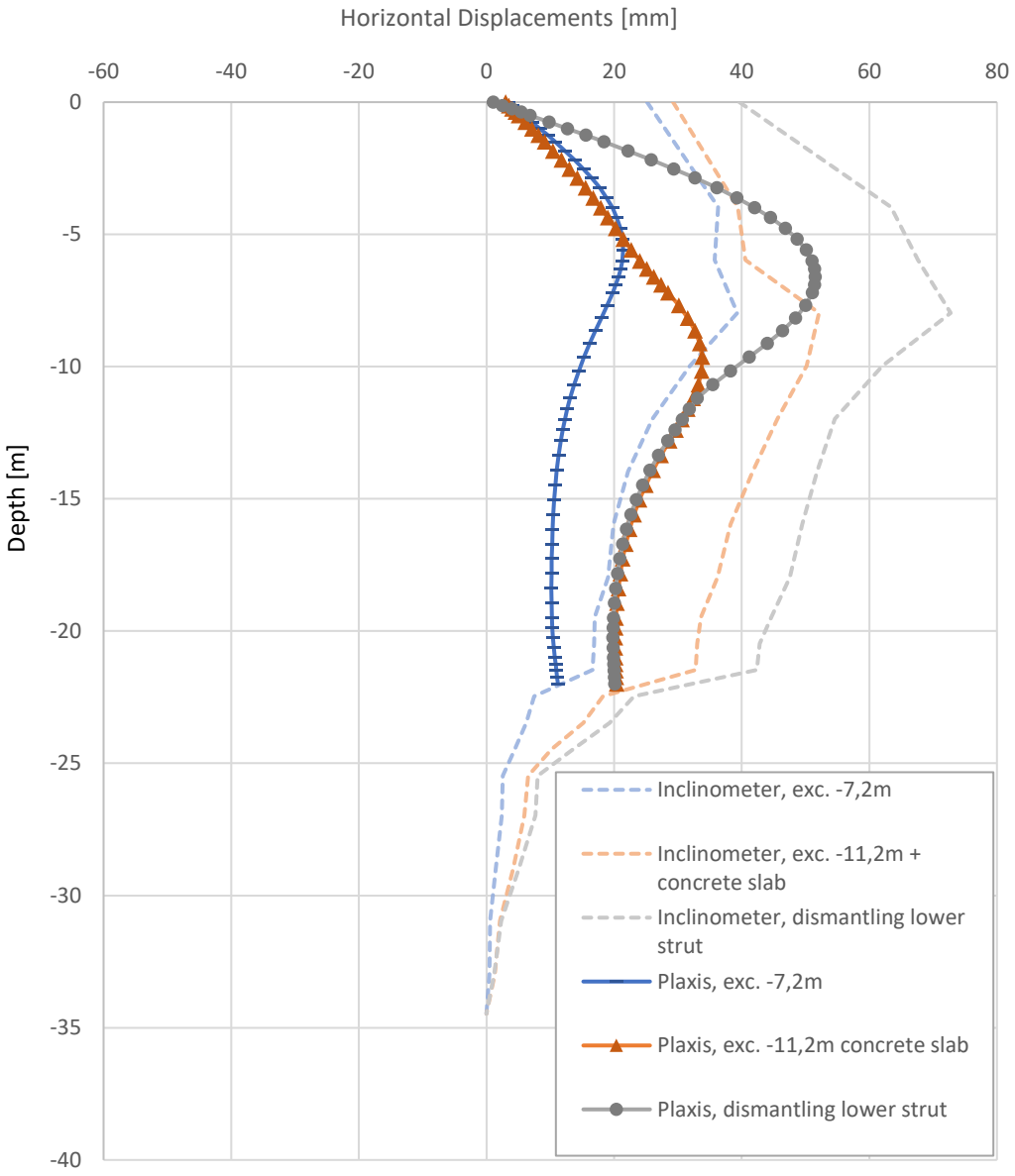

Figure 5.1 *Wall displacement of the base model and inclinometer results. Positive values represent displacements towards the excavation while negative values represent displacements away from the excavation.*

Vertical displacements on the surface of the adjacent soil are shown in Figure 5.2. It suggests that uplift displacements occur close to the excavation while settlements occur further away. When comparing the results to the prism monitoring from Figure 3.9 it is important to remember that the prisms include installation effects. Moreover, the red line in Figure 3.9 is erroneous, due to the sensor being disturbed. Otherwise, the base model is like the monitoring.

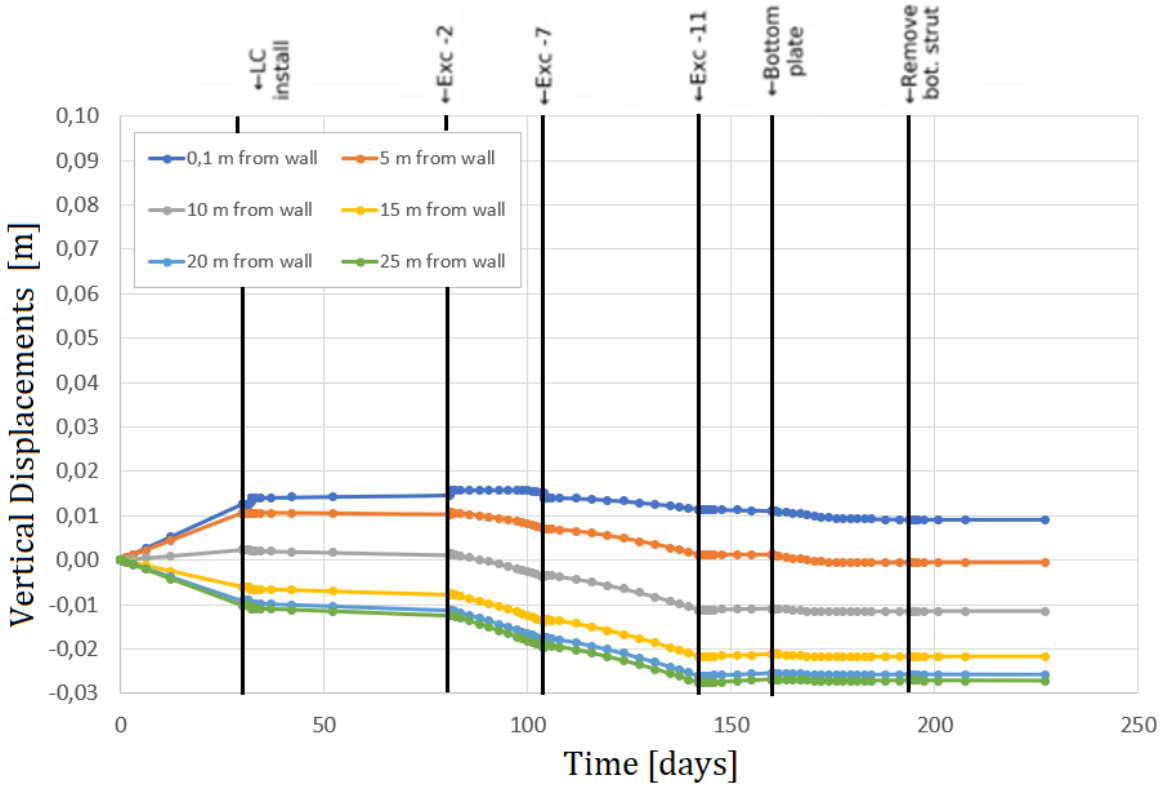

Figure 5.2 Vertical Plaxis displacements on surrounding soil in the base model.

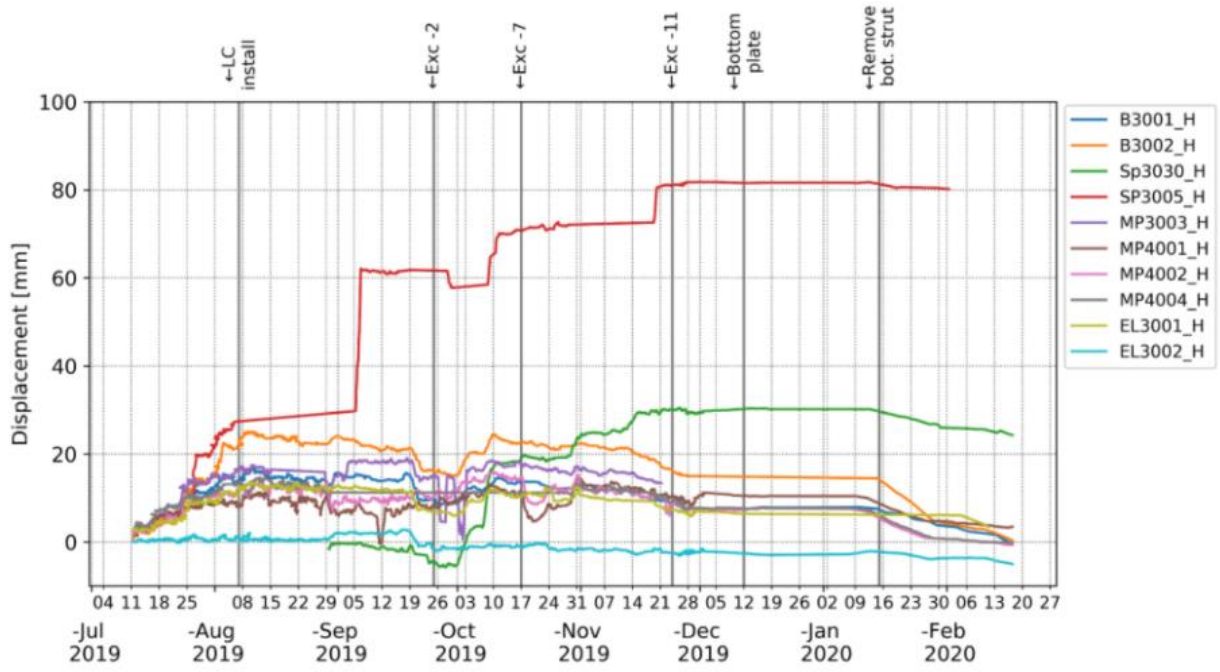

Figure 3.10 (bis) Monitored vertical deformations from the case study site. See Figure 3.9 for placement.

Figure 5.3 shows the forces in the upper and lower struts, for both the base model results and the strain gauge measurements. The results show an underestimation in the upper strut forces and overestimation of the lower strut forces. The overestimation in the lower strut may be due to insufficient small strain stiffness in the soil models. The underestimation of the upper strut forces may be due to the base model not taking LCC installation effects into account, since a volume expansion in the excavation should increase the strut forces, see Chapter 5.2.1.

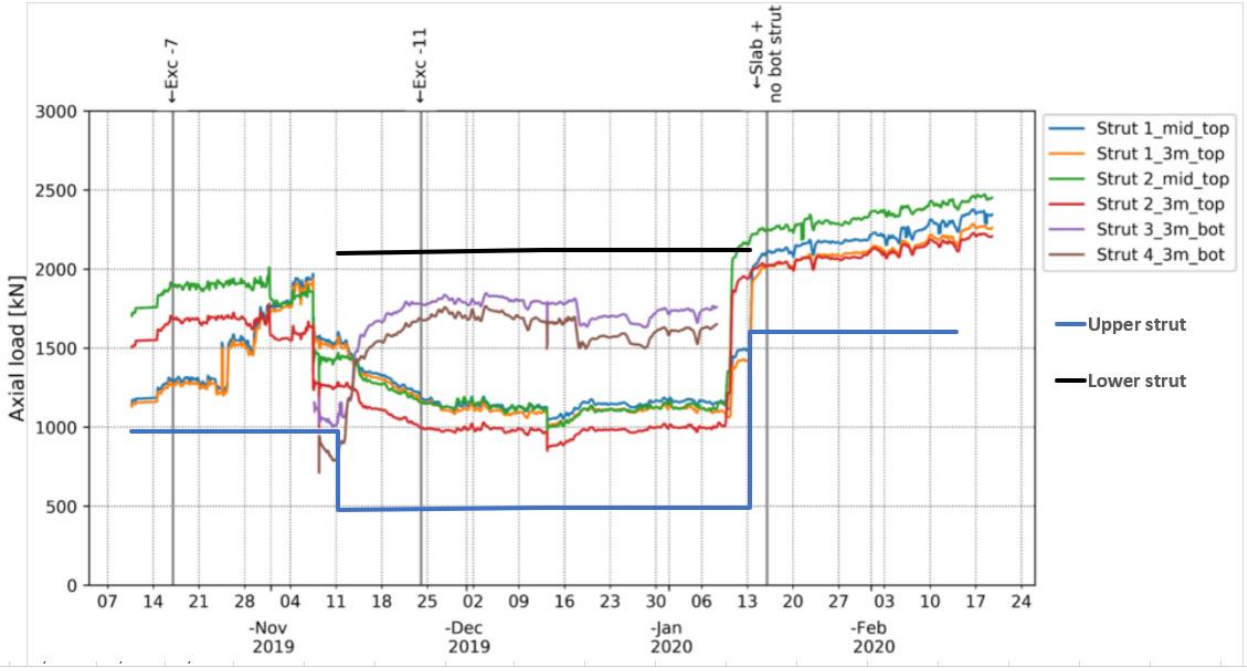

Figure 5.3 Strut forces from the base model and strain gauge data.

5.2 Numerical investigation results

The result of the numerical investigation is shown in Table 5.2. Some of the more complex modelling scenarios gave a better response, but overall, the differences were small. However. modelling volume expansion from LCC installation changed the response which will be discussed in chapter 5.3.

Table 5.2 Numerical investigation results, ranging from insignificant, minor to notable.

Numerical investigation	Horizontal Wall Displacements	Surface Settlement	Strut Forces
Volume expansion from LCC installation	Notable decrease	Notable change	Notable change
LC weak layer 0-11m	Minor increase	Insignificant change	Insignificant change
Vertical LCC grid	Minor decrease	Minor change	Minor increase
Horizontal LCC	Minor increase	Insignificant change	Insignificant change
Weaker Strength/Stiffness in LCC	Notable increase	Notable change	Minor increase
Using different values for $\boldsymbol{R_{inter}}$	Minor decrease	Notable change	Insignificant decrease
OCR of 1 in LCC	Minor increase	Insignificant change	Insignificant change

A weaker LC material above the excavation bottom, 0-11m, slightly affect the result but requires the calibration of an additional material. The weaker layer was expected to mostly affect earlier stages of the excavation when the material was not entirely excavated. In Figure 5.4, the wall displacements are shown for three different excavation stages, comparing the result with and without the weaker LC layer. The result shows that there is no substantial difference in any of the phases, it is therefore not necessary to take into consideration this weaker layer in similar projects. However, the small difference is still a better estimation of the real displacements. If the material properties are at hand, it could be a viable choice, but it is not necessary to receive a good result.

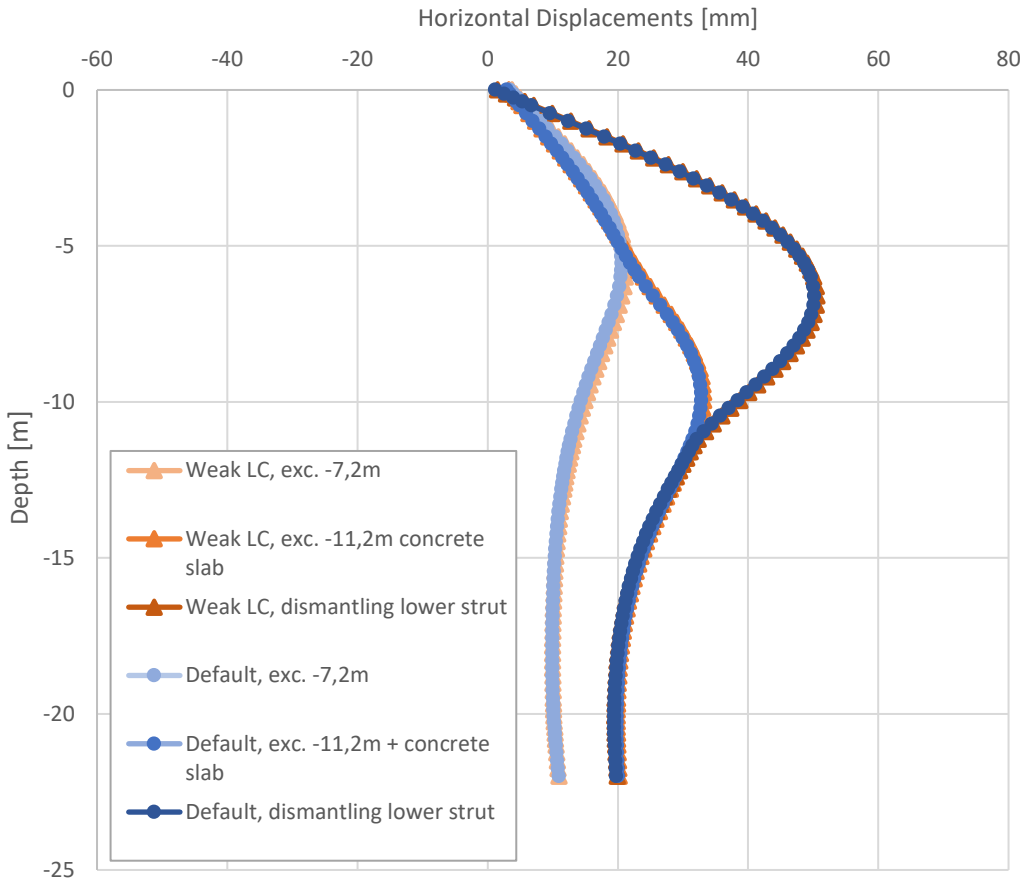

Figure 5.4 Horizontal wall displacements for default scenario and weak LC material 0-11m.

The use of horizontal or vertical layers results in minor differences in the results. The vertical columns decreased the horizontal displacements in the wall and on surrounding ground surface while horizontal columns had a slight increase. However, the model became more unstable with more soil clusters which resulted in pore pressure fluctuations, see Appendix B. The method also requires more work in creating three separate materials. When looking at internal horizontal and vertical effective stresses, there is a difference, see Figure 5.5 and Figure 5.6. However, the maximum value is similarly predicted in the three different models, and the sum of the total stresses in the material is similar. Therefore, the method of creating columns in either direction is not recommended, and a homogenous soil is instead sufficient in an SLS calculation such as this. However, in a study that is near the ultimate limit state, there might be a bigger difference between the scenarios as distinct failure modes will emerge.

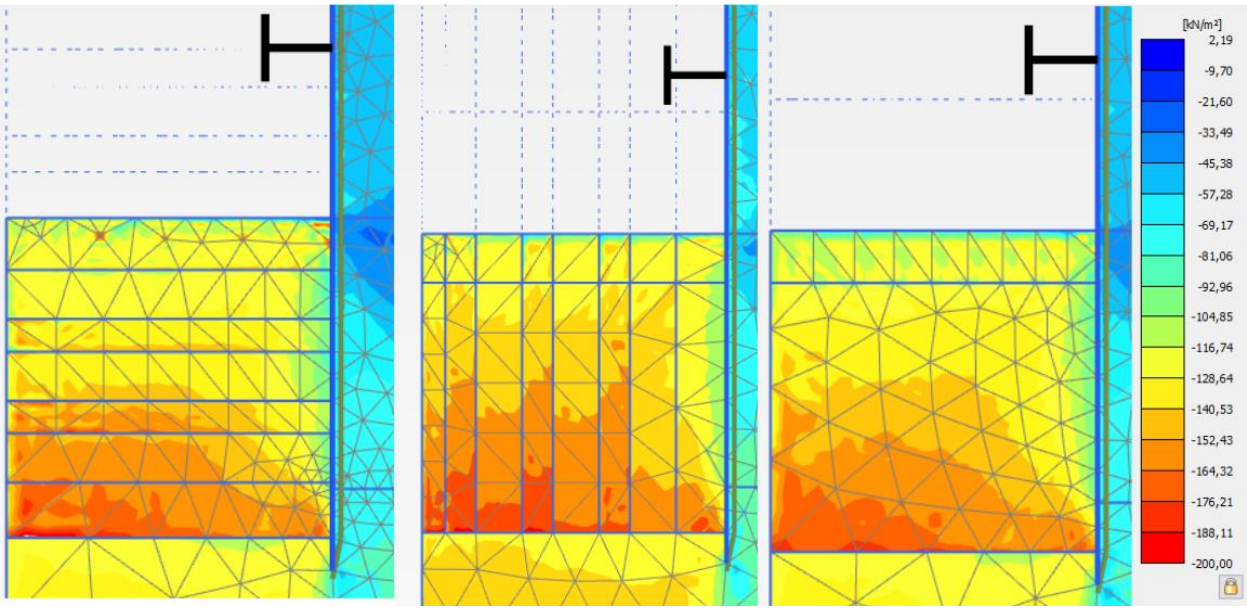

Figure 5.5 *Vertical effective stresses in the passive zone for horizontal columns (left), vertical columns (middle) and homogenous soil (right).*

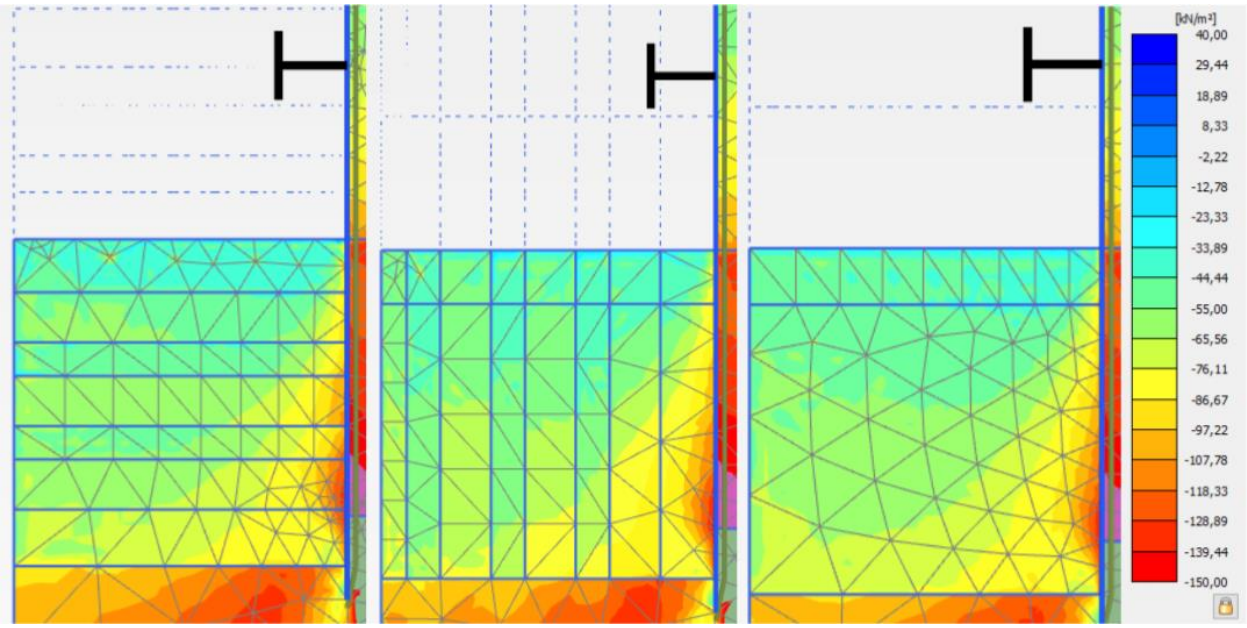

Figure 5.6 *Horizontal effective stresses in the passive zone for horizontal columns (left), vertical columns (middle) and homogenous soil (right).*

The use of an R_{inter}=0,8 resulted in a decrease in the wall displacement and an increase in the heave of surrounding soil. The changes do not correspond to the inclinometer/prism monitoring and hence the result suggests a value of R_{inter}=0,5. This match with the theory as a value of 0,5 takes into consideration the thin clay layer closest to the wall, see Figure 4.17.

Modelling LC in Hardening Soil model can be done assuming an overconsolidated material (OCR=15) or a normally consolidated material (OCR=1). The numerical investigation done during

the parameter determination concluded that an OCR=15 is more appropriate, since the LC laboratory tests suggest the material behaves like an overconsolidated material. Additionally, the numerical investigation during modelling suggests no substantial difference between the two alternatives, and an OCR of 15 results in an easier optimization of material parameters. An OCR of 1 can be used as well but other parameters must be adjusted to this. What is important however is to not have an OCR where the preconsolidation pressure is exceeded during loading, as this causes a misrepresentative change in the behaviour of the LC which does not occur in reality.

Using a 20% weaker LC material to compensate for the overpredictions in the lab sampling method results in a more accurate result in terms of wall deformations and strut forces. Therefore, it is a preferable method when laboratory tests of different amount of LC have been used to gather the material parameters.

5.2.1 Installation Effects

The deformations due to installation effects have a significant impact on the wall and surrounding soil in this case study, this can be seen in the inclinometer 5 displacements in Figure 3.7. Therefore, they cannot be neglected, the question is if the Plaxis model can predict these impacts, or if the effects are better predicted by other methods. The significance of the installation effects would decrease if the final displacement of the wall increases. Therefore, in the case of an ultimate limit state analysis, the neglection of installation effects could be argued more.

A comparison between inclinometer values and Plaxis results considering installation effects are shown in Figure 5.7. The results are similar in trends and values. The Plaxis results are chosen to match the inclinometer in the installation stage. In further stages the trends start to differ because of the fixed anchor in the Plaxis model at -1m holding the wall in its place. However, the values are far more similar than that in a comparison without installation effects, where the maximum wall displacements are only slightly underestimated with 3-4mm. This shows that Plaxis can model installation effects to a high extent.

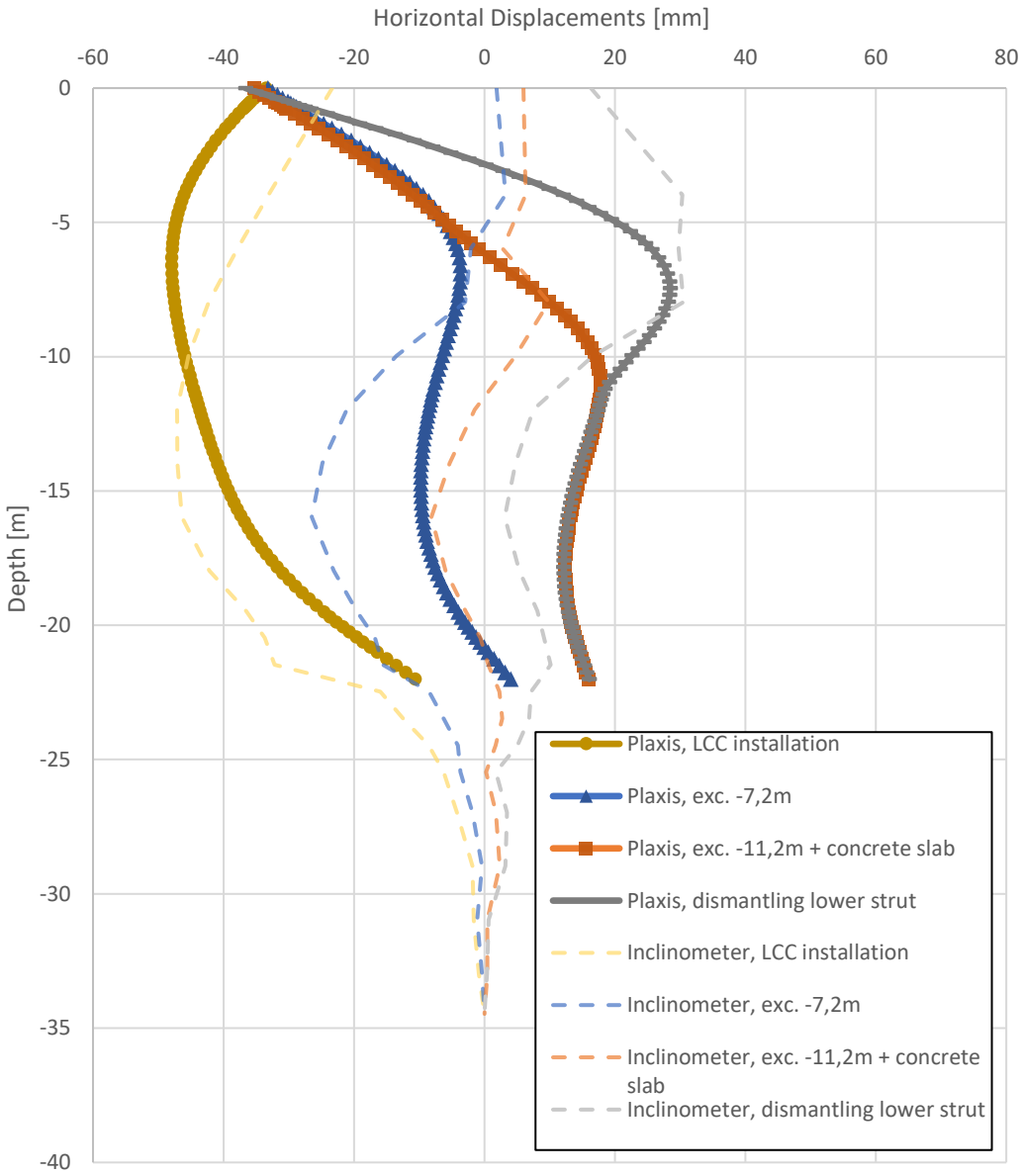

Figure 5.7 Displacements in the wall including installation effects, Plaxis and inclinometer values.

The volumetric expansion, V, used to get similar deformations in the installation phase as the inclinometer data, was an expansion in the x-axis with 0,6 %. For this study, a displacement of around 48 mm was present in the wall, with a total LC area coverage (A) of 64,5 % of the excavation, and a mean LC usage of 60 kg/m^3 (M). This would lead to a volumetric expansion of 1,55x10^{-4} per percent area covered and kg/m^3 LC. This is expressed by equation (5.1).

$$V[\%] = 1{,}55 \cdot 10^{-4} \cdot A \cdot M \tag{5.1}$$

This equation is just an illustration of what is true in this case study, and great uncertainties exist if implemented on other projects. One uncertainty is in the double rows installation which exist in this project.

Vertical displacements on the surrounding ground surface in the Plaxis model with installation effects are shown in Figure 5.8 and can be compared with the prism displacements in Figure 3.10. The results show similar trends with time and distance from the wall. However, the Plaxis results highly overestimate the settlements far away from the wall. This is because of overpredicted settlements in later stages of the excavation, the prediction in the installation phase is fairly accurate. Therefore, including installation effects can be useful to predict displacements, especially in earlier stages.

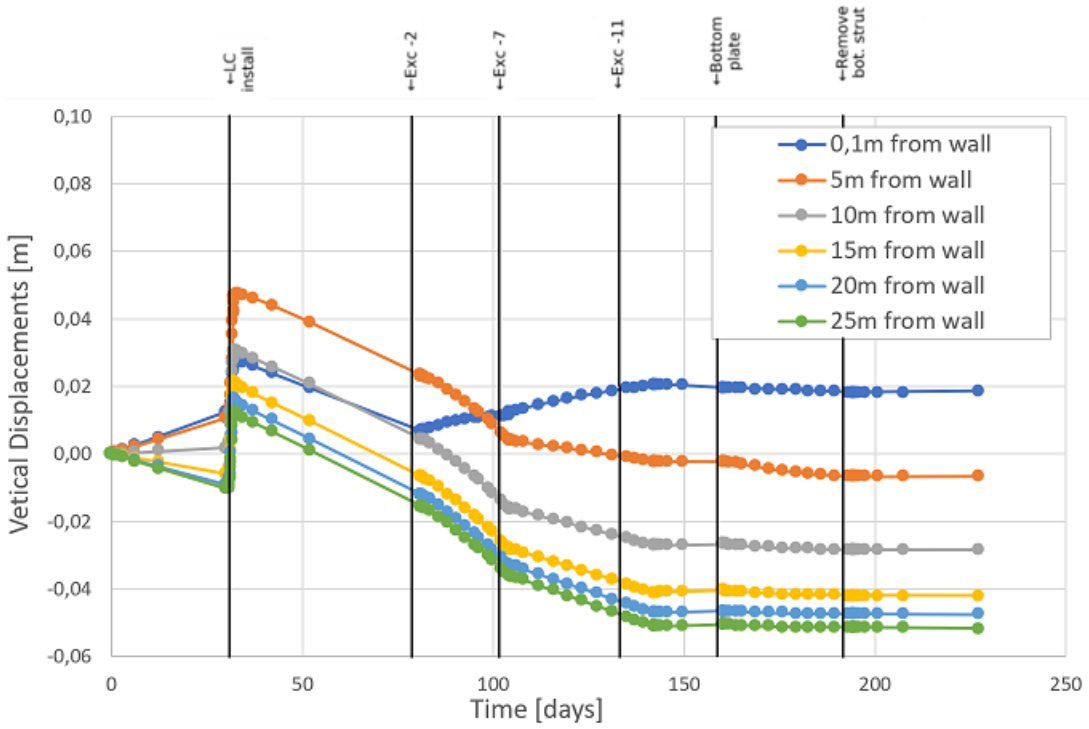

Figure 5.8 *Plaxis settlements on surrounding soil.*

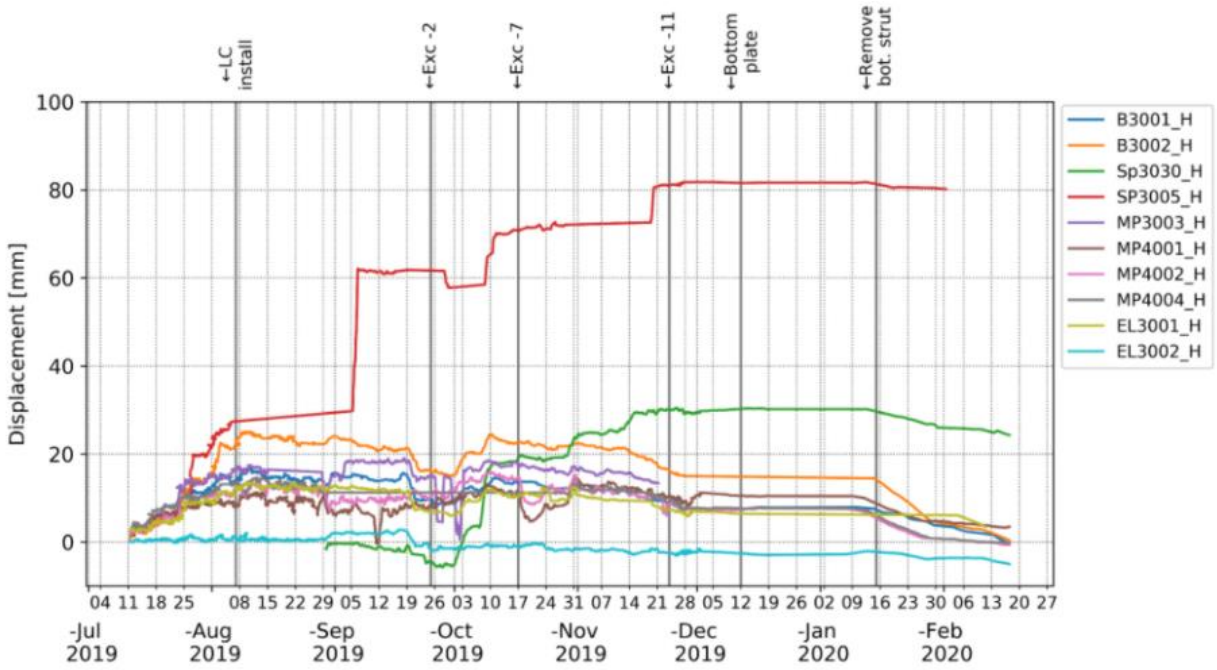

Figure 3.10 (bis) *Vertical displacements of prism field monitoring.*

An alternative potential method is to add the installation effects by hand, this is made in Figure 5.9 by adding an upward displacement by hand to the settlements after the LCC installation. A value of 0,02m (S) is used to match the initial displacements in the LCC installation phase. Like equation (5.1), an equation can be creating from this value as well, depending on the total LC area coverage(A) and the kg/m^3 LC, see equation (5.2).

$$S[m] = 5{,}17 \cdot 10^{-6} \cdot A \cdot M \tag{5.2}$$

The results are like the prism displacements and shows that the method has potential if the correct prediction is made. However, it is just an illustration of what is true in this case study and big uncertainties comes with new projects.

When looking at the strut forces, see Figure 5.10, the installation effects increase the values. This leads to similar forces in the upper strut compared to the strain gauge monitoring, while the lower strut is predicted to take higher forces then in reality. A test was made where the volume expansion was reverted by 50% to compensate for the soil crawling back with time. This did however not affect the lower strut forces, while the upper strut forces were decreased with 300kN.

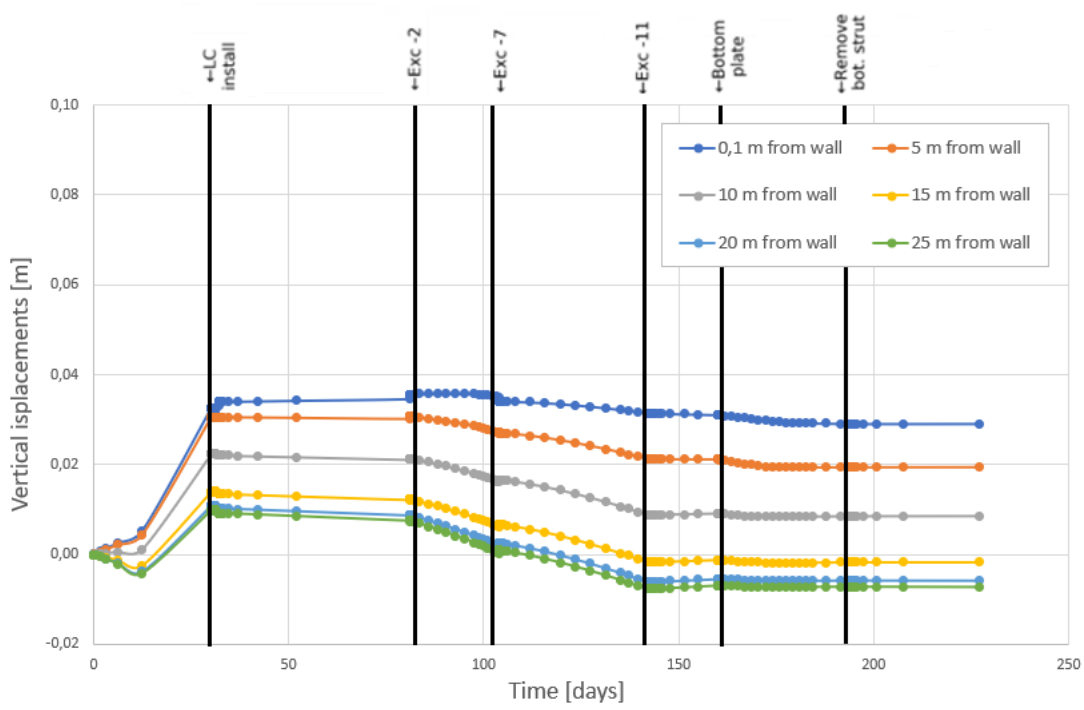

Figure 5.9 Vertical displacements on surrounding soil with hand calculated LC installation effects.

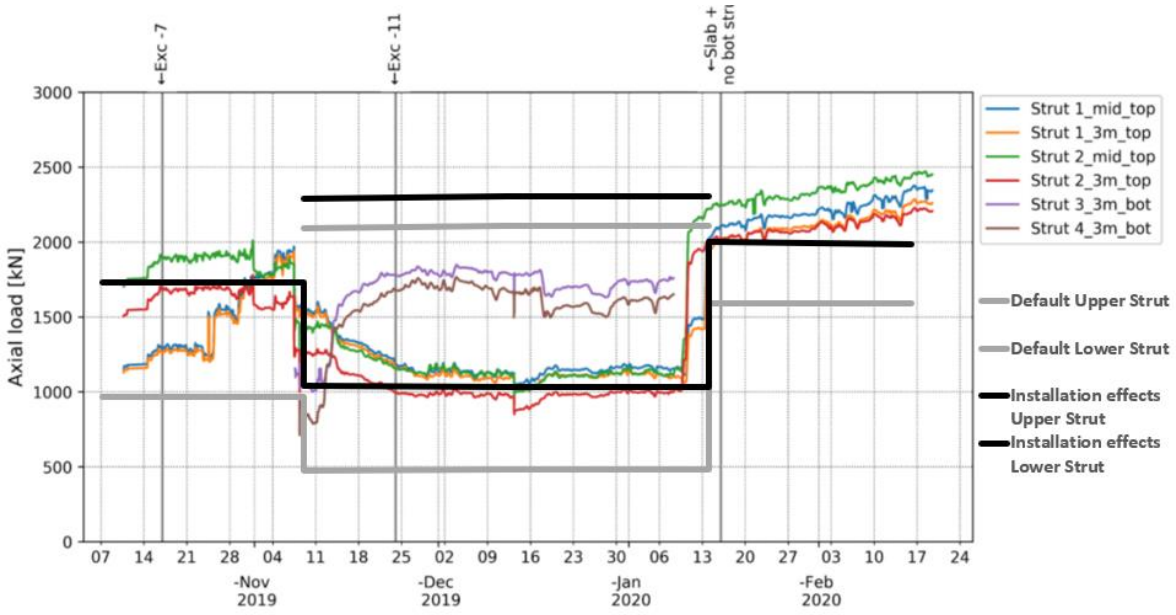

Figure 5.10 Strut forces with installation effects and strain gauge monitoring.

5.2.2 Final Model

The final approach to model the case site is shown in Table 5.3, where the changes from the base model are highlighted in grey. It is the final attempt to model the system response of the excavation as accurately as possible. The decided approach is based on conclusions reached in the chapters above. The most important change in approach from the base model is the addition of volume expansion from LCC installation.

Table 5.3 Description of modelling approach for final model.

Model aspect	Choice for final model
Geometry of LCC	Homogenous soil to represent the entire LCC grid.
OCR of LC	OCR = 15
Value for R_{inter}	R_{inter}=0,5
LC material in excavation	Consider the weaker LC material above excavation bottom.
Strength reduction of LCC	Use –20% strength/stiffness in the LCC.
LC Installation Effects	Include installation effects in the model.

The resulting wall displacements are compared with the inclinometer 5 displacements in Figure 5.11. The maximum displacements of the wall displacements are accurately predicting the trends and quantity of displacements, the maximum deformation in the final stage is slightly overpredicted with 4-5mm. The biggest discrepancy is that the Plaxis wall displacements shows no displacement at the top, since the top strut is fixed in place and highly stiff. In comparison, the inclinometers show some top displacement. This may be due to the entire excavation being rotated to the side by LCC installation at the emergency exit excavation, and by the strut being locked in at maximum displacement.

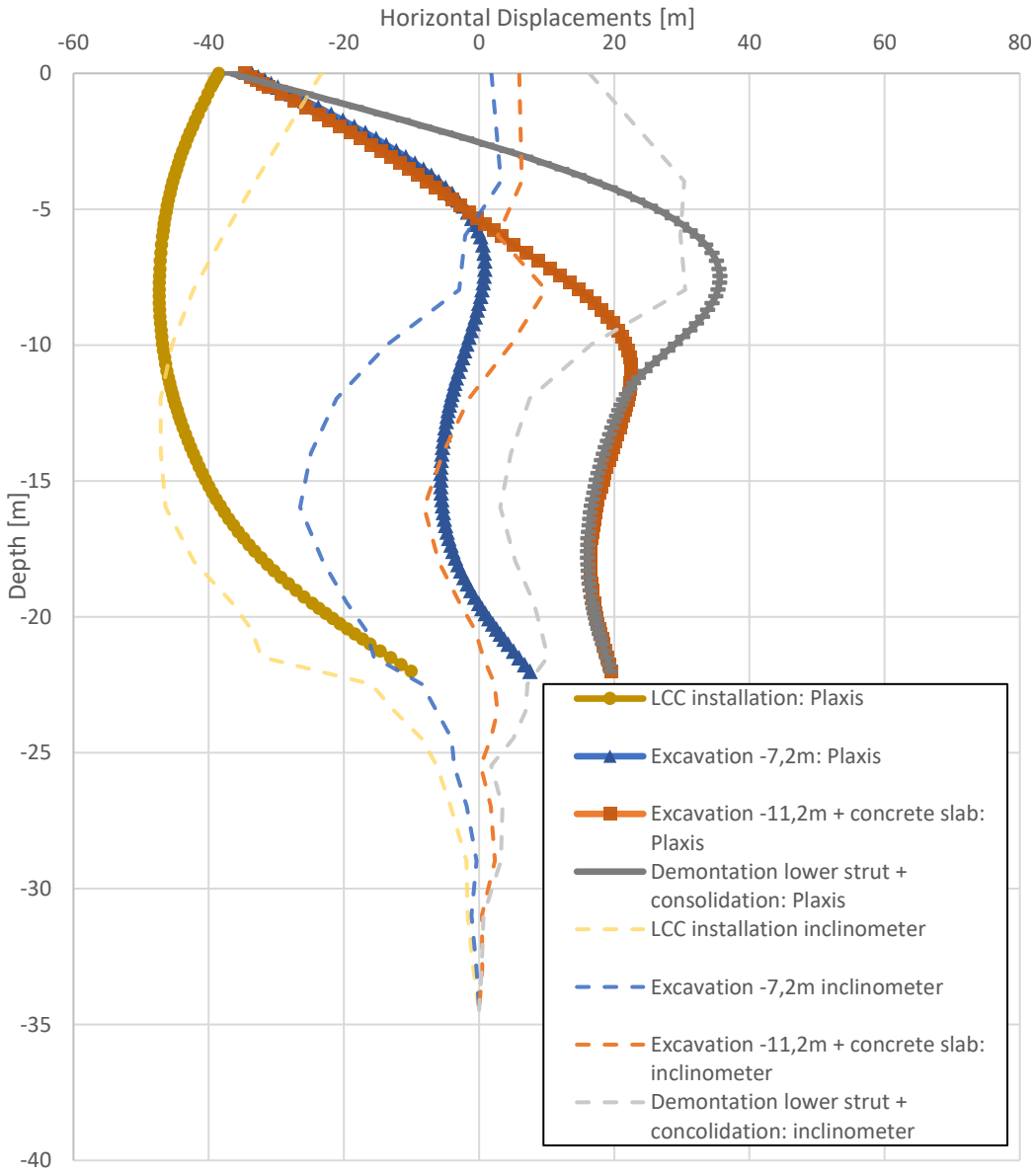

Figure 5.11 Wall displacement of final model vs. inclinometer monitoring.

Settlements on surrounding soil is shown in Figure 5.12 for the final Plaxis result and Figure 3.10 for prism displacements, including installation effects. The two figures show similar trends and values, differences will always be there due to other activities and events that affect the prisms. Furthermore, the Plaxis results can be combined with hand calculations using equation (5.2) to compare the effects far away from the excavation, since the Plaxis model seems to overestimate the settlements there.

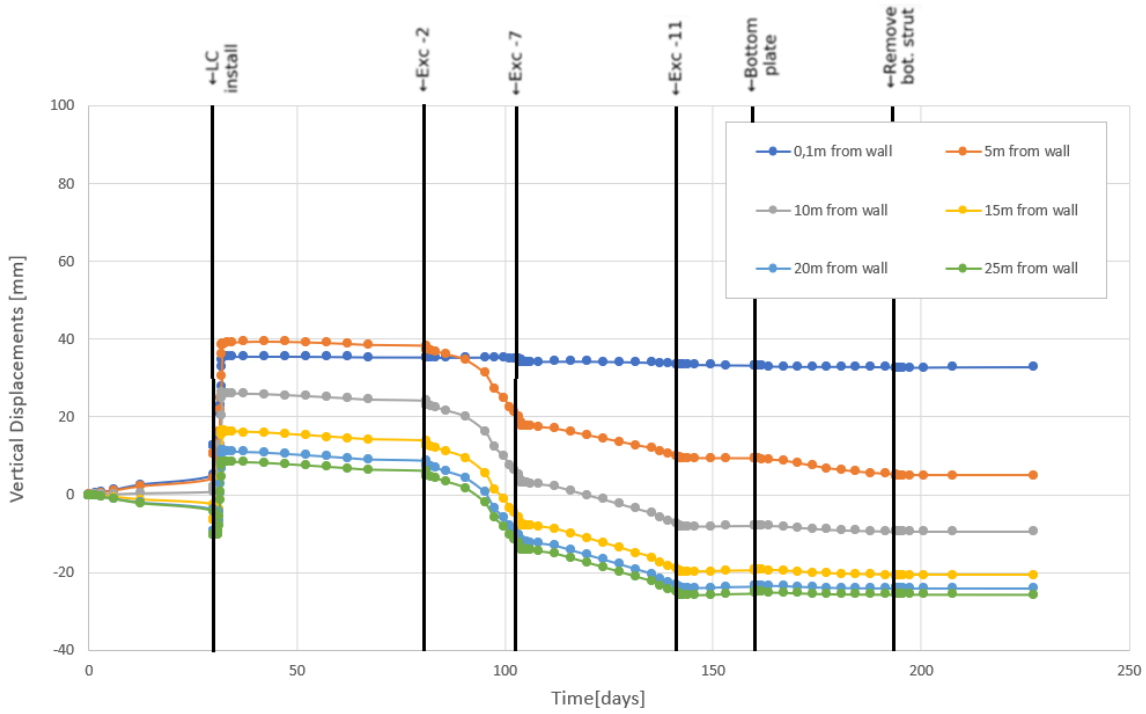

Figure 5.12 Vertical displacements on surrounding soil with final Plaxis model.

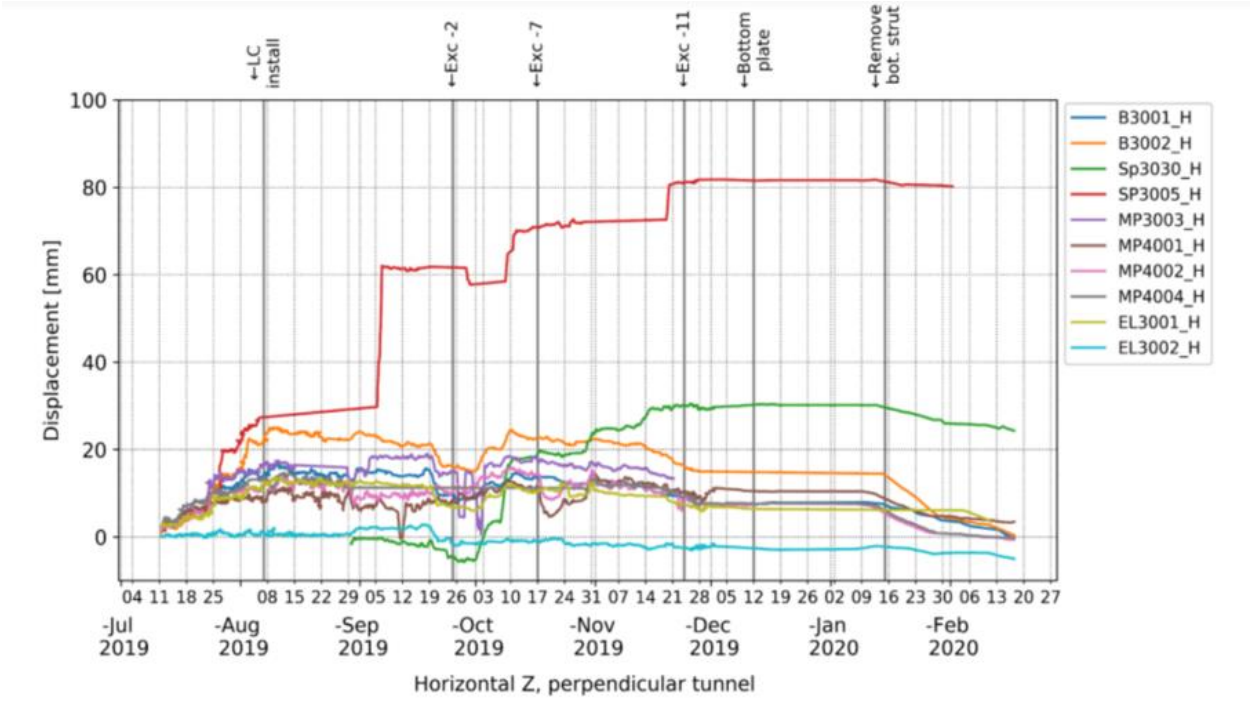

Figure 3.10 (bis) Vertical displacements of field measurement prisms.

Strut forces in the final Plaxis model compared with strain gauge monitoring is shown in Figure 5.13. The final model accurately predicts the upper strut forces while the lower strut forces are overpredicted. The overprediction of the lower strut forces may, as previously stated, be due to

insufficient small strain stiffness in the material inside the excavation. A constitutive model such as Hardening Soil small strain could take this into account, but it requires triaxial soil tests that accurately depict its small strain stiffness, which is uncommon in Sweden and was not at hand in this study. Another solution is to increase overall stiffness, but it would overpredict soil stiffness in larger strains which is unsafe.

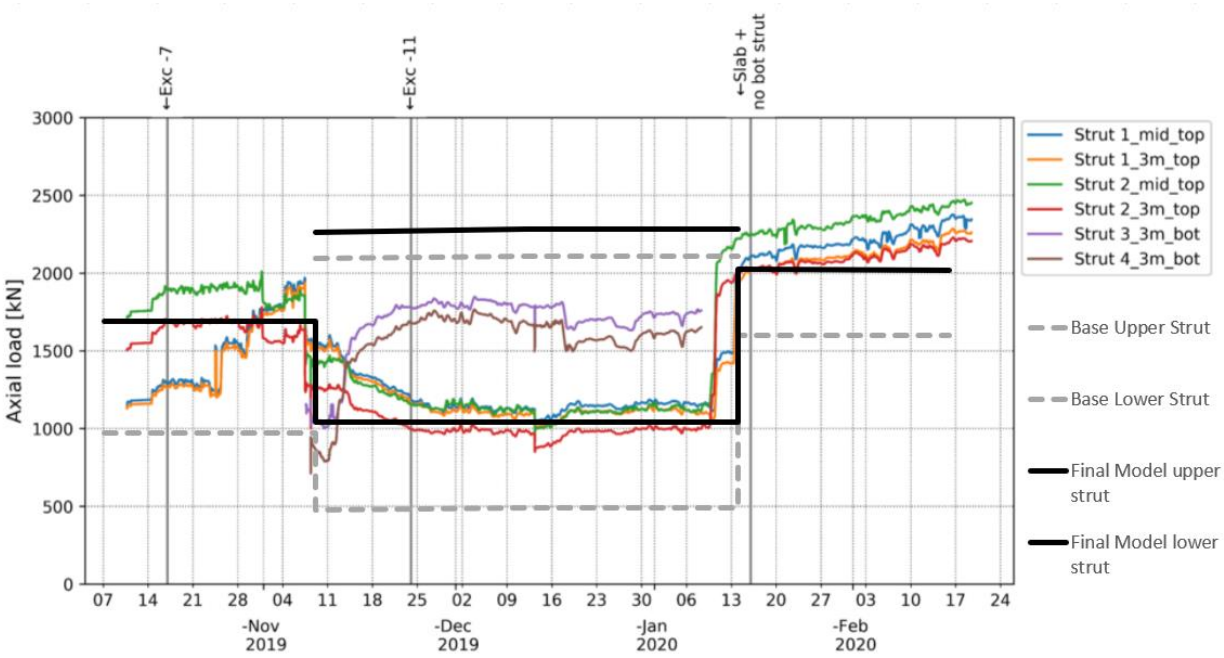

Figure 5.13 *Strut forces with final model and strain gauge monitoring.*

5.2.3 Creep-SCLAY1S state parameters

To determine the impact of Creep-SCLAY1S as the constitutive model used for the surrounding clay body, state parameters are shown and analysed. If they do not change during the simulation, it suggests they are not contributing to the analysis. This does not mean the model is not describing the soil response well, just that the excavation is so stable that the phenomena are not appearing.

Although the aim of the numerical model is to describe the system response, it seems the response in the clay body outside of the excavation is not substantial. Thus, the use of an advanced constitutive model such as Creep-SCLAY1S for modelling short term scenarios in excavations may not be motivated. No considerable effects of the advanced state parameters are seen in the model. Figure 5.14 suggests there is a rotation of the yield surface around some local stress points. Global changes in rotation of the yield surface are small, around 0,05 during the entire excavation period. Similarly, amount of bonding, shown in Figure 5.15, shows some change in local zones but no significant development in the soil body as a whole. This is likely because of the small displacements in the clay body outside of the excavation. Additionally, no creep effect was seen because of the brief time span of the simulation.

In long term stability studies however, the use of Creep-SCLAY1S could be more significant because of the creep, rotation of the yield surface and bonding/destructuration effects.

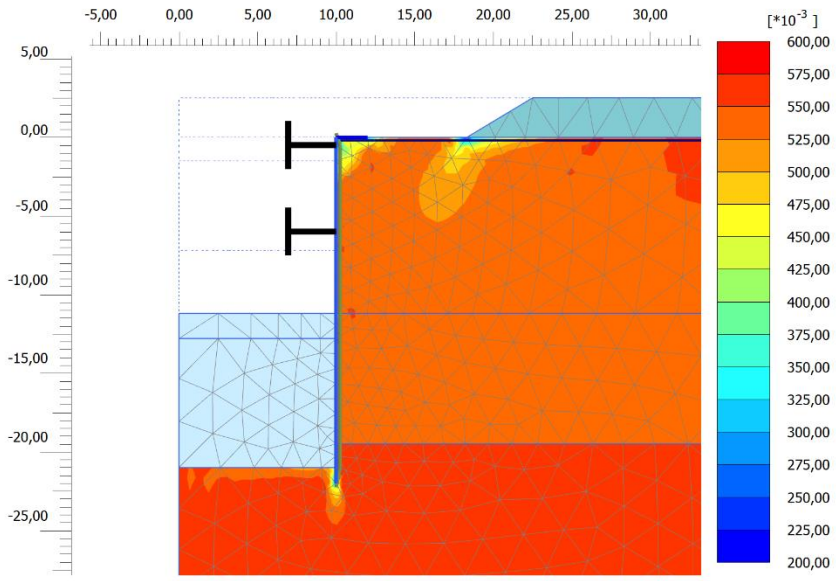

Figure 5.14 Scalar value of the rotation of the yield surface, α, in phase "dismantling of lower strut".

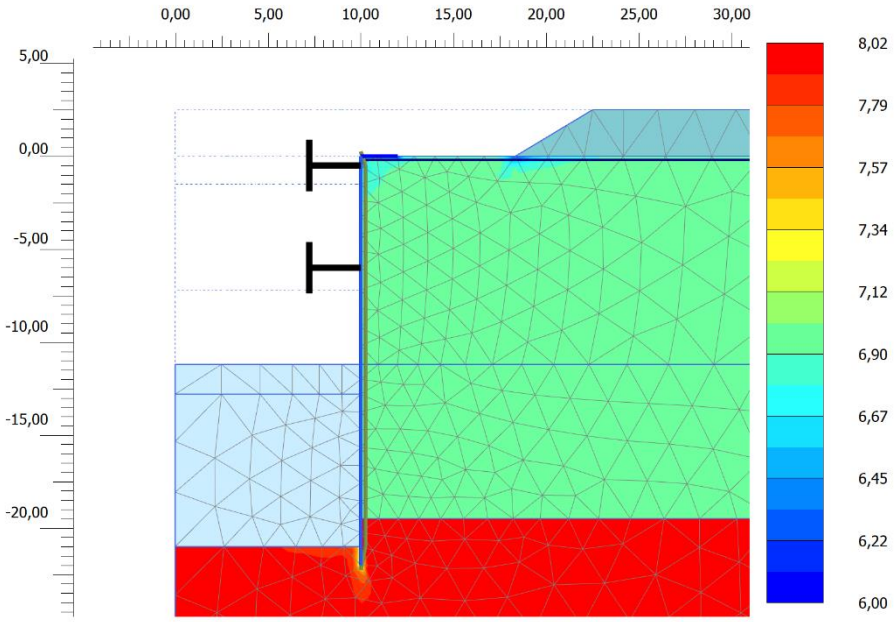

Figure 5.15 Amount of bonding χ in phase "dismantling of lower strut".

5.3 Impact of LCC on Excavation

The expected positive effects from LCC were stated in Chapter 2.2 and three of them will be discussed using the results from this report.

- Reduce impact on surrounding soil.
- Reduce the construction loads in strut and wall.
- Stabilize excavation ground and working foundation, allowing for more efficient work, more heavy machines and facilitate transportation around the excavation.

The final model is now compared with a model excluding LCC in the excavation. The soil inside the excavation is still modelled with Hardening Soil model. The comparison of the wall displacements is shown in Figure 5.16. The results show that LCC decrease the final positive displacements (towards the excavation) of the wall with 20mm, which is a significant decrease. The effects are also evident during the construction of the excavation which increases the safety of the workers. However, the negative displacements (away from the excavation) can create problems with heave close to the excavation.

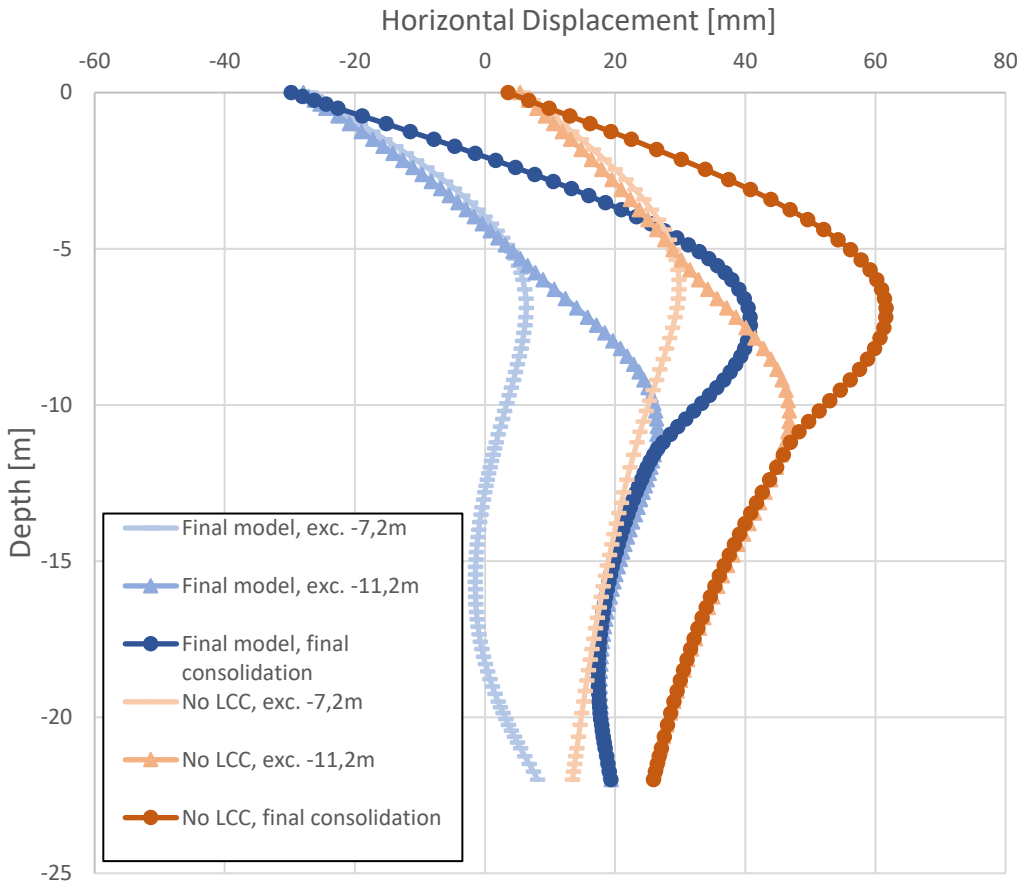

Figure 5.16 Displacements of the with wall final model and without LCC.

A comparison of the vertical displacements on surrounding soil is shown in Figure 5.17. The results show that LCC decrease the settlements on soil far away from the excavation. This is an important improvement to an excavation in an urban area as settlements can damage surrounding

buildings. However, there is an increase on heave close to the excavation, which could disturb the working process. One of the claimed positive effects of the LCC is "stabilization of work foundation" which partly refers to the hardening of the soil in the excavation, but also the decreased displacements close to the excavation. This is true after the installation as the curve is more stable after that point, but during the installation phase it may have the opposite effect and should be taken into consideration.

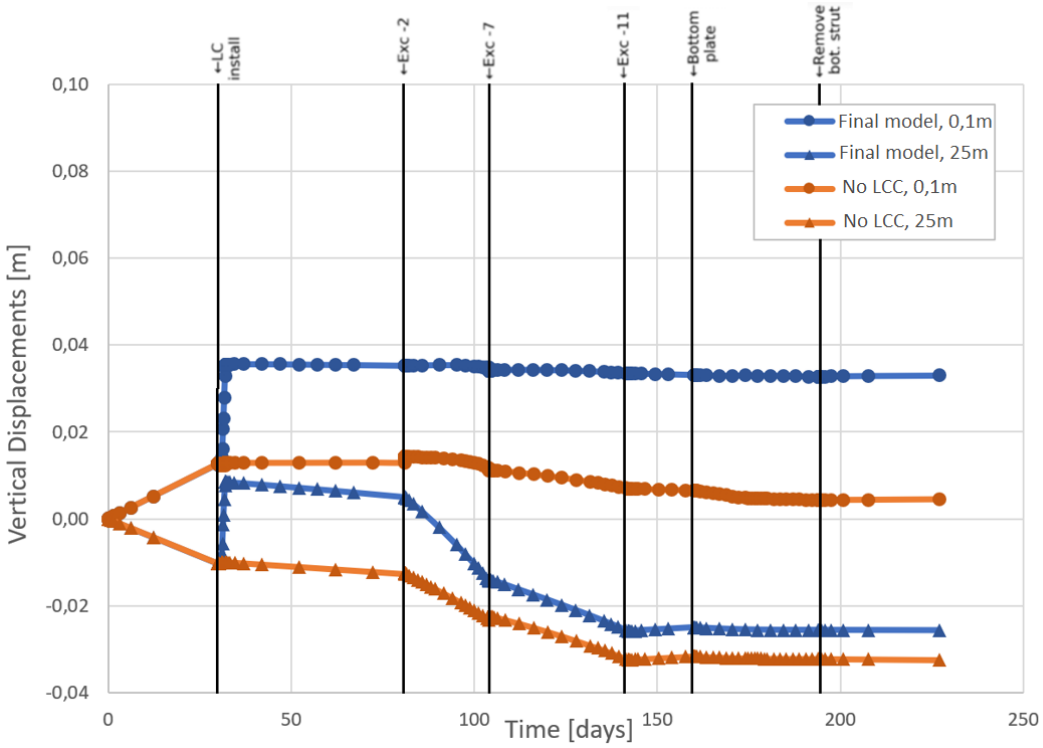

Figure 5.17 Settlements on surrounding soil with final model and without LCC.

A comparison of the strut forces is shown in Figure 5.18. It shows a significant increase in the strut forces with the LCC. This is due to the installation effects causing the SPW to be pushed out, hence increasing pressure on the SPW. When including the contraction of the soil in the model in chapter 5.2.1, the strut force increase is still present in both struts. One of the said positive effects of LCC, brought up in Chapter 2.2, is a decreased force on struts, which is not found looking at the SLS. This however highly depends on when the struts are installed and the impact of the LCC installation can be decreased if the ground is allowed to stabilize before strut installation. The conclusion is that LCC can increase the strut forces if struts are installed quickly after the installation.

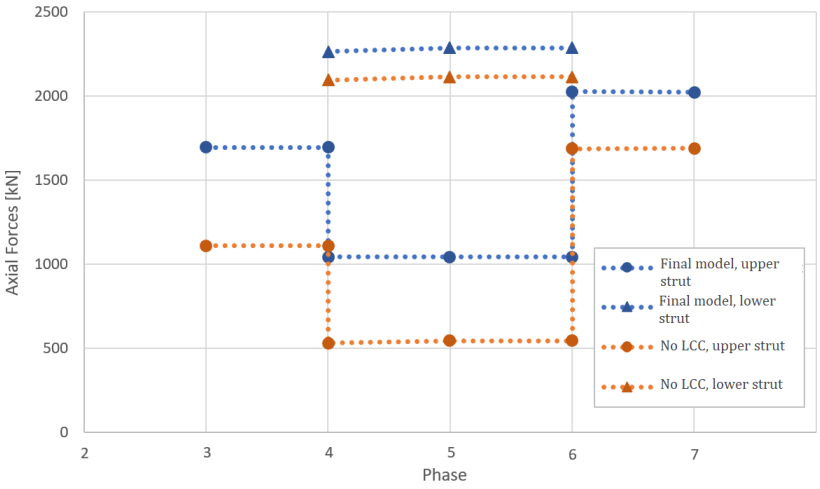

Phase 1	Maximal deformations after LC-installation
Phase 2	Excavation down to -2m, installation of upper strut
Phase 3	Excavation down to -7,2m, installation of lower strut
Phase 4	Excavation down to -11,2m
Phase 5	Casting of bottom concrete slab
Phase 6	Dismantling of lower strut
Phase 7	Consolidation

Figure 5.18 Strut forces for final model and without LCC.

6 Further Discussion

The numerical investigation has shown that the LCC installation effects have a significant impact on the system response, while the material quality and LCC geometry is less significant.

In this study, strut forces increase significantly with LCC due to the impact of its installation effects as well as upheave in the working foundation, while the wall displacements and settlements decrease. This suggests that LCC have both negative and positive impacts in the serviceability state. In an ultimate limit state, the structural support from LCC might have a bigger positive effect on the strut forces than the negative impact from installation effects, causing decreased strut forces overall.

The effects of the overlapping LCC grid have proven to decrease wall displacements and settlements on surrounding soil. Overly conservative predictions will overestimate the needed struts and material when using overlapping columns, which has negative impact on both economy but also environment in terms of CO_2 emissions.

Although uncertainties still exist, the study shows it is possible to model the system response of an excavation with LCC in the passive zone to a satisfactory level. This is promising for future urban excavation designs. Dry deep mixing can be a part of the toolkit for geotechnicians to reduce carbon emissions and cost, but it must be evaluated case by case what excavation design is most suitable. Although it was possible to back calculate the installation effects in this study, there is no way of predicting the amount of installation effects during design. To manage the uncertainty, a numerical investigation with different volume expansions could be executed.

6.1 Sources of Error

The results from this project have shown good accuracy in trends and values when compared to monitoring, but there are some known uncertainties that is considered and discussed in this chapter. Important to note is that error sources do not necessarily contradict the results in this report, as the results come from comparisons and differences in the models rather than from raw values.

- Lab tests are used when determining the boundaries of the parameters. Hence deviations in e.g., temperature and how the test is mixed can occur. Also, the LC lab tests are from 100 kg/m^3 cement while the real LC in the case study are 40 to 80. Only the strongest part of the LCC in the field can successfully be extracted and used for testing while the weaker parts can crumble and become unusable. Thus, the triaxial field tests that was compared with the triaxial lab test are potentially an overestimation of the material strength and hence not fully representative.
- The Creep-SCLAY1S optimization process was highly dependent on the oedometer tests. A total of 6 parameters were optimized with one output graph and hence a set of wrong parameters in the simulated test can still match perfectly with the field test. The optimization process was carried out multiple times with test results as guidance to prevent this error.
- Plaxis 2D cannot fully model the 3D geometry such as the LCC grid and the emergency exit 10m away from the cross section. This means some 3D phenomena is not fully modelled.

6.2 Further Research

The following are some topics that could be studied in further research:

- This report has focused on the actual response of the excavation. Further research is needed on the ultimate limit state, and the best way of modelling LCC where failure is a problem.
- How to model LCC installation effects in similar studies using finite element analysis.
- Understand what impact LCC has on long-term stability, and if it can be an effective method to decrease maintenance cost, vibrations, and comfort of constructions.
- Study the impact of Creep-SCLAY1S as a constitutive model for deep excavations, a sensitivity study could be executed by doing a comparison between Creep-SCLAY1S and a simpler constitutive model such as SCLAY1, NGI or the Soft Soil model.
- Additional triaxial tests could be executed in E02 Centralen, that captures the small strain stiffness response. Then, it could be studied if the constitutive model Hardening Soil small strain in the passive zone gives more realistic passive earth pressures and system response.

7 Conclusion

The study has investigated the effect of LCC in the passive zone of the excavation in E02 Centralen. It approached the problem through a rigorous computational technique based on homogenisation, that model's complex 3D effects in computationally effective 2D analysis. The aim was to accurately model the short-term system response of the site, and to analyse the effects of the LCC. Creep-SCLAY1S is used in the clay body to investigate its function in such a scenario.

Overall, the investigation shows that it is important to capture all processes, such as installation effects, to accurately describe the behaviour of a deep excavation. Sensitivity analyses are key to understand what parts of the model is of greatest importance.

The following conclusions can be drawn regarding the effects of LCC on the excavation:

- The wall deformations are decreased, partly because of the installation effects and partly because of the added stiffness of the LC.
- The heave in the working foundation close to the wall is high during LCC installation, but then stabilizes for future stages compared to displacements where no LCC was used.
- The settlement on surrounding soil is decreased with the use of LCC, which is positive for surrounding structures.
- Strut forces are significantly increased when using LCC because of the installation effects. This might not be the case in ultimate limit state studies or if the ground is allowed to stabilize before the strut installation.

Conclusions on how to best model LCC with an overlapping column grid in a short term SLS case study is shown in following bullet points:

- A homogenous soil to represent the entire grid is recommended, while separating eventual layers is preferable but not necessary.
- Parameter determination was shown to have less impact then modelling assumptions and decisions such as how to include installation effects. Setting the LC material to always over- or normally consolidated have both been successful, while the interface reduction factor has a little more impact and is preferably considering that the wall is interfacing in-situ clay.
- Volume expansion from installation of LCC is confirmed to have a considerable importance in the system response of the excavation and should be taken into consideration in the SLS. The volumetric expansion function in Plaxis has potential in modelling wall displacements.
- The advanced parameters of the Creep-SCLAY1S model are not developed during the simulation. A simpler model may be sufficient for this type of study.

References

Alén, C., Sällfors, G., Bengtsson, P.-E., & Baker, S. (2006). *Provbankar Riksväg 45/Nordlänken: Bankar på kalkcementpelarförstärkt jord – Beräkningsmodell för sättningar.* Linköping: Svensk Djupstabilisering.

Bjerrum, L. (1973). *Problems of soil mechanics and construction on soft clay soils and structurally unstable soils (collapsible, expansive and others).* Moscow: Proc. 8th ICSMFE,.

Björkman, T., Isaksson, J., & Yannie, J. (2020). *Projekterings-PM Geoteknik, Utökad produktionsuppföljning, KC i passivzonen.* Gothenburg: Trafikverket, NCC.

Broms, B. (1998). *Progressive failure of lime, lime/cement and cement columns.* Stockholm: Proceedings of the International Conference: Dry Mix Methods for Deep Soil Stabilization.

Graham, J., Nooman, M. L., & Lew, K. V. (1983). Yield states and stress–strain relationships in a natural plastic clay. *Canadian Geotechnical Journal 20,* 502-516.

Gras, J., Sivasithamparam, N., Karstunen, M., & Dijkstra, J. (2017). Strategy for consistent model parameter calibration for soft soils using multi-objective optimisation. *Computers and Geotechnics*, 164-175.

Gras, J.-P., Sivasithamparam, N., Karstunen, M., & Dijkstra, J. (2018). Permissible range of model parameters for natural clay. *Acta Geotechnica,* 13:387–398.

Grimstad, G., Degado, S. A., Nordal, S., & Karstunen, M. (2010). *Modelling creep and rate effects in structured anisotropic soft clays.* 69-81: Acta Geotech, 5.

Hedman, P., & Kuokkanen, M. (2003). *Hållfasthetsfördelning i kalkcementpelare –Fältförströk i Strängnäs.* Linköping: Arbetsrapport 29. Svensk Djupstabilisering.

Heidelberg. (2006). *Supported excavations in soft soil deposits.* Berlin: Springer.

Ignat , R., Baker, S., Karstunen, M., Liedberg, S., & Larsson, S. (2020). Numerical analyses of an experimental excavation supported by panels of lime-cement columns. Volume 118. *Computers and Geotechnics*.

Ignat, R. (2018). *Ground Improvement by Dry Deep Mixing Lime-Cement Column Panels as Excavation Support.* Stockholm: KTH, Royal Institute of Technology.

Ismail-Zadeh, A., & Tackley, P. (2010). Computational methods for geodynamics. *Cambridge University Press*.

Karlsrud, K., Eggen, A., & Nerland, O. (2015). *Some Norwegian Experiences Related to Use of Dry-Mixing Methods to Improve Stability of Excavations and Natural Slopes in Soft Clays.* San Fransisco: In Proceedings of the Deep Mixing Conference.

Karstunen, M., & Amavasai, A. (2017). BEST soil: Soft soil modelling and parameter determination. Gothenburg: Department of Architecture and Civil Engineering, Chalmers University of Technology.

Karstunen, M., & Koskinen, M. (2004). Anisotropy and destructuration of Murro clay. *Proc., A. W. Skempton Memorial Conf., R. J.Jardine, D. M.Potts, and K. G.Higgins, eds., Vol. 1, Thomas Telford, London*, 476–487.

Karstunen, M., Krenn, H., Wheeler, S., Koskinen, M., & Zentar, R. (2005). Effect of anisotropy and destructuration on the behavior of. *Int J Geomech*, 5(2):87–97.

Kitazume, M., & Maruyama, K. (2006). External stability of group column type deep mixing improved. *Soils and Foundations, Vol. 46(3)*, 323-40.

Kitazume, M., & Maruyama, K. (2007). Internal stability of group column type deep mixing improved. *Soils and Foundations, Vol. 47(3)*, 437-55.

Kitazume, M., Yamamoto, M., & Udaka, Y. (1999). *Vertical bearing capacity of column type DMM.* Stockholm: In Proceedings of the International Conference: Dry Mix.

Kivelö, M. (1998). *Stabilization of embankments on soft soil with lime/cement columns.* Stockholm: KTH Royale Institute of Technology.

Knappet, J., & Craig, R. (2012). *Craig's Soil Mechanics.* Oxford: Spon Press.

Korhonen, K. H., & Lojander, M. (1987). Yielding of Perno clay. *In Proceedings of the 2nd International Conference on Constitutive Laws of Engineering Materials, Tucson, Ariz, Elsevier, N.Y. Vol. 2*, 1249-1255.

Koskinen, M., Karstunen, M., & Wheeler, S. J. (2002). Modelling destructuration and anisotropy of a natural soft clay. *Proc., 5th European Conf. Numerical Methods in Geotechnical Engineering, P.Mestat, ed., Presses de l'ENPC/LCPC, Paris*, 11–20.

Larsson, S. (2005). State of practice report–Execution, monitoring and quality control. *International Conference on Deep Mixing,*, 732-785.

Larsson, S., Malm, R., Charbit, B., & Ansell, A. (2012). Finite element modeling of laterally loaded limecement columns using a damage plasticity model. *Computers and Geotechnics, Vol. 44*, 48-57.

Leoni, M., Karstunen, M., & Vermeer, P. A. (2008). Anisotropic creep model for soft soils. *Géotechnique 58(3)*, 215-226.

Phillips, A., & Sierakowski, R. (1965). On the concept of yield surface. *Acta Mechanica*, 29-35.

Potts, D. M. (2003). Numerical analysis: a virtual dream or practical reality? *Géotechnique*, 535-573.

Schanz, T. V. (1999). The hardening soil model: Formulation and verification. *International symposium "Beyond 2000 in computational geotechnics"* , (ss. 281-296). Amsterdam.

Sivasithamparam, N., Karstunen, M., & Bonnier, P. (2015). Modelling creep behaviour of anisotropic soft soils. *Comput Geotech*, 69:46–57.

Sivasithamparam, N., Karstunen, M., Brinkgreve, R. B., & Bonnier, P. G. (2013). Comparison of two anisotropic creep models at element level. *Proc. International Conference on Installation Effects in Geotechnical Engineering*, 72-78.

Starting Point Teaching Entry Level Geoscience. (den 19 03 2020). *Analytical Models*. Hämtat från Starting Point Teaching Entry Level Geoscience: https://serc.carleton.edu/introgeo/mathstatmodels/Analytical.html

Trafikverket. (2014). *Technical requirements for geoconstructions (Trafikverkets tekniska krav för*. Sweden: The Swedish Transport Administration, Publ. TDOK 2013:0667.

Trafikverket. (den 20 04 2020). *Så bygger vi västlänken*. Hämtat från Trafikverket: https://www.trafikverket.se/nara-dig/Vastra-gotaland/vi-bygger-och-forbattrar/Vastlanken---smidigare-pendling-och-effektivare-trafik/Om-Vastlanken/sa-bygger-vi-vastlanken/

Trafikverket. (2021). *TDOK 2015:0480, Klimatkrav i planläggning byggskede underhåll och på teknisk godkänt järnvägsmateriel.*

Västsvenska paketet. (u.d.). *The west swedish agreement*. Hämtat från https://www.vastsvenskapaketet.se/english/

Wheeler, S. J., Näätänen, A., Karstunen, M., & Lojander, M. (2003). An anisotropic elastoplastic model for soft clays. *Can. Geotech. J.*, 40(2), 403–418.

Wood, T. (2018). *Fullskaleförsök DDM (Dry Deep Mixing) i passivzon, Delprojekt E02 Centralen, Västlänken.* Göteborg: Trafikverket.

World Business Council for Sustainable Development. (2002). *The cement sustainability initiative.*

Wu, B., Ito, K., Mori, N., Oya, T., Taylor, T., & Yanagimoto, J. (2020). Constitutive Equations Based on Non-associated Flow Rule for the Analysis of Forming of Anisotropic Sheet Metals. *International Journal of Precision Engineering and Manufacturing-Green Technology volume 7*, 465–480.

Yu Yin, Z., & Karstunen, M. (2011). Modelling strain-rate-dependency of natural soft clays combined with anisotropy and destructuration. *Acta Mechanica Solida Sinica*, Vol. 24, No. 3.

Appendix A

Graphs from parameter determination

Appendix A contains figures from the parameter determination process.

- Graphs of laboratory tests, displaying which test is chosen for optimization.
- Figures of the optimized curves. First set of figures displays plots of all laboratory tests, and what test is chosen for the optimization process.

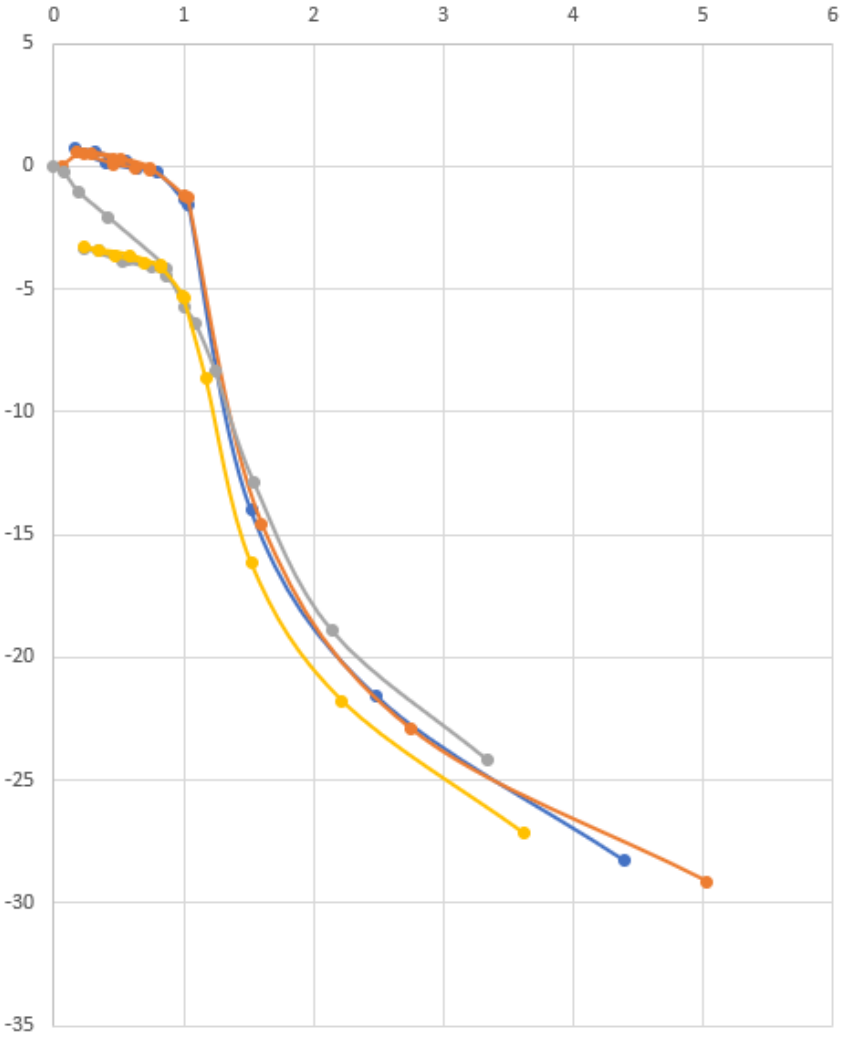

Figure A 1 *Plot of all IL tests for clay depth 0-20m evaluated for optimization of parameters. The blue test was selected, since it is a sensible median test.*

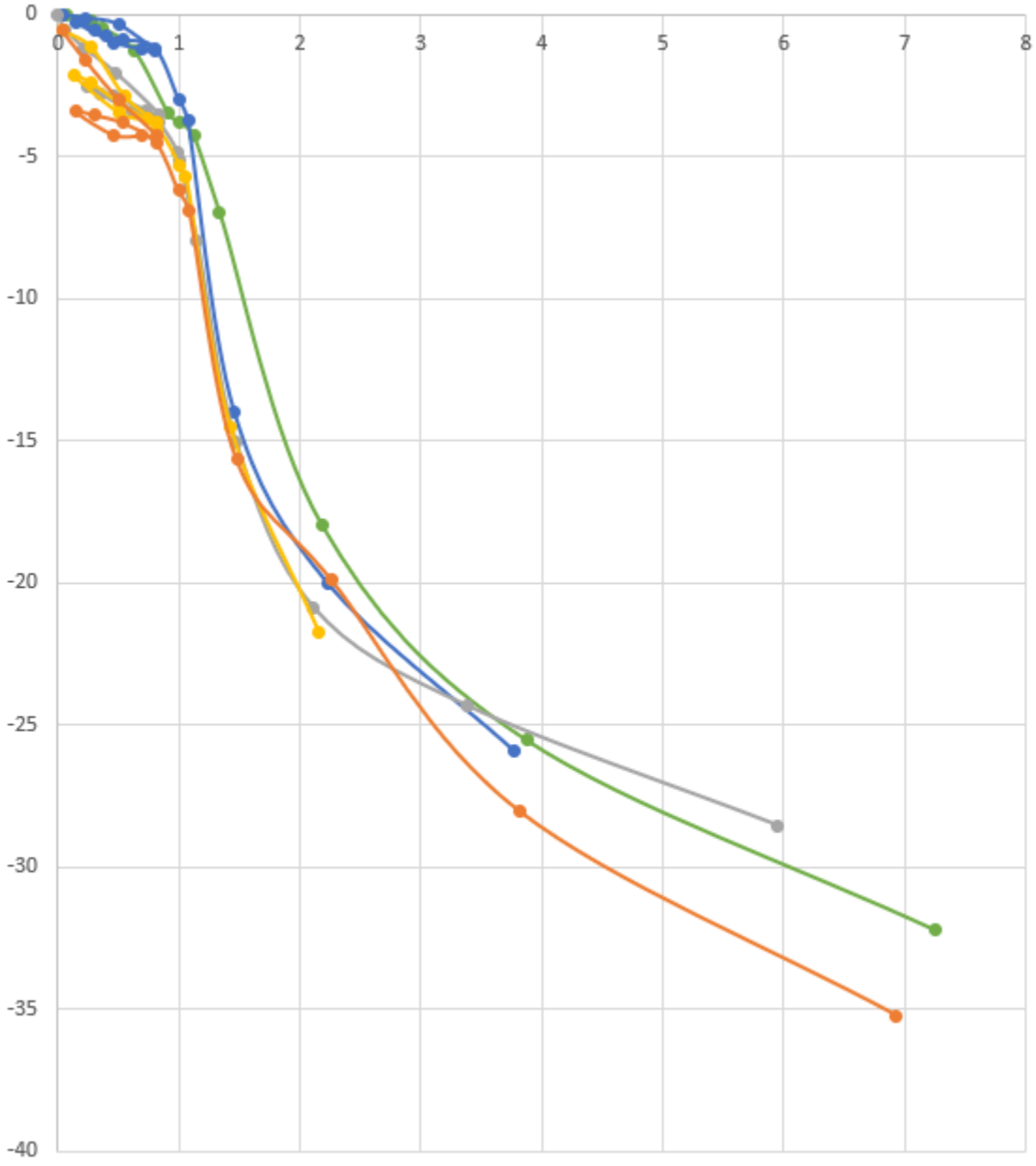

Figure A 2 *Plot of all IL tests for clay depth 20-45m evaluated for optimization of parameters. The blue test was selected, since it is a sensible median test.*

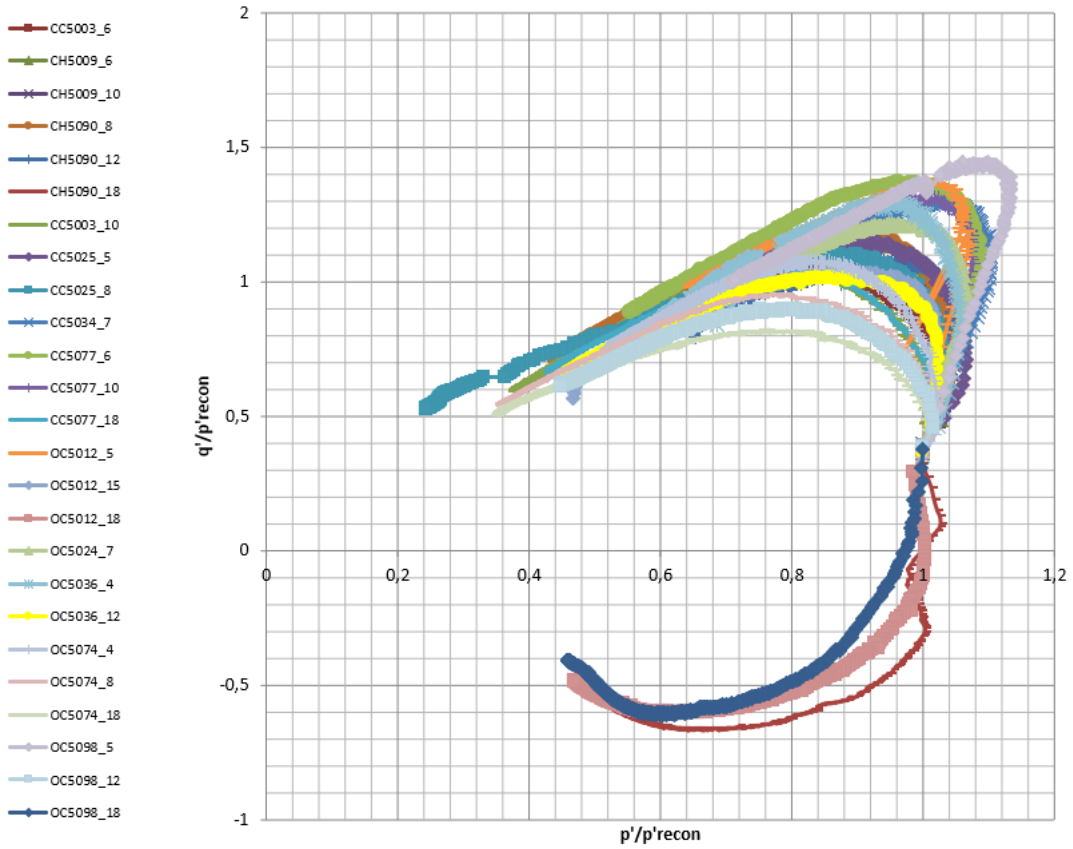

Figure A 3 *Plot of all CADC/CADE tests for clay depth 0-20m evaluated for optimization of parameters. The bright yellow CADC test was selected, as well as the dark blue CADE test.*

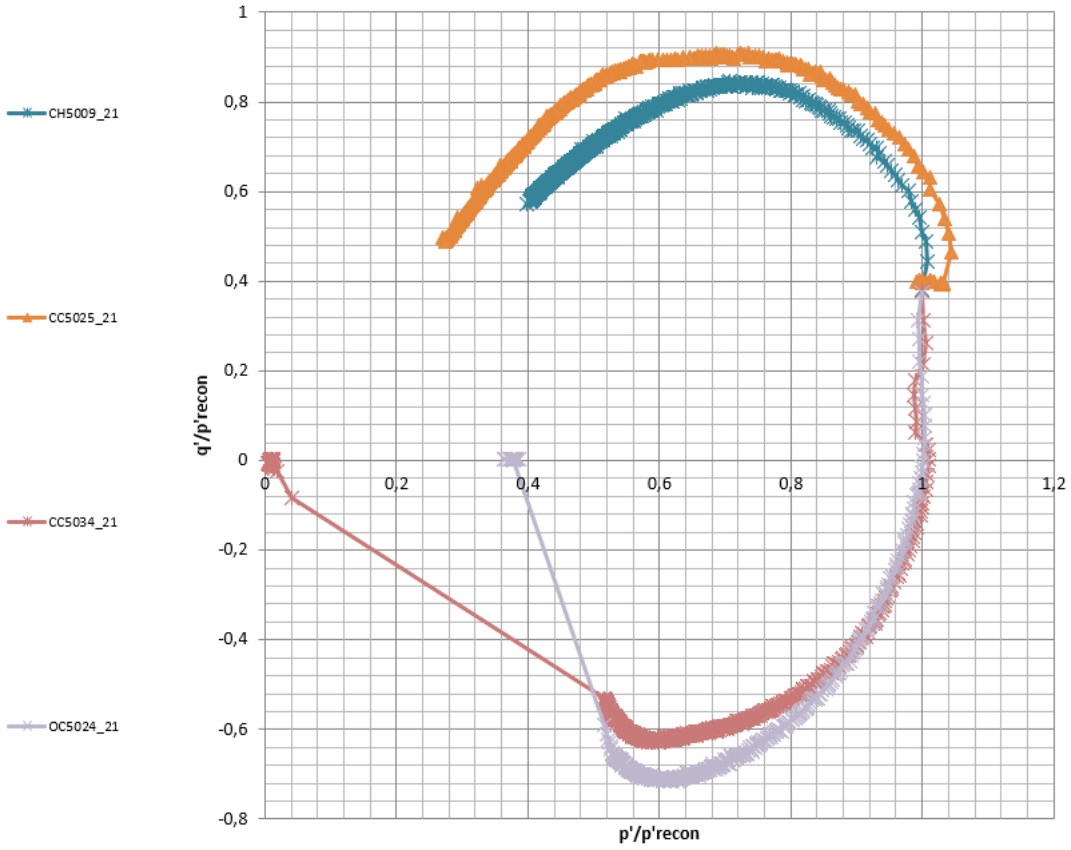

Figure A 4 *Plot of all CADC/CADE for depth 20-45m clay tests evaluated for optimization of parameters. The orange CADC test was selected since it starts nearest the calculated in situ stress state. The grey CADE test was selected.*

Following is set of figures displaying the optimized curves from the parameter optimization process.

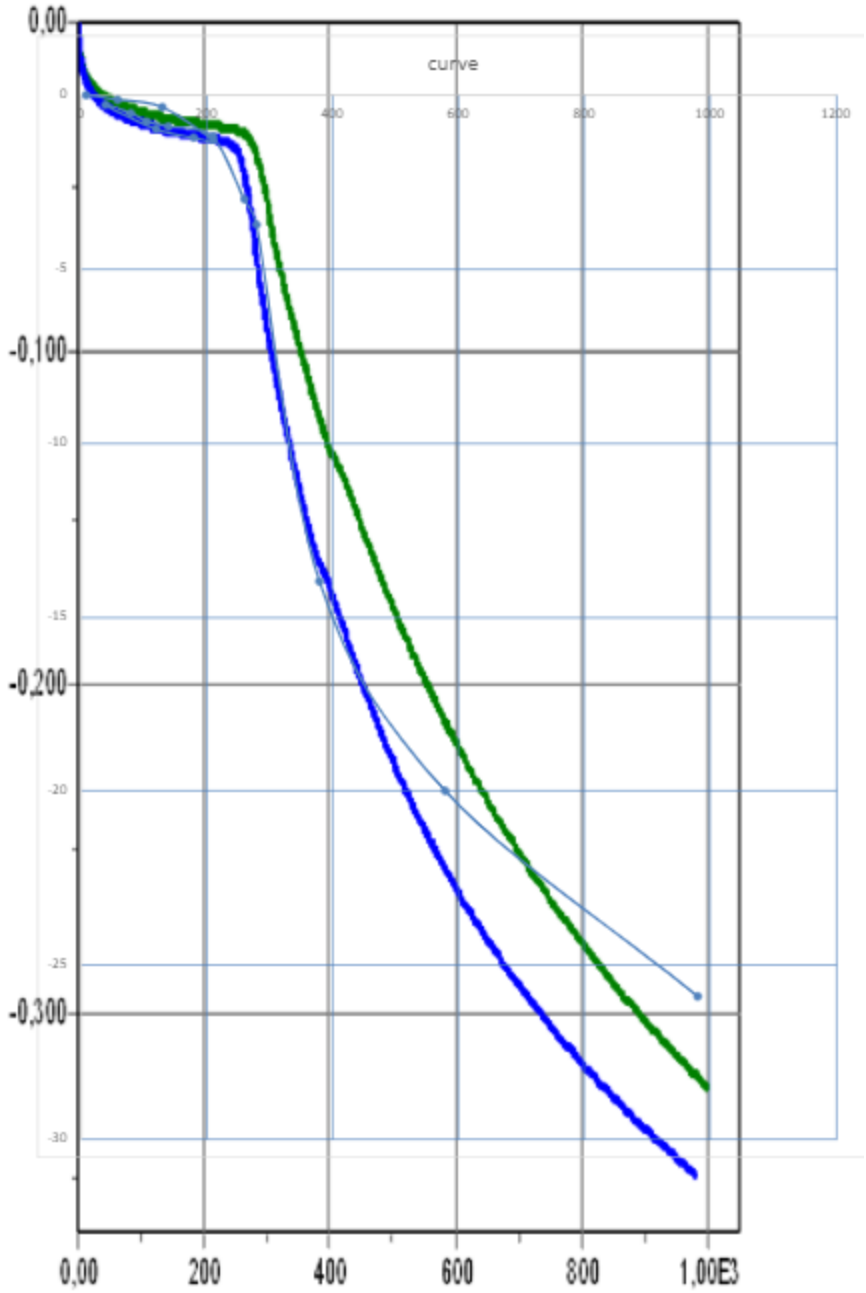

Figure A 5 *Optimized oedometer curve for Creep-SCLAY1S layer 20-45m. Green graph is pre-optimization and blue post-optimization.*

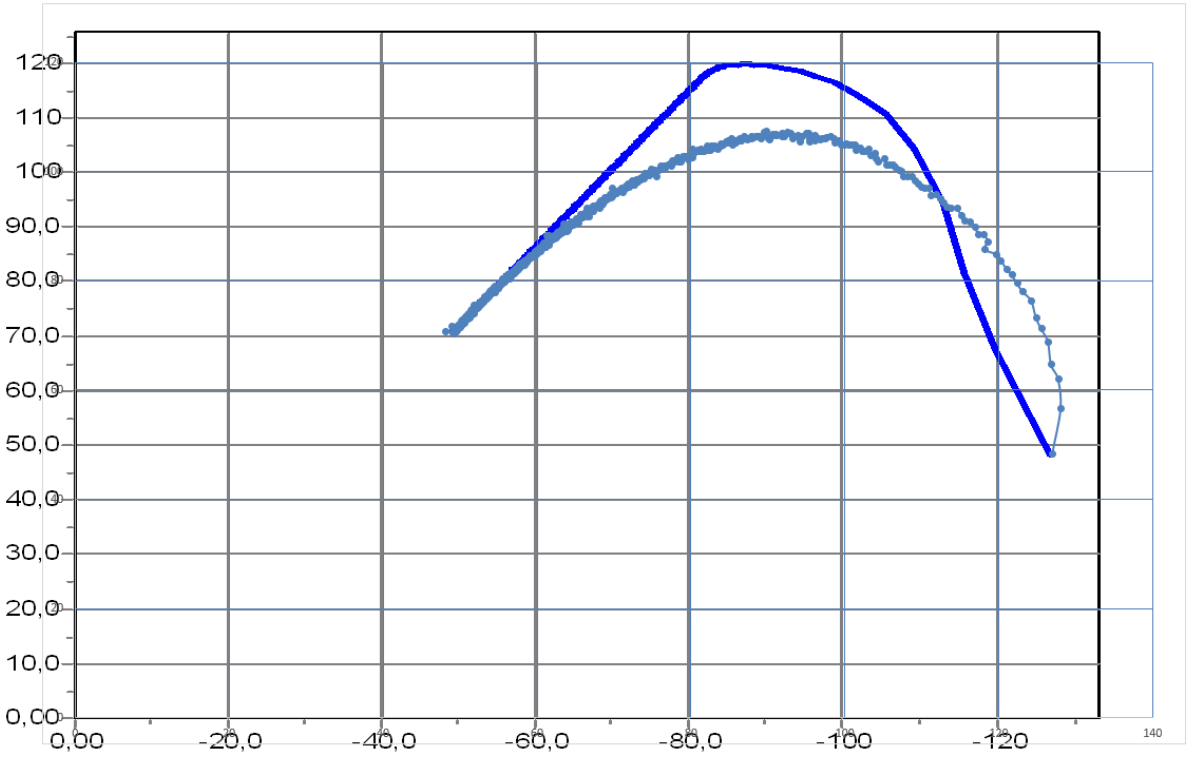

Figure A6 Optimized Triaxial CADC curve for Creep-SCLAY1S layer 20-45m.

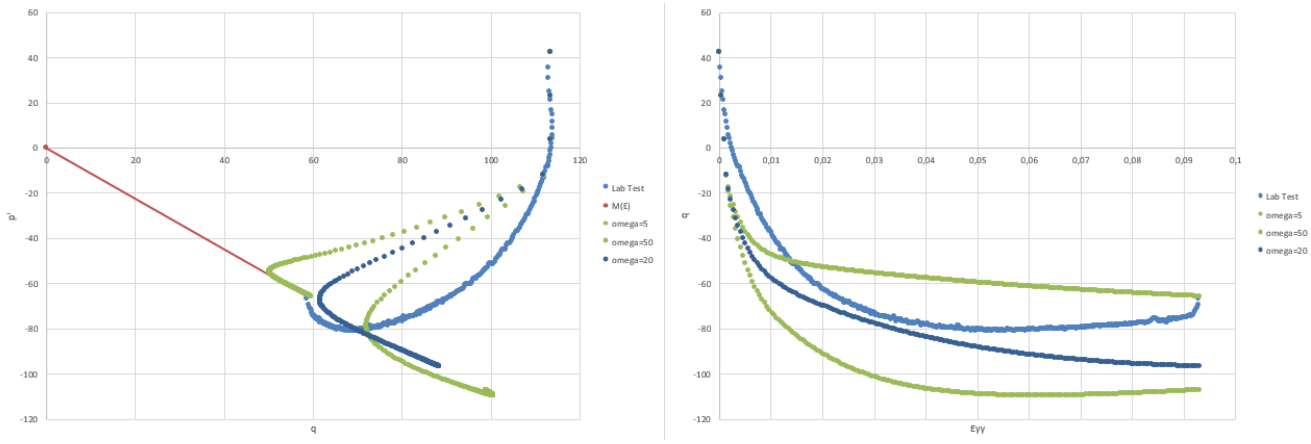

Figure A 7 Optimized Triaxial CADE curve for Creep-SCLAY1S layer 20-45m. Green graphs are during the optimization process and dark blue post-optimization. The light blue curve is the lab test.

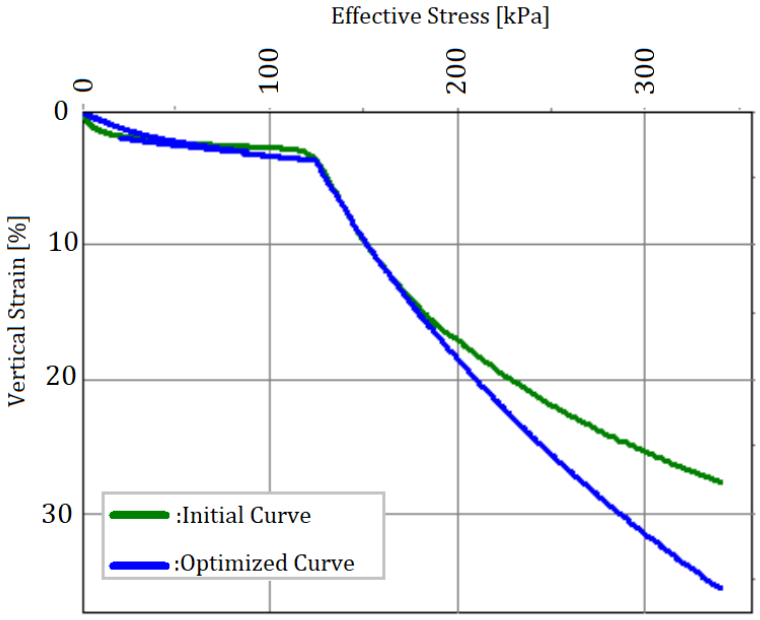

Figure A 8 Converting Creep-SCLAY1S parameters to Hardening soil by optimizing IL.

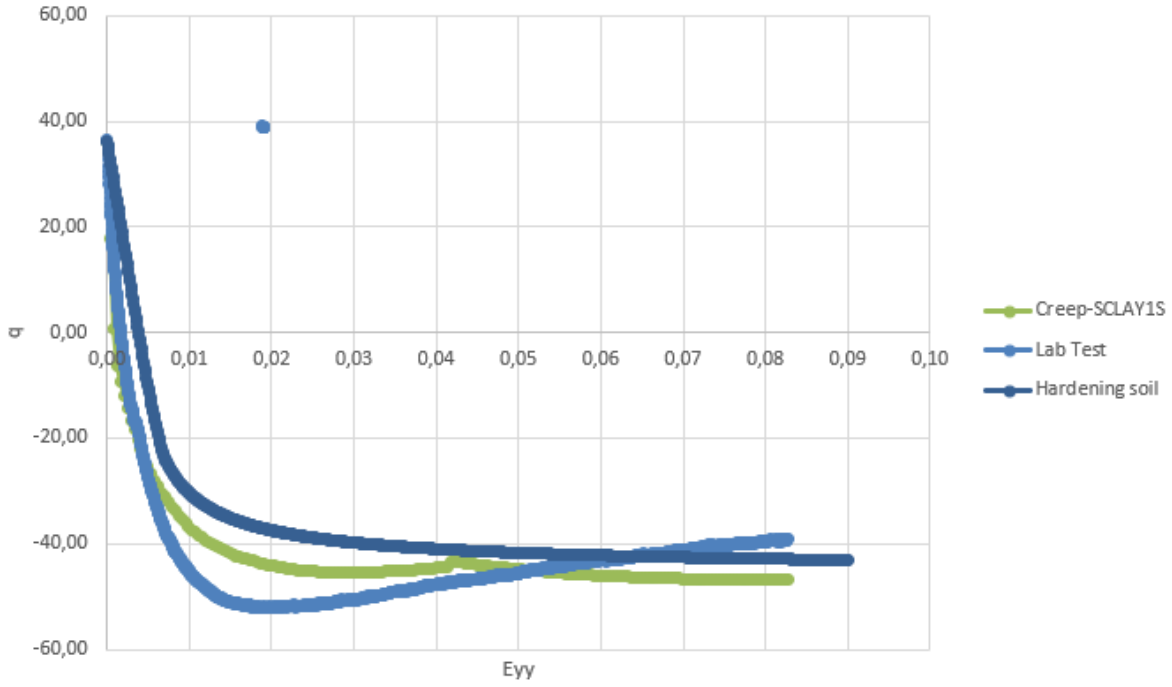

Figure A 9 Converting Creep-SCLAY1S parameters to Hardening soil by optimizing triaxial CAUE.

Appendix B

Graphs from Numerical Modelling

Appendix B contains figures from the numerical model.

- Phases of the excavation
- Final mesh with different geometries.
- Illustrations of excess pore pressures with and without columns.

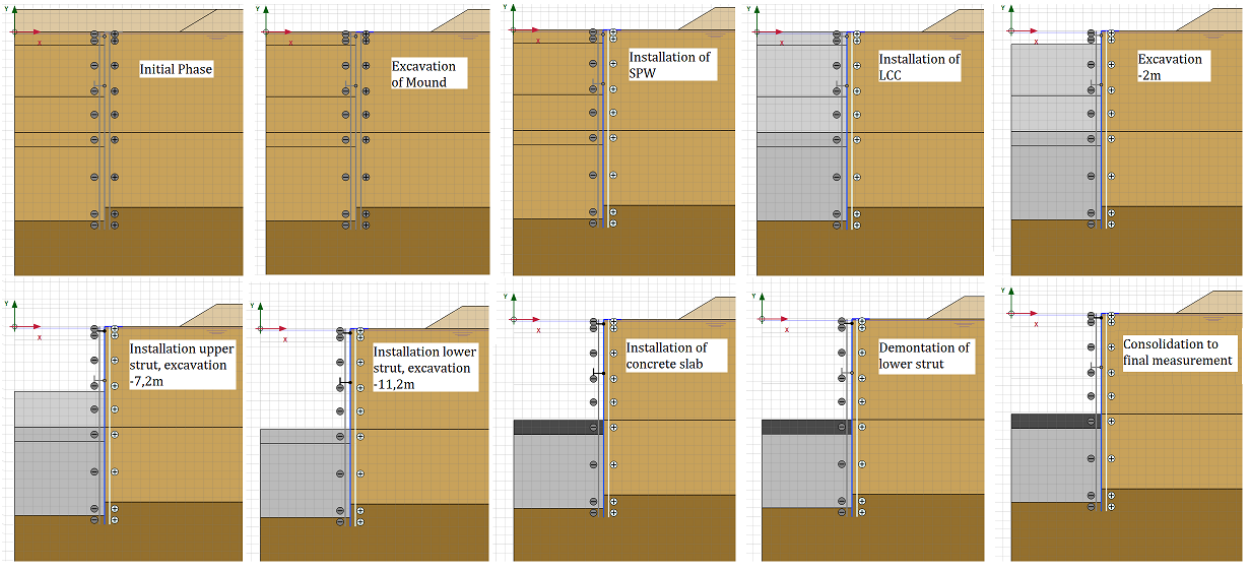

Figure B 1 Illustration of all phases in the Plaxis model.

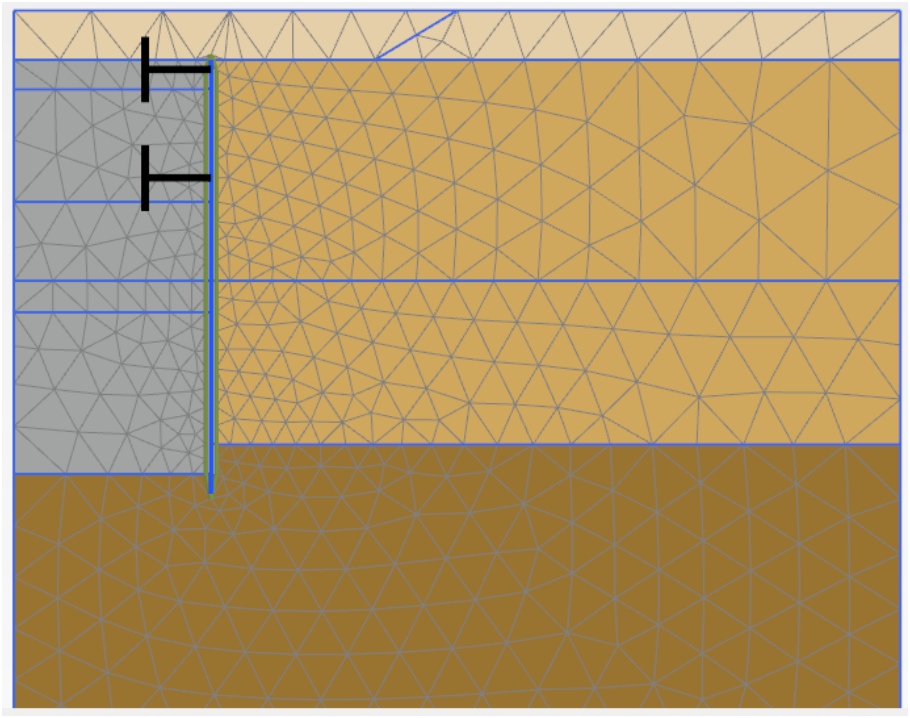

Figure B 2 Final mesh used in the numerical model with homogenous soil.

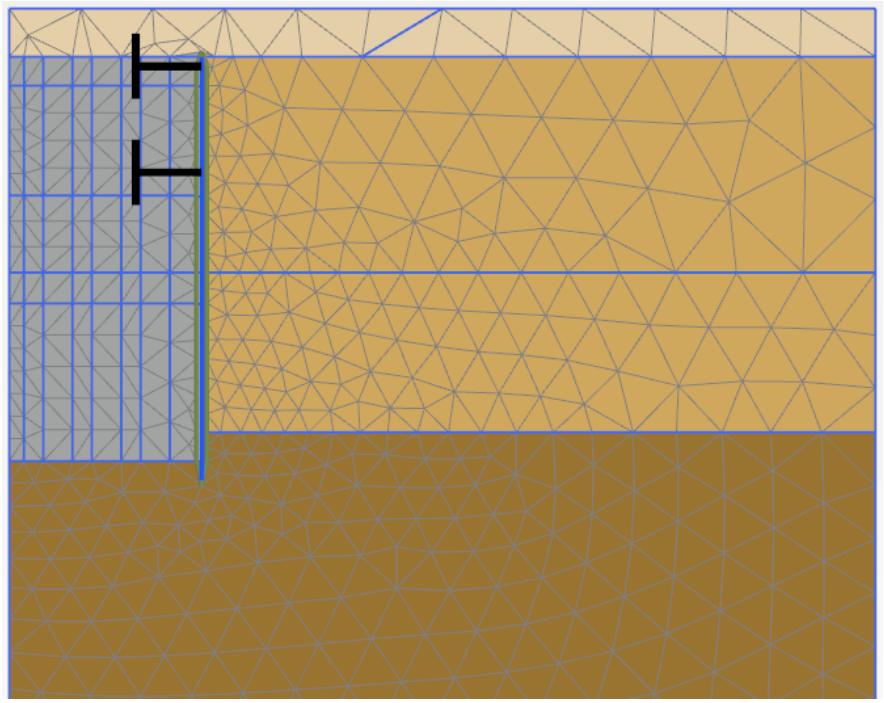

Figure B 3 Final mesh used in the numerical model with columns.

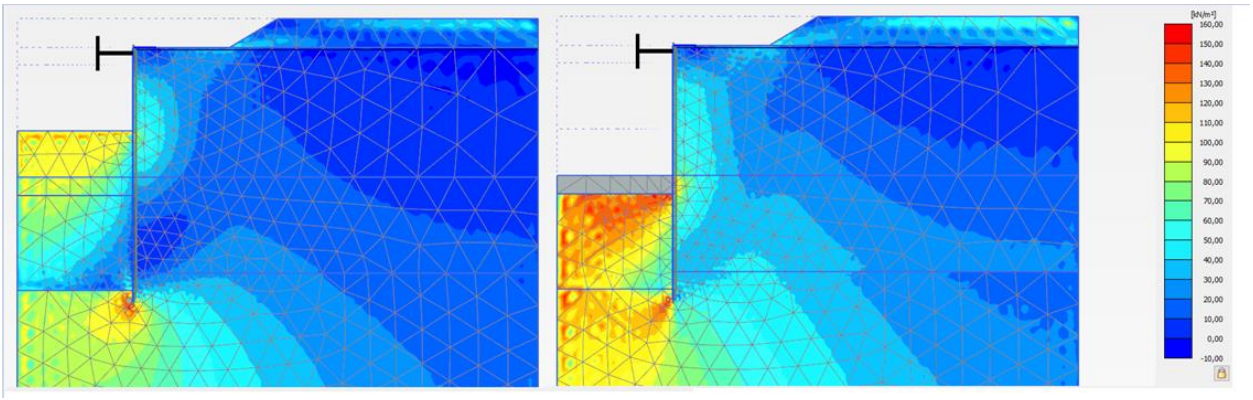

Figure B 4 Excess pore pressures in final model, excavation to -7,2m (left) and final consolidation stage (right).

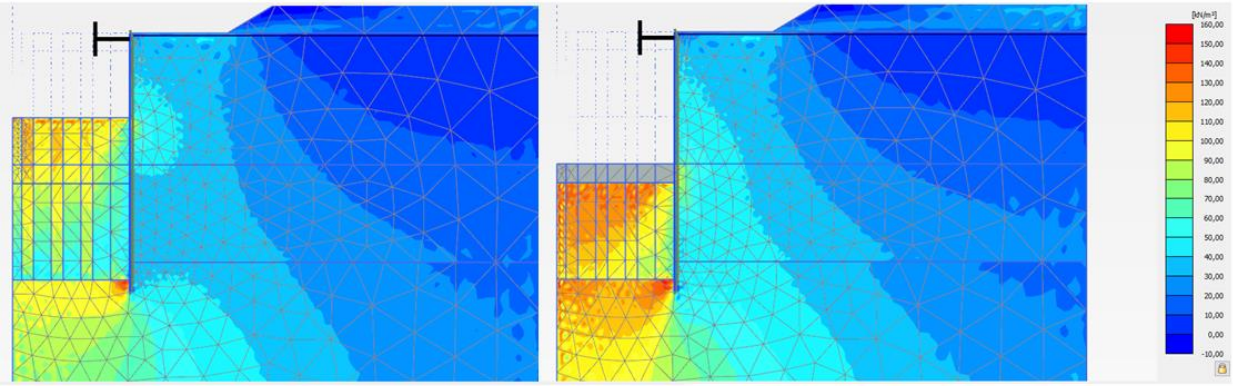

Figure B 5 Excess pore pressures with vertical columns, excavation to -7,2m (left) and final consolidation stage (right).

DEPARTMENT OF ARCHITECTURE AND CIVIL ENGINEERING

CHALMERS UNIVERSITY OF TECHNOLOGY

Gothenburg, Sweden 2021
www.chalmers.se